Doctoral Dissertation
Doctoral Program in Energy Engineering (32th Cycle)

Investigation and Modelling of Porous Solid Sorbents and Bio-based Ionic Solvents for the Separation of CO_2 from Flue gas

Elahe Davarpanah

* * * * * *

Supervisors
Prof. Guido Saracco, Supervisor
Prof. Simelys Hernández, Co-Supervisor

Doctoral Examination Committee:
Prof. Patricia Benito, University of Bologna
Prof. Francesco Maurellio, Mediterranea University of Reggio Calabria

Politecnico di Torino, April 2020

I hereby declare that, the contents and organisation of this dissertation constitute my own original work and does not compromise in any way the rights of third parties, including those relating to the security of personal data.

Elahe Davarpanah
Turin, April 20, 2020

Summary

This work is focused on the investigation of innovative materials for CO_2 capture from flue gas streams in a post-combustion carbon capture process. Porous solid sorbents and bio-based ionic liquids are applied to accomplish the objective of our study by adapting and modifying their properties, which contribute to a higher system efficacy and lower energy requirement. The results obtained from solid sorbent performance are modeled for a Temperature Swing Adsorption (TSA) system and validated using the experimental results.

In **Chapter 1** of this thesis, the main technologies developed for CO_2 removal from flue gases along with their pros and cons are described. Different types of materials used in these technologies are discussed with the main focus on the application of porous solid sorbents including a natural zeolite known as Clinoptilolite (Clino) and bio-based Ionic liquid famous as Amino-acid Ionic Liquid ([AA][IL]).

In **Chapter 2** the application of clinoptilolite for CO_2 separation from industrial processes at moderate temperatures in the range of 50 °C - 100 °C is studied in detail. Besides evaluating the sorbent in its raw form, the properties and the adsorption performance of cation-exchanged modified clinoptilolite are also investigated. The capability of zeolites in exchanging cations makes them a unique and potential sorbent with a basic structure for CO_2 separation purposes. In this work, the effect of alkali (Na^+) and alkaline metal (Ca^{2+}) cations on adsorption features are evaluated. Several tests are performed to understand the kinetic and equilibrium behavior of the sorbent as well as its CO_2 uptake performance and efficiency. The sample's characterization is done by means of EDX, XRD and N_2 physisorption analysis giving insight into the chemical composition and porous structure of the sorbent. Moreover, the adsorption isotherm for pure CO_2 at different temperatures is measured with the volumetric method. Using the results obtained

from adsorption isotherms at two different temperatures, the isosteric heat of adsorption is evaluated. The adsorption isosteric heat profile verified the presence of strong sites on the structure of the zeolite leading to the formation of different species. To understand the nature of these species contributing to the isosteric heat of adsorption the IR spectroscopy analysis is carried out. The results obtained from this comprehensive study indicated the high thermal stability of untreated clinoptilolite which causes an increase in the sorbent CO_2 loading uptake. In perspective, the improved adsorption capacity of clinoptilolite, versus the state-of-the-art zeolite 13X, at high temperature makes it a potential sorbent for CO_2 removal from flue gases, with temperature ranges between 80°C and 100 °C.

In **Chapter 3** the zero-length column (ZLC) method for measuring the diffusion and transport mechanism of CO_2 into the sorbent is described in detail. Later the method is used to evaluate the mass transfer behavior for Clino, K-Clino, Na-Clino and Cs-Clino. The results obtained confirmed that the nature of CO_2 adsorption on Clino and its cation exchanged forms is equilibrium controlled. Alternatively, the sorbent adsorption capacity is evaluated by measuring the CO_2 equilibrium isotherms and adsorption breakthrough curves. The adsorption robusticity of the sorbent is examined by repeating the adsorption (20°C, 35 °C, 50 °C and 65 °C) and desorption (100 °C and 300 °C) at different temperatures and through different cycles.

Chapter 4 discusses a mathematical model developed for a one-column fixed-bed reactor to investigate the dynamic behavior of CO_2 adsorption process. The model is validated with the experimental data obtained from the same system using commercial zeolite 13X. The process is considered to work in a three stages of adsorption, desorption, and cooling. Temperature Swing Adsorption (TSA) configuration is devoted to the regeneration phase by heating the system up to 85 °C. The operability of each phase is exploited through a one-dimensional model using mass, energy and momentum balances. The input parameters for equilibrium data are obtained by conducting equilibrium experiments for pure component and by fitting the data with single and dual-site Langmuir isotherm. The parameters obtained from the adsorption equilibrium model is used to investigate the kinetic parameters necessary for building the numerical model.

Chapter 5 is dedicated to the absorption study carried out by using amino acid-based ionic liquids [AA][IL] with a lower environmental impact and energy demand comparing to conventional solvents (e.g. amines). Four choline-based amino acids ([Cho][AA]): Alanine, Glycine, Proline, and Serine, that are task-specific for this purpose are tested. The drawbacks related to the high viscosity of these ILs were limited by applying DMSO as a solvent, which is chosen because it

is a polar aprotic liquid with low toxicity, low vapor pressure, and relatively low price. The absorption measurements are performed at constant operational conditions of 20 °C (using circulating thermal bath) and 1 bar. The optimal concentration of IL in DMSO (12.5 and 25 wt%) is examined through preliminary tests performed with various concentration of DMSO. The solution of these ionic liquids in DMSO showed promising properties for CO_2 removal from a simulated flue gas mixture with 17 vol% CO_2 in Ar. Indeed, the higher absorption efficiency is the outcome of diluting the IL in the DMSO, which contributes to minimize the CO_2 mass transfer limitation toward the ILs absorption. These solutions are potentially competitive due to their low cost, low environmental impact, easy processability (due to their low viscosity) and good regenerability for the production and storage of highly pure CO_2.

Finally, in **Chapter 6** the principle findings of this dissertation to create a cost-effective process through application of Clinoptilolite zeolite and Bio-based ionic liquids are discussed.

Acknowledgment

I would like to express my deepest regards to Prof. Guido Saracco for giving me the opportunity to start the research in this topic at Politecnico di Torino.

Then, I would like to thank my supervisor Dr. Simelys Hernandez for her patience and advices throughout my Ph.D. period. Her passion and persistence for her work had been an encouragement for me.

It was an honor to collaborate with Carbon Capture Group at the University of Edinburgh. Special appreciations to Prof. Stefano Brandani and Dr. Enzo Mangano for their support and guidance. Also, I would like to thank to Dr. Rhys Lioyd, Dr. Maarten Verbraeken and Roberto Mennitto for being very kind and helpful in the laboratory. Finally, thanks to Dr. Ishan Sharma, Dr. Mauro Luberti and Jinyu Wang for their advices and help during my stay in Edinburgh.

As for the collaboration with RSE Milano, I have had a great help and technical insights from Eng. Antonio De Marco and Eng. Luigi Bisone. Also, I am thankful for obtaining experimental data from Silvia Canevese, Maurizio Notaro and Walter Prandani.

I present my gratitude to ASJA Ambiente S.p.A for providing me scholarship grant to pursue this PhD programme. Here I am thanking to Eng. Stefano Re Fiorentin and Eng. Guido Maia.

As part of my collaboration with other research groups at Politecnico di Torino and IIT I thank to Dr. Marco Armandi, Dr. Sergio Bocchini, Dr. Marco Piumetti and Giulio Latini with whom I was able to make some publications.

The support of my parents was very valuable and encouraging. Nothing would have been possible without their help.

My thoughts go to my siblings Elham, Amin and my brother-in-law Masoud. My love goes to my niece, Toranj for her valuable smile and energy.

Thanks to Tavi, my love, for supporting me in my difficult periods of the Ph.D and being a great motivation.

Finally, thanks also to my colleagues and friends, especially to Mohsen Shiea for giving me technical support and hints.

I would like to dedicate this thesis to my loving parents and my beloved ones Toranj, Tavi, Elham, Amin and Masoud.

CONTENTS

List of Tables

List of Figures

Chapter 1

Introduction

Abstract

The growing greenhouse gas emission during the last decades has motivated researchers seeking solutions to mitigate this issue. CO_2 is the major greenhouse gas released into the environment from different fossil fuel industrial sources responsible for producing electricity/heat and providing energy for the transportation system. Despite the extensive investigations on renewable energies, fossil fuels are still the main source of energy. This pushes scientists toward developing processes for capturing CO_2 from fossil fuel combustion and though limiting its emission into the atmosphere. Regarding this issue, different techniques were developed for CO_2 capturing purposes. However, challenges such as high cost of operation, low profit, low integrability with a specific process and low concentration of CO_2 in the flue gas, are the main barriers for generating a profitable and practical CO_2 capture method.

1.1 CO_2 capture technologies

The technologies developed for CO_2 capture from industrial flue gases up to date are pre-combustion, oxyfuel combustion, and post-combustion. The choice of the CO_2 capture process strongly depends on the flue gas discharge source as well as its operating cost and energy consumption [1,2]. All the existing CO_2 capture approaches are designated in Figure 1-1 together with a brief description of each technology [3]:

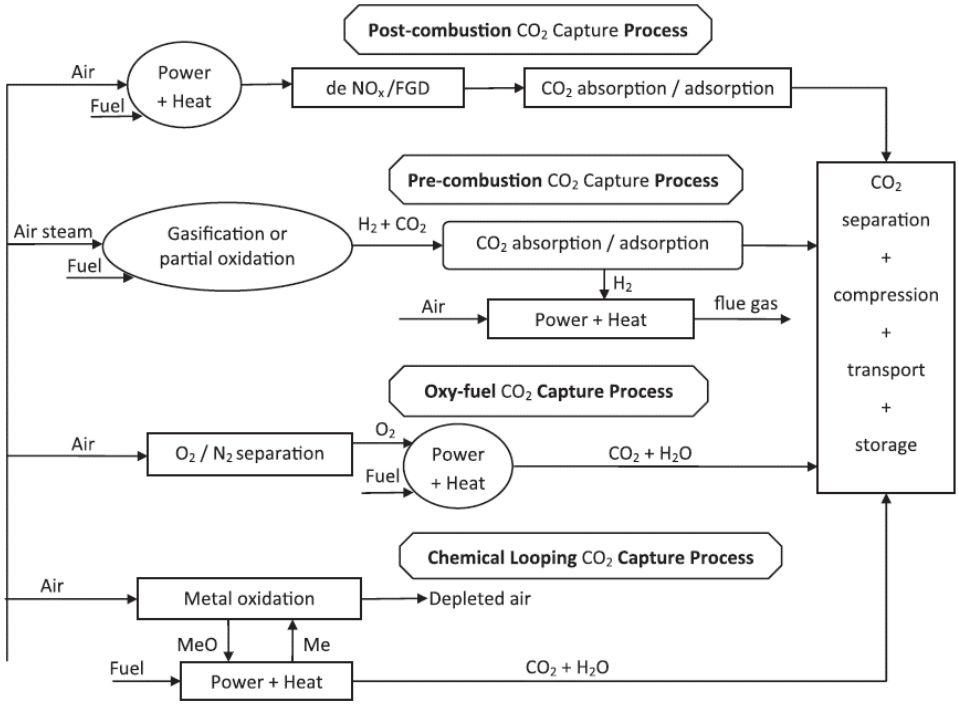

Figure 1-1. CO_2 capture technologies: Post-combustion, Pre-combustion and Oxyfuel combustion [1].

Post-combustion capture is considered among the most retrofitting CO_2 capture technologies as it can be upgraded to the existing power plant constructions. Here, several different processes can be used to separate CO_2 from the industrial exhaust gas streams, which in some cases could demand a high energy penalty. To decrease the energy consumption and lowering the process costs, it is essential to pick the most appropriate separation method with low regeneration energy, low cost, and high capture efficacy.

Pre-combustion capture is typically used for integrated gasification combined cycles (IGCC) in which initially the fuel is gasified to produce CO_2 and H_2. Though CO_2 is captured from the fuel before combustion and though will not generate any CO_2 after burning [4]. Several separation techniques can be applied to remove CO_2 from the product stream while H_2 will be used as a source of energy. The main drawbacks related to this process is the necessity of having an input stream with a high concentration of CO_2 as well as its high operating costs.

Oxyfuel combustion is established on burning the fuel with a rich oxygen stream instead of combustion in air. This results in the production of steam and CO_2 with higher concentration and makes the CO_2 capture easier. Nevertheless, the high cost of pure oxygen production from the air makes this process not economically convenient.

The advantages and disadvantages [5] of all these processes are briefly reported in Table 1-1.

Table 1-1. Advantages and disadvantages of CO_2 capture technologies.

Technology	Advantages	Disadvantages
Post-combustion	• Retrofit technology applicable to the existing coal-fired plants	• Low concentration of CO_2 in the flue gas • The low partial pressure of CO_2, leading to the need for larger recycling volumes
Pre-combustion	• The high CO_2 concentration in the synthesis gas • High CO_2 pressure leading to the low cost of compression	• Applicable to new power plants with an integrated gasification plant
Oxy-combustion	• Retrofit technology • The high concentration of CO_2 in the flue gas	• Expensive for the necessity of having a pure O_2 stream; • Adding energy costs for cooling the CO_2 recycled stream

Along with the proper choice of CO_2 separation technology, the type of sorbent material used is playing a significant role. Efforts have been put to introduce cost-effective, highly CO_2 capture efficient and kinetically fast adsorbents/absorbents to develop practical means for CO_2 capture separation. In this regard, to reduce the cost of operation specific-task sorbents need to be tailored to work properly for a definite separation process, with designed operating temperature and pressure. Indeed, each separation technique requires to be initially evaluated for the targeted application. Commercial processes for CO_2 separation are absorption, adsorption, membrane application, and cryogenic techniques. In this thesis, our focus is on the absorption and adsorption technologies for CO_2 separation within a post-combustion carbon capture process.

1.2 Post-combustion carbon capture

1.2.1 Absorption separation

The absorption process is the first method applied for CO_2 removal from industrial flue gases. In this technique, CO_2 is separated from the exhaust gas by using solvents, capable of absorbing CO_2 physically (occurs under low temperature or high pressure) or chemically (based on the acid-base reaction). The conventional solvents used industrially are monoethanolamine (MEA) and diethanolamine

(DEA) and methyl diethanolamine (MDEA) [4]. Amine scrubbing is a chemical absorption with a high CO_2 uptake capacity of almost 85 %. In this process initially, the NO_x and SO_2 are removed from the flue gas. Whereas the CO_2-riched stream is treated in a separate adsorption and desorption plant composed of two separation columns. The absorption column is assigned for stripping the CO_2 from the flue gas and desorption vessel is considered for the regeneration of the solvent at high temperature or under vacuum. CO_2 separation with amine solutions is a highly efficient and fast process; however, it is corrosive, degradable, environmentally toxic and expensive due to the high energy requirement for regeneration. Such disadvantages make amine scrubbing less favorable, thus creating interest in developing cost-efficient and environmental-friendly absorption techniques with low energy demand.

An alternative replacement for amine solvent are Ionic Liquids (ILs), referred to as green solvents. ILs are molten salts at room temperature, used as potential solvents for CO_2 separation due to their very low vapor pressure, low volatility (less environmental impact), low viscosity, thermal stability, high CO_2 solubility, and selectivity. In this process, the flue gas stripping is carried out at a low temperature and the solvent regeneration is performed at an elevated temperature below the ILs boiling point [6]. In **Chapter 5** of this thesis, the application of bio-based ILs for CO_2 separation from industrial exhaust gases is discussed more in detail.

1.2.2 Adsorption separation

The adsorption process is a CO_2 treatment technique in which porous solid sorbents are used to remove the CO_2 from the flue gas streams. Solid sorbents are promising materials as compared to liquid solvents due to their lower energy penalty in the regeneration phase and their higher thermal stability. The CO_2 interaction with the solid sorbent is mostly a physical interaction with a weak Van der Waals force. The solid materials used for CO_2 separation purposes have normally a high surface area and a large pore sizes distribution. The most used ones are activated carbon, silica-based sorbents, zeolites and MOFs. The choice of employing a proper sorbent for CO_2 capture application depends on its structural properties including its surface area and pore size as well as the process operating condition like temperature and pressure (as important factors for a cost-effective process). The adsorption process is performed in parallel adsorption units composed of fixed bed reactors packed with the sorbent that operates in cycles. The adsorption can be carried out under high pressure or low temperature regarding the application and the specification of the sorbent. Alternately, the regeneration process is carried out in a pressure swing adsorption (PSA) or temperature swing adsorption (TSA) process. The CO_2 uptake capacity and material selectivity together with the energy consumption and process cost efficiency are all indicators for choosing the appropriate sorbents for CO_2 treatments. A more detailed description of solid sorbents for CO_2 separation applications along with a thorough explanation of adsorption operation is given in section 1.3 and <Chapter 2.

1.2.3 Carbon capture and utilization

An essential factor to be considered is the feasibility of converting waste CO_2 into useful commodities by integrating the CO_2 capture process into a sustainable economy. The enormous amount of CO_2 discharged into the environment annually and the potential of CO_2 circular economy has triggered the interest towards CO_2 utilization. The captured CO_2 can be applied in an integrated process of carbon capture and utilization (CCU) to produce valorized products such as chemicals and fuels including methanol, formic acid and the conversion of CO_2 into polymers [7]. Alternatively, CO_2 can be used directly in an enhanced gas or oil recovery (EOG, EOR) applications in larger scales. Considering the techno-economic CCU process, different pathways for both CO_2 capture and utilization are investigated based on the potential sources and prospective industries.

1.3 Materials for CO_2 Capture: A Review of Solid and Liquid-based Sorbents

Several classes of solid and liquid sorbent materials including carbonaceous materials, zeolites, amine-based supported sorbents, amine-based solvents and conventional ionic liquids are used in CO_2 capture processes. Indeed, the choice of sorbent contributes to creating a cost-effective process with lower environmental impact. For an efficient process with high adsorption capacity, selectivity and fast kinetics, an accurate selection of materials that can adapt to the process operation conditions is the key point. In the past decades, efforts have been put forth in developing new materials or modifying the currently used sorbents for CO_2 separation from flue gases, bearing in mind the energy penalty reduction and the CO_2 treatment performance improvement.

Conventional solvents such as monoethanolamine (MEA) and diethanolamine (DEA) are mainly used in CO_2 capture technologies due to their high capacity and selectivity. In this process, CO_2 interacts chemically with amine molecules, which encounters a large heat of absorption and resulted in strongly absorbed CO_2 molecules, requiring a high energy input in the regeneration step. The high amount of energy penalty makes this process economically inconvenient on a large scale. The other disadvantages of amine solutions are their high volatility leading to solvent loss and degradability, causing environmental toxicity [8]. The high operational cost and energy requirements are the main motives for not having yet any functional large-scale CO_2 capture plant. Regarding this issue, several research works have been concentrated on finding novel materials and solvents with high energy competence and cost-efficiency. This includes applying innovative solid adsorbent, liquid-based sorbents and membrane in different physical or chemical processes [9].

Among the liquid-based sorbents can be mentioned the conventional amine solvents, organic solvents and ionic liquids (ILs). Diverse methods are applied to increase the CO_2 uptake of solid materials such as the impregnation of functional

groups by modifying the support materials or by grafting technique [10]. Similarly, the absorption efficiency of liquid-based solvents such as ionic liquids can be improved by modifying the functional groups present in their structure. The performance of different sorbent materials is evaluated considering their CO_2 capture capacity, selectivity, stability, durability during application in consecutive cycles, regenerability and kinetics. Apart from these properties their environmental impact and their adaptability to large scale industries are important parameters. In this chapter, a comprehensive literature review of both solid sorbents and liquid sorbent with emphasis on zeolite and functionalized amino acid ionic liquids are discussed. In Table 1-2 all the important parameters affecting the techno-economic aspects of the sorbent materials adsorption/absorption behavior are defined.

Table 1-2. Advantages and disadvantages of CO_2 absorption and desorption separation technologies [2].

Technology	Sorbents	Pros	Cons
Adsorption	• Zeolite • Activated Carbons • Mesopore Silica • MOFs	• High adsorption capacity • Low regeneration energy	• Thermal, chemical and mechanical instability • low adsorption kinetics
Absorption	• Amine-based absorbent (MEA and DEA)	• Retrofitted technology • Suitable for use in low CO_2 concentration • High recovery and purity	• The high energy input for solvent regeneration • Degradation and toxicity
	• Ionic Liquid	• Thermal stability • Low toxicity • Low volatility • High absorption capacity	• High viscosity

1.4 Solid Sorbents: Zeolites

For solid sorbents to be practically effective parameters including structural properties of the sorbent and the operational process conditions need to be coordinated. The sorbent properties affecting the CO_2 adsorption performance are pore dimensions, polarity, basicity, cation distribution, the kinetic diameter of pores and structural stability. However, the process requirements for an optimized CO_2

separation are the adsorption capacity, selectivity, kinetics, economical cost and heat of adsorption [11].

Zeolites are microporous crystalline solids existing as natural and synthetic structures. Their framework is formed by silicon, aluminum and oxygen in a three-dimensional well-defined structure of [SiO_4] and [$(AlO_4)^-$]. The cage-like porous structure of zeolites makes available the presence of alkali, alkaline and metallic cations that compensate the negative charge introduced by [$(AlO_4)^-$]. The extra-framework cations help to increase the adsorption capacity of the sorbent. The structural properties and composition of zeolites such as their pore size, their channel distribution and the Si/Al ratio are important constraints affecting their adsorption behavior. Besides, the presence of cationic sites with different strengths and exchangeable cations with diverse polarizing power are alternative factors affecting CO_2 adsorption [12]. Cationic zeolites with high cation content on their framework are effective CO_2 adsorbents that can adsorb CO_2 at ambient temperature and low CO_2 partial pressures of 0.1 bar.

Other influencing features are the adsorbent type, dimension and physico-chemical characteristics. The adsorbed molecule dimension needs to be less than the zeolite pore size in order to penetrate into the zeolite cavities. For CO_2 capture purposes, the zeolite to be chosen has to have a pore diameter bigger than the CO_2 molecule size (3.3 Å). Instead, the sorbent polarity influences the material selectivity, which is in fact associated with CO_2 adsorption mechanism and formation of stronger bonds [13]. Molecules with sturdier quadrupole moments interact strongly with the cationic sites present on the zeolite structure. The quadripole moment can be described as two electrical dipoles that interact with the cations and opens the cavity gates for the CO_2 molecule to enter [14]. The quadrupole moment of gases differs as following $CO_2 > CO > N_2 > H_2 > CH_4 \approx Ar$ [12]. The affinity and selectivity of these gases are defined with their binding strength or the quadrupole moment, which in the case of CO_2 (4.30×10^{-26} cm^2) is 3 times bigger than N_2 (1.52×10^{-26} cm^2) [15]. Moreover, the linear assembly of the CO_2 molecule contributes to the higher adsorption selectivity of CO_2 as compared to CH_4 and N_2 [16].

The CO_2 undergoes physical (Physisorption) or chemical (Chemisorption) adsorption at the zeolite surface. The physisorbed CO_2 requires less energy to be recovered from the sorbent as compared to the chemisorbed one. The CO_2 capacity of the sorbent is influenced by the operating condition like temperature and pressure. A low temperature and high pressure favor the adsorption process due to the exothermic nature of CO_2 adsorption. The high affinity of water of zeolites is an important limiting factor that can decrease the CO_2 adsorption capacity of a zeolite by 20%. The H_2O molecule due to its high polarity can strongly interact with cations on the zeolite's surface and form some carbonate species.

The synthesized zeolites such as type X and A have been broadly studied for CO_2 capturing processes. Among these types of zeolites, various literature reviews have mentioned zeolite 13X belonging to Faujasite structure (FAU) as the most promising adsorbent for CO_2 separation from flue gases [17–23]. The high CO_2 adsorption performance of zeolite 13 X is associated with its porous structure and

the large size of pores. The channels in 13X composed of 12-membered rings connected to four other cages with a dimension of 7.4 Å [24]. The high affinity of CO_2 compared to CH_4 and N_2 [25] makes it a potential sorbent for CO_2 capture from flue gas. The CO_2 uptake of zeolite 13X is reported to be about 2 - 3 mol/kg at 0.1 atm and 20 °C [26,27]. The main cation on the structure of zeolite 13X that plays an important role on its adsorption performance is Na^+ [28,29]. Despite the promising CO_2 adsorption performance of zeolite 13X, its main drawbacks are its high heat of adsorption (50 – 60 kJ/mol) and strong hydrophilicity. This leads to the occupation of strong sites with water and to a decrease in the adsorption efficiency of the sorbent.

Other types of zeolite, including natural zeolites such as chabazite and clinoptilolite, are considered like cost-effective sorbents with a high CO_2 selectivity. The cation exchanged capability of clinoptilolite makes it a potential sorbent for different separation applications including CH_4 purification and CO_2 separation from flue gases [30]. The capturing capacity of clinoptilolite at ambient temperature and atmospheric pressure is about 2 mol/kg, while the adsorption capacity of zeolite 13X is almost 12 mol/kg. This is due to the high Si to Al ratio in clinoptilolite [31].

1.4.1 Natural Zeolites: Clinoptilolite

Clinoptilolite is a member of the natural zeolite family (heulandite (HEU)) formed with a two-dimensional channel structure composed of 10 membered-rings (channel A) and 8 membered-ring (channels B and C) as shown in Error! Reference source not found. The dimension of its channels are: channel A = 7.2Å× 4.4 Å, channel B = 4.7Å× 4.1 Å, and channel C = 5.5Å× 4.0 Å [32]. The ratio of Si/Al for clinoptilolite varies in the range of 4 to 5 imposing a negative charge on the clinoptilolite framework. The cations presence on the structure of clinoptilolites such as Na^+, K^+, Ca^{2+} and Mg^{2+} are compensating the negative charges. The presence of multi-layered cations and their exchange capability is making them a multifunctional adsorbent with high tuneability. Cations location in the framework is depending on the size and charges of the cation. Different sites existing on the clinoptilolite structure are including M(1), M(2), M(3) and M(4). Where M(1) located in channel A is occupied by Na^+, M(2) in channel B and is occupied mainly with Na^+ and Ca^{2+}, M(3) is engaged with K^+ and Ba^{2+} and M(4) site is occupied with Mg^{2+} [33] as also presented in **Figure 1-3**.

The key factors affecting the CO_2 adsorption capacity and selectivity of clinoptilolite are the type of cations with their relevant charge and location. The potential of clinoptilolite in exchanging cations makes it a noteworthy adsorbent that can be tailored for various gas separations such as CO_2/CH_4, H_2/CO_2 and CO_2/N_2. To enhance the adsorption properties of natural clinoptilolite several structural modifications can be performed including adjusting the distribution of extra-framework cations with optimized size and charge, Si/Al ratio and pore sizes [31].

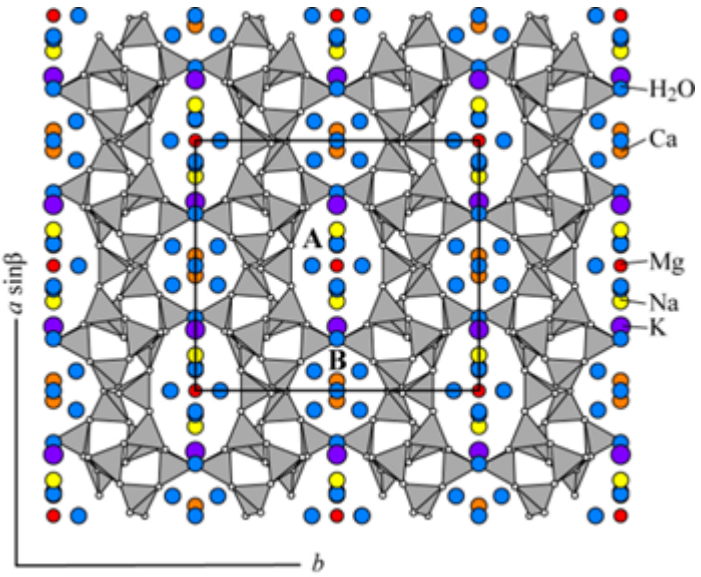

Figure 1-2. Clinoptilolite Structure from IZA Commission of Natural Zeolites [19].

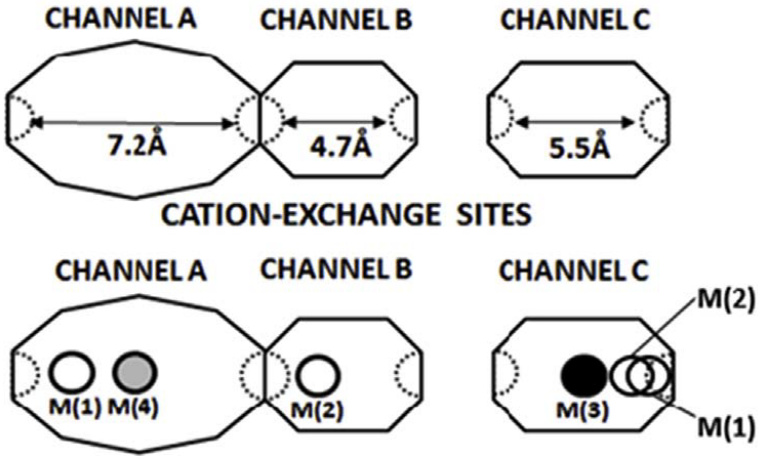

Figure 1-3. Location of different channels and sites on the clinoptilolite structure [32].

1.4.2 Ion-exchange clinoptilolite

Cation-exchange modification is a potential method for improving the adsorption performance of natural clinoptilolite. The induced extra-framework cations with different sizes and charge densities can be used to tailor the adsorption efficacy of the sorbent for capturing the CO_2 from the flue gas streams. The exposed cations induce changes in the electrical field and polarity of the sorbent structure. Along with the electrical charge, the position of the cation on the zeolite is considered as a limiting factor for the CO_2 mass transfer and kinetics.

Cation exchanged modification has been carried out through different experimental methods using solutions of chloride, nitrate and hydroxide. The results obtained show a growth in the CO_2 adsorption capacity by increasing the

cations charge density [35,36]. Though for alkali metal cations the trend of adsorption capacity observed is changing in the following order $Li^+ \approx Na^+ > K^+ > Rb^+ > Cs^+$ [32]. This shows that along with the electrical charge, the size of cations is contributing to the sorbent adsorption performance too. Indeed, smaller cations such as Li^+ and Na^+ are occupying less space though make the basic sites and the pore channel available to the adsorbed gas. The alkaline earth metal cations exchanged in clinoptilolite improved the adsorption capacity in this order: $Ba^{2+} > Sr^{2+} >> Be^{2+} \approx Mg^{2+} > Ca^{2+}$. Kennedy D. A. and Tezel, F. H. [32] have reported that the higher adsorption performance of Ba^{2+} and Sr^{2+} comparing to the smaller cations is attributed to the occupation of different sites by each cation. Ba^{2+} and Sr^{2+} are occupying locations in the vicinity of M(1) and M(2) sites [37]. This results in the easier interaction of CO_2 with the channel opening while the smaller cations are limiting the CO_2 access to the pores as they are positioned in the middle of the pores. G. Aguilar-Armenta [37] presented the CO_2 uptake at the equilibrium for clinoptilolite changes in different alkali cations as follows $Ca^{2+} \approx Na^+ > K^+$. However, their work showed a faster kinetics behavior in the K^+ and Ca^{2+} exchanged samples.

Previous studies done on the adsorption performance of clinoptilolite mainly discussed the adsorbent CO_2 uptake, while the kinetic or equilibrium behavior of the sorbent have been rarly studied. In this thesis, the dynamic and kinetics adsorption behavior of clinoptilolite is studied by analyzing the adsorption breakthrough curves, CO_2 adsorption isotherms, in-situ FTIR analysis and kinetics measurements using the zero-length-column (ZLC) technique.

1.5 Liquid-based Solvents

Ionic liquids are organic salts designed with cation and anion blocks in the form of stable liquids at room temperature (room temperature ionic liquid, RTILs). They are called green solvents due to their low vapor pressure and low biodegradability, which help to minimize the atmospheric contamination and reduce health concerns. The applications of ionic liquids have been studied for different chemical processes and industries [38]. Their low volatility, extensive variety, thermal stability, tunability and high CO_2 solubility make them more environmentally friendly solvents for CO_2 capture than organic solvents such as ammonia, alkaline amine and piperazine [39,40]. One of the main drawbacks of ionic liquids is their high viscosity. However, due to a variety of cations and anions combination, it is feasible to synthesize ionic liquid with an acceptable range of viscosity. Alternatively, diluting ionic liquids with water or other green solvents is a practical way of reducing their viscosity. Ionic liquid used for CO_2 capture are classified into groups of room-temperature ionic liquids (RTILs), task-specific ionic liquids (TSILs) and supported ionic liquid membrane (SILMs).

1.5.1 Ionic Liquids for CO_2 capture

A large number of ILs have been investigated for CO_2 capture technologies among which the most used anions and cations, as reported by R. Mahinder and T.W. de Loos [41], are shown in **Figure 1-4**.

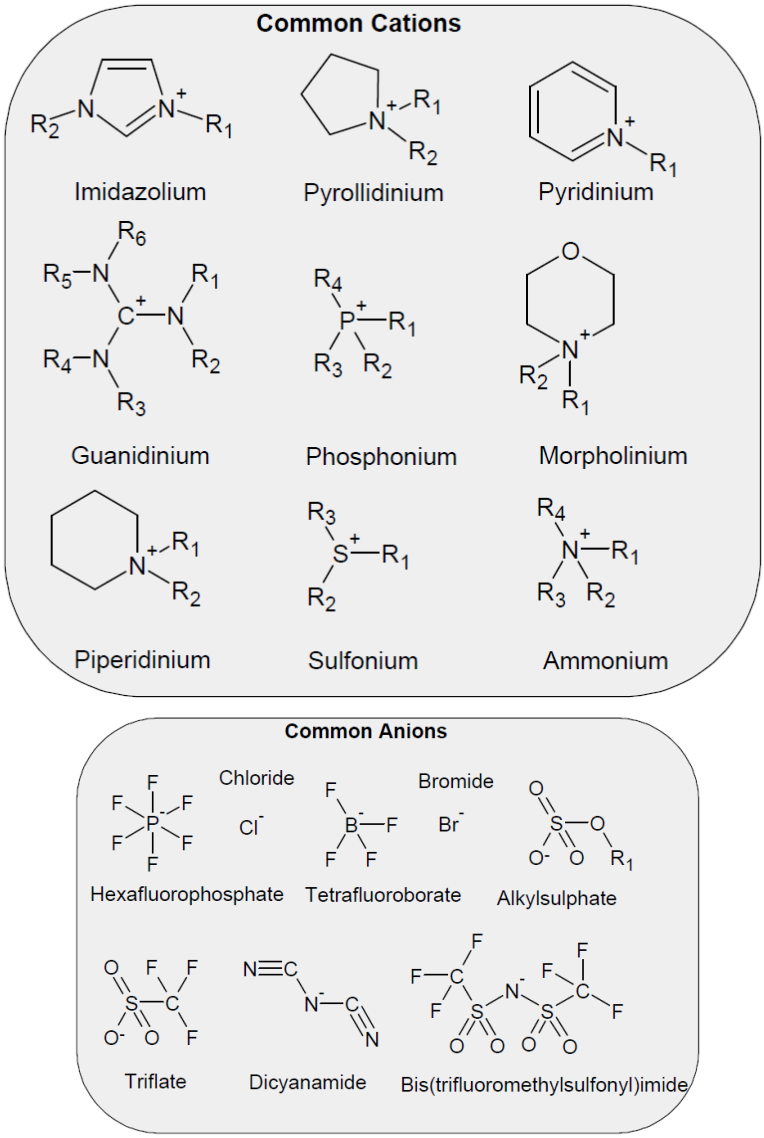

Figure 1-4. Common cations and anions of ionic liquids [41].

Both cation and anion are playing a significant role in designing ionic liquids with high CO_2 solubility [42]. However, studies have indicated a minor influence of cations on CO_2 dissolution as compared with anions [43]. The effect of cations is associated with the length of the alkyl chain; longer chains improve the CO_2 solubility. Among the studied anions and cations, the ILs composed of fluoroalkyl anions [44] and imidazolium cations [45] groups exhibited a better CO_2 absorption performance. The possibility of tuning the structure of the ionic liquid provides the viability of designing functionalized ionic liquids with desirable properties and

adsorption capacities. The principal interaction of CO_2 molecule with ILs can be either physical or chemical. In conventional ILs, the CO_2 interaction with the solvent is a physical one, since there are no functionalized groups present in the solvent. Whereas, the functionalized ILs forms strong chemical bonds with CO_2.

The key factors to be considered before selecting a proper IL for CO_2 absorption are: high CO_2 absorption capacity, low CO_2 dissolution enthalpy and high CO_2 selectivity [45]. The absorption enthalpy is associated with the CO_2 regeneration energy (system energy requirement). Instead, the selectivity is connected with the predominant components present in the flue gas, which can be a mixture of $CO_2/O_2/N_2$, CO_2/H_2 and CO_2/CH_4 as well as they can contain impurities such as H_2S, SO_x and H_2S [46]. Different studies have shown that generally, the N_2 and O_2 solubilities in ILs are inferior to CO_2, while hydrocarbons solubilities are moderately comparable to CO_2 [47–49]. In the following subsections, different types of ionic liquids with their particular absorption mechanisms are described. Much effort is put on describing the structure of a class of functionalized ionic liquids with amino acid groups.

The CO_2 solubility in conventional solvents is investigated by comparing Henry's constants for each ILs showing a high selectivity of CO_2 over N_2, H_2, O_2 and CH_4. These studies proved that the higher CO_2 solubilities are associated with the excess enthalpy of dissolution of CO_2 in ILs. Further, the interaction between the CO_2 and ILs indicated that the Van der Waals forces dominate the CO_2 solubility behavior comparing to electrostatic interaction and hydrogen bonds [50]. Physical CO_2 absorption capacities in mol CO_2/kg IL for a large group of conventional solvents are reported by M. Radmin [46]. The solubilities are shown for pressure up to 5 MPa although the highest amount of CO_2 absorbed for these solvents at atmospheric pressure is about 0.6 mol CO_2/kg IL.

1.5.2 Amino acid-based Ionic Liquids

Amino acid ionic liquid (AAILs) are ILs with amine-functionalized groups of amino acids such as lysine (Lys), alanine (Ala), Serine (Ser), Glycine (Gly) and Proline (Pro). The tunability of ILs makes it possible to build different ILs by using amino acids both as anions and cations. However, as discussed before anions are playing a more significant role in the CO_2 absorption efficiency as compared to the cations. Though, several works have synthesized AAILs with amino acids tethered to the anion group of IL. The reported stoichiometry for the reaction of CO_2 and ILs with amine group tethered in the cation and anion are respectively 1:2 (CO_2/ILs) and 1:1 (CO_2/ILs) [51]. The possession of equimolar stoichiometry for AAIL-CO_2 comparing to pure amino acids, ethanolamine and conventional ILs make AAILs a potential absorbent for industrial use. The main reactions between CO_2 and AAIL are shown in **Equation (1-1)** and **Equation (1-2).**

$$CO_2 + R^-NH_2 \leftrightarrow R^-N^+H_2CO_2^- \quad (1\text{-}1)$$

$$R^-N^+H_2CO_2^- + R^-NH_2 \leftrightarrow R^-NHCO_2^- + R^-N^+H_3 \quad 1\text{-}2)$$

Thus, the interaction of CO_2 with amine-functionalized solvents represent a mixture of carbamates ($RNH\text{-}CO_2^-$), ammonium ions (RNH^{+3}) and carbamic acids ($RNH\text{-}CO_2H$) at equilibrium. Lowering the temperature or increasing the partial pressure shifts the equilibrium to higher CO_2 uptake. Similarly, there are other factors contributing to CO_2 absorption enhance including increasing the size of the cation [46], CO_2 interaction at the surface of IL [52] and using solvents for lowering the ILs viscosity. A large number of studies are performed to measure the CO_2 absorption properties of AAILs such as absorption capacity and kinetics [51,53,54]. The main drawback of utilizing the AAILs for CO_2 absorption is their high viscosity. This has led to the investigation of methods to reduce the ILs viscosity and several works reported mixtures of ILs with water [55], low viscosity ILs and supported IL materials [52]. In this thesis, the CO_2 absorption performances of several synthesized AAILs is studied in terms of absorption capacity and absorption rate. Moreover, the ILs regarded high viscosity problem has been investigated and reduced by using a dimethylsulfoxide (DMSO) as an organic solvent, which helps to remove the barrier for CO_2 mass transfer into IL.

1.6 Goals and Objectives

This thesis aims to expand the knowledge in the application of promising solid materials (natural zeolites) and the liquid-based sorbents (ionic liquids) for CO_2 capture purposes. The potential behavior of such materials for CO_2 separation is evaluated considering several parameters including their CO_2 capture capacity, stability, kinetics, selectivity and cyclic performance along with their cost-effectiveness and environmental impact.

In this regard, the adsorption dynamics and kinetic performance of an economically low-cost zeolite in different cation-exchanged forms are studied. The first part of the work has been carried out at laboratories of Politecnico di Torino through a complete cycle of synthesizing and characterizing the samples. Later, the samples were tested, and their adsorption breakthrough curves and dynamic behavior were analyzed. The activity on zeolite adsorption behavior was continued later, in a 6 months research visiting period at the University of Edinburgh, by using the Zero Length Column (ZLC) technique that is a fast method used to characterize the equilibrium and kinetic properties of different solid sorbents. The experimental conditions are chosen considering flue gases condition within the range of low to high temperatures of 20 °C – 75 °C and CO_2 partial pressure of 0.1 bar. Furthermore, the cyclic behavior of all samples is predicted by using a mathematical adsorption model, developed in collaboration with ASJA Ambiente Italia SpA and Research on Energy System (RSE) SpA. The model is validated using experimental data.

The 2nd part of this thesis is focused on the absorption properties of novel bio-based ionic liquids performed in collaboration with the Center for Sustainable Future technologies (IIT@Polito) of the Italian Institute of Technology. The

absorption efficiencies of different amino acid ionic liquids are discussed considering any transport limitation to CO_2 into ionic liquids. As a state of the art, the diluted mixture of these ionic liquids in the organic solvent has been suggested to remove the barrier to CO_2 mass transfer in comparison to the pure ionic liquid or ILs in solution with water. The present dissertation is organized as follows:

Chapter 1 discusses a review of novel porous materials and ionic liquids applied for carbon capture. The main factors influencing the sorption performance of these materials are discussed in detail as well as their limitations for CO_2 capture. The state-of-the-art materials developed are summarised and the opportunity of tailoring materials with higher efficiency, lower environmental impact and higher industrial practicability are reported.

Chapter 2 introduces the application of a cost-effective natural zeolite (clinoptilolite) for CO_2 capture from industrial flue gases. Here, the possibility of enhancing the CO_2 uptake capacity for clinoptilolite by implementing cation exchange modification is discussed. Later, the dynamic behavior of untreated and cation exchanged clinoptilolite is investigated by performing adsorption tests at operating condition (middle temperatures) found in post-combustion carbon capture process.

Chapter 3 provides details on the ZLC method used to explore the CO_2 adsorption kinetic of natural zeolite. Here, the results obtained from the kinetic measurements are discussed while the CO_2 capacities for all samples are calculated from their breakthrough curves. The CO_2 isotherm for all samples is obtained through volumetric measurements.

Chapter 4 discusses the experimental data demonstrated in chapter 3. The mathematical model developed for interpreting the dynamic behavior of the system is provided. The model is used to simulate the behavior of the zeolite on a larger scale while the experimental data are used for parameters validation.

Chapter 5 introduces a family of bio-based ionic liquids applied for the CO_2 separation processes from simulated industrial flue gases. Their synthesis method and their structural properties are described and compared with the state-of-the-art solvents. The absorption performance of these novel ionic liquids along with their limiting parameters are discussed in this chapter. To overcome the diffusion barrier to CO_2 interacting with ILs and to decrease the ILs viscosity a dilution method is suggested, in which ILs are mixed with the DMSO organic solvent. The increased absorption capacity and the lower environmental impact of this process is explained thoroughly.

Chapter 6 summarized all the sorption results obtained from both natural clinoptilolite and bio-based ionic liquids, including their limiting factors, CO_2 uptake capacities, kinetics and their environmental impacts. The possibility of reducing the operating costs is discussed through the opportunity of using natural zeolite at a higher temperature up to 80 °C without affecting the adsorption capacity. Moreover, the superiority of ionic liquids used in this thesis over conventional solvents and ILs are discussed. The impact of reducing the IL viscosity by using DMSO on its CO_2 absorption performance is overviewed.

To sum up, for a CO_2 separation process to be retrofitted, environmentally friendly, cost-effective and with a high CO_2 uptake capacity, the correct technology and sorbent material have to be selected, to create a further market and application for any sorbent. The author believes that the proposed materials in this thesis, including natural clinoptilolite and bio-based amino acid ionic liquids for CO_2 capture, can contribute to the achievement of this goal.

Chapter 2

2 CO_2 Adsorption on Natural Clinoptilolite and 13X Zeolites: Effect of Temperature and Role of the Adsorption Sites

This chapter of the thesis has been submitted for publication to the Journal of Environmental Management with the following description:

*E. Davarpanah, M. Armandi, S. Hernández, M. Piumetti *, R. Arletti, S. Bensaid, D. Fino, CO_2 capture on clinoptilolite and 13X zeolites: Effect of temperature and role of the adsorption sites.*

Abstract

In this study, the adsorption capacity of the natural zeolite clinoptilolite for capturing waste carbon dioxide (CO_2) emitted from different sources is investigated. The aim of this work is to introduce a low-cost zeolite with high CO_2 loading capacity to be applied directly to CO_2 streams from industrial processes with moderate outlet temperatures (e.g. within the 333 - 353 K temperature range). The dynamic CO_2 adsorption capacity of bare and ion-exchanged (with Na^+ and Ca^{2+}) clinoptilolite are evaluated in a fixed-bed reactor operating in the 293 – 338 K range and the obtained breakthrough curves are compared to those of commercial 13X zeolite. On the other hand, CO_2 adsorption isotherms under equilibrium conditions are used to measure the isosteric heat of CO_2 adsorption (q_{iso}) of the sorbents, and to investigate the effect of pre-treatment temperature. The high q_{iso} measured on 13X (i.e. 50 – 42 kJ/mol) over a wide coverage range is mainly responsible for the drastic decrease in CO_2 adsorption capacity with the temperature increase. Indeed, whereas the adsorption capacity as measured from the

breakthrough curves at 293 K on 13X largely exceeds that of ion-exchanged and bare clinoptilolite, this latter sorbent shows the highest CO_2 uptake at 338 K.

Besides structural and compositional characterization by means of standard techniques (EDX, XRD and N_2 adsorption at 77 K), the nature of the surface species contributing to the observed q_{iso} was investigated by means of FTIR spectroscopy of adsorbed CO_2. With bare clinoptilolite, CO_2 forms linear adducts onto K^+ and (less abundant) Mg^{2+} cations, and carbonate-like species onto basic sites, all the species being only partially reversible at beam temperature. The exchange with Na^+ ions leads to the increase in q_{iso} over the entire investigated coverage range, likely due to the formation of linear adducts onto both single ($Na^+\cdots O=C=O$) and dual ($Na^+\cdots O=C=O\cdots Na^+$) cationic sites.

The improved adsorption capacity of clinoptilolite at high temperature (over 323 K) versus the state-of-the-art zeolite 13X makes it a potential sorbent for CO_2 removal from flue gases by minimizing the input energy required to the system.

Keywords: Clinoptilolite, CO_2 capture, Natural zeolite, Cation exchange, adsorption sites

2.1 Introduction

The growing environmental concerns have led to the development of new technologies aiming to reduce the levels of CO_2 in the atmosphere. Nowadays, the main techniques used for post-combustion CO_2 capture include solid adsorption, solvent scrubbing and membrane separation processes [56,57]. However, the solvent scrubbing process undergoes large energy costs associated with the high heat of adsorption and solvent regeneration. Instead, solid sorption exhibits favorable advantages including no corrosivity, low volatility and low energy penalty. Among the sorbents used for CO_2 separation processes, zeolites could be promising materials due to their textural and structural properties, polarity, and cation exchange potential [18,56,57]. Different zeolites have been investigated for CO_2 treatment applications, including natural and synthetic materials, modified zeolites and zeolitic imidazolate frameworks (ZIFs).

In this scenario, natural zeolites, such as clinoptilolite (belonging to HEU zeolite family), could be interesting materials for CO_2 separation technologies as they exhibit promising adsorption capacity, along with high abundancy and relatively low costs. For instance, the prices for clinoptilolite typically range from \$100 to \$600 per metric tons, depending on the effective zeolite content and processing as well as with the country of origin and market prices [58]. Therefore, these natural materials can be suitable candidates for gas treatment technologies either in their "original" form or by implementing structural modifications.

Clinoptilolite is formed by two parallel channels composed of ten membered-rings (A channel with an aperture of 3.0 x 7.6 Å) and eight membered-rings (B channel with an aperture of 3.3 x 4.6 Å). These channels interconnect with eight-membered rings oriented along the a-axis (C channel with aperture 2.6 x 4.7 Å)

[32]. The main interaction between CO_2 molecule and clinoptilolite is physisorption by Van der Waals forces and electrostatic bonds.

Tailoring the CO_2 loading capacity and selectivity of clinoptilolite can occur by improving the sorbent pore size (to be fitted for the CO_2 molecule with a kinetic diameter of 3.3 Å), active surface area (to have a stronger polarization effect) and pore volume (to have higher contact area and stronger polarization) [59,60]. The coordination and distribution of cations on clinoptilolite affect the adsorption equilibrium and diffusion of gases within the zeolite. Indeed, the degree of freedom for cations within the clinoptilolite channel system depends on the size of the channel, cations species and the diffusing molecules [61,62]. For clinoptilolite the sites on the eight and ten membered-rings in the direction of the c-axis are occupied by Na^+ and Mg^{2+} in channel A, Ca^{2+} in channel B and K^+ in channel C [63].

Different studies have investigated the impact of cation distribution on the exchanged capacity of clinoptilolite and proved that clinoptilolite due to its extra framework cations has high cation exchange potential [62,64–66]. The cation exchange property of clinoptilolite makes it a potential sorbent for CO_2 treatment applications by selectively introducing polar cations into its structure. Formerly, the CO_2 uptake of alkali and alkaline earth cation-exchanged clinoptilolite has been measured by C. Colella [11] and D.A. Kennedy [67]. Their results showed the CO_2 adsorption capacity is changing as following $Cs^+ > Rb^+ > K^+ > Na^+ > Li^+$ and $Ba^{2+} > Sr^{2+} > Ca^{2+} > Mg^{2+}$. Similar works characterized the multi-component (CO_2, CH_4 and N_2) equilibrium kinetics of adsorption and selectivity for the Na^+, Ca^{2+}, K^+, Mg^{2+} exchanged clinoptilolites [33,64,68,69].

Indeed, the cation exchange modification on clinoptilolite can effectively increase its CO_2 adsorption capacity but that is not enough for achieving our objectives. For creating a cost-effective and economically feasible CO_2 capture process by decreasing the total energy penalty it is necessary to adapt the process operational condition with the flue gas temperature and pressure. Obviously, this strongly depends on the release source of flue gas that can be power plant exhaust or vehicle exhaust which are normally below 100 °C. For this reason, it is essential to investigate the performance of cation exchanged clinoptilolite not only at ambient temperature but also at higher temperatures near to flue gas exit temperature. The preceding literature reviews on clinoptilolite only addressed the cation exchange impact on the CO_2 adsorption uptake at ambient temperatures (293 K – 303 K) and atmospheric pressure. However, none has been addressed the feasibility of utilizing clinoptilolite in a cation-exchanged form at higher temperatures as compared to the flue gas outlet temperature of the industrial or automotive exhaust.

Therefore, in the present study, much effort has been put forth to determine the adsorption performance and efficiency of clinoptilolite for CO_2 capture from industrial flue gases at moderate temperatures (*e.g.* 333 K – 338 K). For this purpose, the dynamic CO_2 adsorption capacity of bare and ion-exchanged (with Na^+ and Ca^{2+}) clinoptilolite were evaluated in a fixed-bed reactor operating under the flue gas stream (10% vol. CO_2 in N_2) in the 293 – 338 K range. Then, the obtained breakthrough curves were compared to those of commercial zeolite 13X. Na^+ and

Ca^{2+} are chosen since they are owning comparable effective ionic radius of 1.00 Å and 1.02 Å, respectively, whereas having different charge densities. Moreover, single-component CO_2 adsorption isotherms (*i.e.* under equilibrium conditions) were used to measure the isosteric heat of CO_2 adsorption (q_{iso}) of the sorbents and to investigate the effect of pre-treatment temperature. Besides structural and compositional characterization by means of standard techniques (i.e. EDX, XRD and N_2 adsorption at 77 K), nature of the surface species contributing to the observed isosteric heats of adsorption was investigated by means of FTIR spectroscopy of adsorbed CO_2. To the best of our knowledge, this is the first IR study on CO_2 adsorption on clinoptilolite or other natural zeolites belonging to the heulandite (HEU) framework type.

2.2 Materials and experimental methods

2.2.1 Materials preparation

The Clinoptilolite (obtained from Zeolado, Greece) is in the form of powder with particle sizes ranging between 250 μ and 500 μ.[70]. The cation exchanged clinoptilolite is prepared using aqueous solutions of sodium chloride (NaCl) and calcium chloride ($CaCl_2$). In the initial step, clinoptilolite is washed with deionized water, filtered and dried at 353 K. Later, the ion-exchanged process is carried out by mixing a ratio of 1 g of clinoptilolite in 250 mL of 0.6 N cation salt solution. During this process the solution is stirred for 2 h at the temperature of 323 K, afterward, it is washed and centrifuged three times. Finally, the samples are dried in the oven at 338 K for 24 h. Before performing the adsorption tests the samples are calcinated at 773 K. For comparison purposes, the adsorption performance of commercial zeolite 13X (obtained from GRACE®) with a similar range of particles is also evaluated.

2.2.2 Samples characterization

The sample composition is measured on each sample by energy-dispersive X-ray (EDX) analysis (Aztec, Oxford Instruments) on three different areas of about 0.1 mm2: the average values (wt%) are reported in **Table 2-1**.

2.2.3 N_2 and CO_2 adsorption isotherms.

N_2 adsorption/desorption isotherms at 77 K are collected on Quantachrome – Autosorb 1C. Specific surface area (SSA), total pore volume (VT) and micropore (VMP) volume of the adsorbents are measured on samples previously out-gassed at 573 K. SSA was calculated according to both Langmuir and BET methods. VT was measured at $P/P^0 = 0.90$, whereas VMP was calculated according to the t-plot method. The same instrument was used for CO_2 (99.995% purity) adsorption

isotherms at 283 and 303 K, on samples previously out-gassed at 573 K. Equilibration time for each point was set to 5 min.

From CO_2 adsorption isotherms recorded at 303.1 and 283.1 K, the corresponding values of isosteric heat of adsorption q_{iso} were obtained through the Clausius–Clapeyron equation:

$$\left[\frac{\partial \ln p}{\partial T}\right]_n = -\frac{q_{iso}}{RT^2} \quad (2\text{-}1)$$

which takes in the present case the form:

$$q_{iso}(n) = \frac{\ln\left[p(303.1\ K)/p(283.1\ K)\right]_n}{{}^1/_{303.1} - {}^1/_{283.1}} \quad (2\text{-}2)$$

2.2.4 IR Spectroscopy of adsorbed CO_2

For IR measurements, the powders are pressed as thin self-supporting wafers (ca. 8 mg cm-2) and are outgassed at 573 K for 3 h in a homemade quartz cell equipped with (IR transparent) KBr windows. The IR spectra are recorded at 2 cm^{-1} resolution on a BRUKER EQUINOX-55 spectrometer equipped with a mercury cadmium telluride (MCT) cryodetector. IR spectra are recorded by dosing at room temperature (r.t.) increasing amounts of CO_2 ($7.5*10^{-3}$ - 112.5 Torr equilibrium pressure range) on the outgassed samples. The IR spectra of Clino and Na-Clino are normalized with respect to the wafers density (ca. 10 mg cm^{-2}). Difference spectra in **Figure 2-10** are obtained by subtracting the IR spectrum of the naked wafer (before CO_2 adsorption). After CO_2 adsorption, an evacuation step at IR beam temperature (B.T.) is performed in order to check the reversibility of the interaction. Spectra were taken after 1, 5, 15, 30, 60, 120 and 180 minutes outgassing. Only after 2 h outgassing, no significant changes are observed in the spectra.

2.2.5 XRD measurements

X-Ray Powder Diffraction (XRPD) measurements are performed on an X Pert PANalytical diffractometer (Cu Kα radiation) equipped with a PiX accelerator detector. Samples are ground and high purity α-Al_2O_3 was added (10 wt%) as an internal standard to carry out the amorphous phase quantification (QPA) using the combined Rietveld and reference intensity ratio (RIR) method [71] powder data are collected on a flat zero background sample holder. Diffraction intensities are recorded from 5 to 120 2θ with a counting time of 300 sec/deg. Data analysis is performed using the GSAS package [72] with the EXPGUI interface [73]. The results of quantitative phase analyses (QPA) are reported in **Table 2-2** and observed and calculated pattern in **Figure 2-3**.

2.2.6 CO_2 breakthrough curves

The adsorption and desorption measurements are conducted using an experimental set-up including a reactor with a fixed sorbent bed, furnace and a gas analyzer as shown in **Figure 2-1**. In this system, the sorbent is placed in a quartz U-shape reactor with a sorbent bed height and a diameter of 3 cm and 1 cm respectively. The reactor is located in the Tube Furnace Lenton® (LTF) which is connected to the inlet gas through a stainless steel tube with an outer diameter (O.D.) of 1/6". While the outlet gas is recovering in an Emerson X-Stream® gas analyzer that can measure different gas components. The gas analyzer measures the CO_2 volume fraction expressed in ppm in the outlet gas every minute. A K-type thermocouple monitored the operating condition for temperature during the process. A Bronkhorst® mass flow controller controls the gas inlet flow rate.

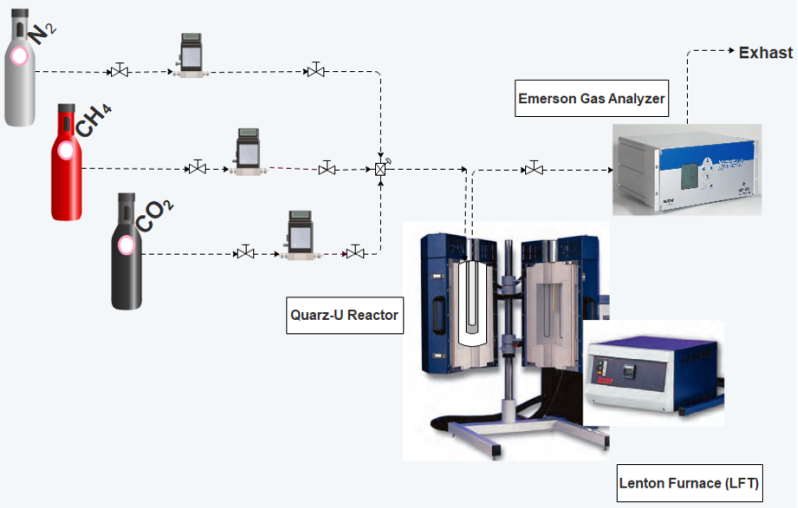

Figure 2-1. The experimental set-up used for performing the adsorption and desorption tests.

Adsorption tests measurements are carried out on the mixtures of 10 vol.% CO_2 in N_2 (assuming the flue gas composition) within a temperature range of 293 K – 338 K. Initially, the adsorbents are degassed at 373 K for 1 h and after that, the system is cooled down to the experimental temperature. The total flow of the gas mixture used is 40 mL/min. However, to evaluate the effect of gas contact time with the sorbent on the shape of CO_2 breakthrough curves a higher flow rate (80 mL/min) is also tested. During the adsorption experiment, the CO_2 volume fraction in the outlet gas is recorded with the gas analyzer until the concentration of the analyzed gas at the inlet of the reactor and outlet of the analyzer became equal. In each adsorption experiment the adsorbed amount of CO_2 is calculated using the following equations:

$$V_{CO2_{adsorbed}} = \int_{t0+\Delta t}^{tf} (1 - C_{CO2_{out}}) d(Q_{out} t) \quad (2\text{-}3)$$

$$n_{CO2_{out}(t)} = \frac{y_{CO2} PV}{RT} \quad (2\text{-}4)$$

Where $C_{CO2_{out}}$ is the volumetric concentration of the CO_2 recorded by gas analyzer at each time, $Q_{out}\left(\frac{m^3}{s}\right)$ is the outlet volumetric flow rate of the reactor for each time and $\Delta t\ (s)$ is the time presumed delay of the gas analyzer. Moreover, the adsorption loading capacities respecting to the weight of loaded zeolite is calculated by:

$$\alpha_{zeolite} = \frac{n_{CO2_{adsorbed}}}{m_{sorbent}} \quad (2\text{-}5)$$

Following adsorption, the regeneration process is executed by heating and purging the system respectively at 358 K with a flux of pure N_2 (100 mL/min). The rate of temperature change for heating is held at 1 K/min until the system temperature reached the set point. The desorption process was completed once the concentration of the CO_2 in the out-flowing gas measured by GC reached 1 vol.% of the CO_2 concentration at the inlet. Finally, the sorbent bed is cooled down to the desired adsorption operating temperature.

The regeneration efficiency expresses in **Equation (2-6)** shows the reversibility of the absorption process.

$$\eta = \frac{n_i}{n_0} \quad (2\text{-}6)$$

Where the n_0 are the moles of CO_2 adsorbed and n_i is the amount of CO_2 recovered in the adsorption phase.

2.3 Results and discussion

2.3.1 Structural and compositional characterization

The chemical composition of clinoptilolite (Clino), cation-exchanged samples (Na-Clino, Ca-Clino), and 13X are reported in **Table 2-1**. As a whole, it appears that the most abundant cation in Clino is K^+, followed by Ca^{2+}, Mg^{2+}, Na^+ and $Fe^{2+/3+}$. The sum of the cationic charges roughly balances the zeolite negative charge brought by Al^{3+}, in agreement with the very limited cation exchange capacity of kaolinite [74], which was found to be the main component of the clay mineral impurities (vide infra). The relevant increase in sodium content in Na-Clino provides evidence on the effectiveness of the cation-exchanged process, which took place mainly at the expense of Ca^{2+}. Smaller differences in cations content are

instead observed between Clino and Ca-Clino. A slight decrease in Al content in ion-exchanged samples is observed, possibly due to delamination occurring during the exchange [75], or to the loss of naturally occurring extra framework Al^{3+}.

The QPA performed with the Rietveld method as shown in **Table 2-2** and **Figure 2-3** indicates that both pristine and Na^{+} exchanged samples show very similar results. In particular, both samples show the same phases: clinoptilolite as the main component, kaolinite and illite as clay minerals, and a fraction of the amorphous phase. The pristine sample shows a slightly high level of clay minerals if compared to the exchange one (5.8 wt% vs 4.8 wt%). Overall, the QPA analyses indicate that the exchange treatment does not influence the mineralogical composition of the samples.

The nitrogen physisorption isotherms of the investigate adsorbents are reported in **Figure 2-2** and the corresponding values of Specific Surface Area (SSA), Total Pore Volume (VT) and Micropores Volume (VMP) are gathered in **Table 2-3**. As expected, 13X zeolite shows type I isotherm, most of its pore volume being due to microporosity. On the other hand, both Clino and Na-Clino show definitely lower SSA and pore volumes. Both Clino and Na-Clino isotherms are similar and exhibit a hysteresis loop of H3-type [76] in the 0.45 – 0.99 P/P0 range. This feature is commonly observed for clinoptilolite samples [61,77–79] and can be attributed to capillary condensation in mesopores of the amorphous fraction or in the space between the zeolite crystallites. At very low relative pressures, a scarce increase in adsorbed N2 volume adsorption is observed, resulting in a very limited VMP. The low VMP and SSA of Clino and Na-Clino samples are likely due to the difficult accessibility of the narrow microporosity by N2 molecules at 77 K, while they are accessible to CO_2 at room temperature (vide infra). Actually, the channel apertures characterizing the framework of HEU type zeolites are definitely smaller than those of the FAU framework type.

Table 2-1. The elemental composition as measured by EDX analysis.

Sample	Cations content / mmol g^{-1}						Si/Al Atomic ratio
	Na	Mg	K	Ca	Fe	Al	
Clino	0.12	0.32	0.78	0.50	0.20	2.43	4.79
Na-Clino	1.46	0.15	0.30	0.03	0.07	2.14	5.75
Ca-Clino	0.000	0.3	0.53	0.9	0.25	2.48	4.77
13X	4.93	0.11	0.04	0.10	0.11	5.60	1.50

Table 2-2. QPA results obtained with Clino and Na-Clino.

	Clino	Na-Clino
	QPA results (wt.%)	
Clinoptilolite	66.4 (1)	65.3 (1)
Illite	0.8 (2)	1.2 (2)
Kaolinite	4.0 (2)	4.6 (2)
Amorphous phase	28.8 (1)	28.8 (1)
Refinement statistic		
R_{wp} (%)	0.089	0.108
Rp (%)	0.059	0. 670
RF^2 (%)	0.086	0.087

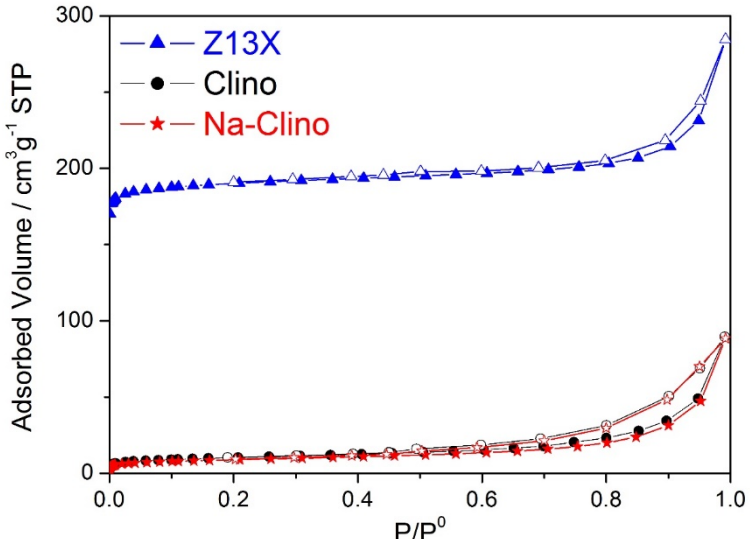

Figure 2-2. N_2 adsorption/desorption measured at 77 K on the samples 13X (blue triangles), Clino (black circles), and Na-Clino (red stars).

Table 2-3. N_2 physisorption parameters measured for raw clinoptilolite and zeolite 13X.

N_2 Physisorption Property	Clino	Na^+Clino	Zeolite 13X
BET Surface Area ($m^2 g^{-1}$)	37	32	745
Langmuir Surface Area ($m^2 g^{-1}$)	39	33	815
Total Volume ($cm^3 g^{-1}$)	0.14	0.14	0.44
t-plot Micropore Volume ($cm^3 g^{-1}$)	0.005	0.004	0.3
t-plot micropore Area ($m^2 g^{-1}$)	11	9	700

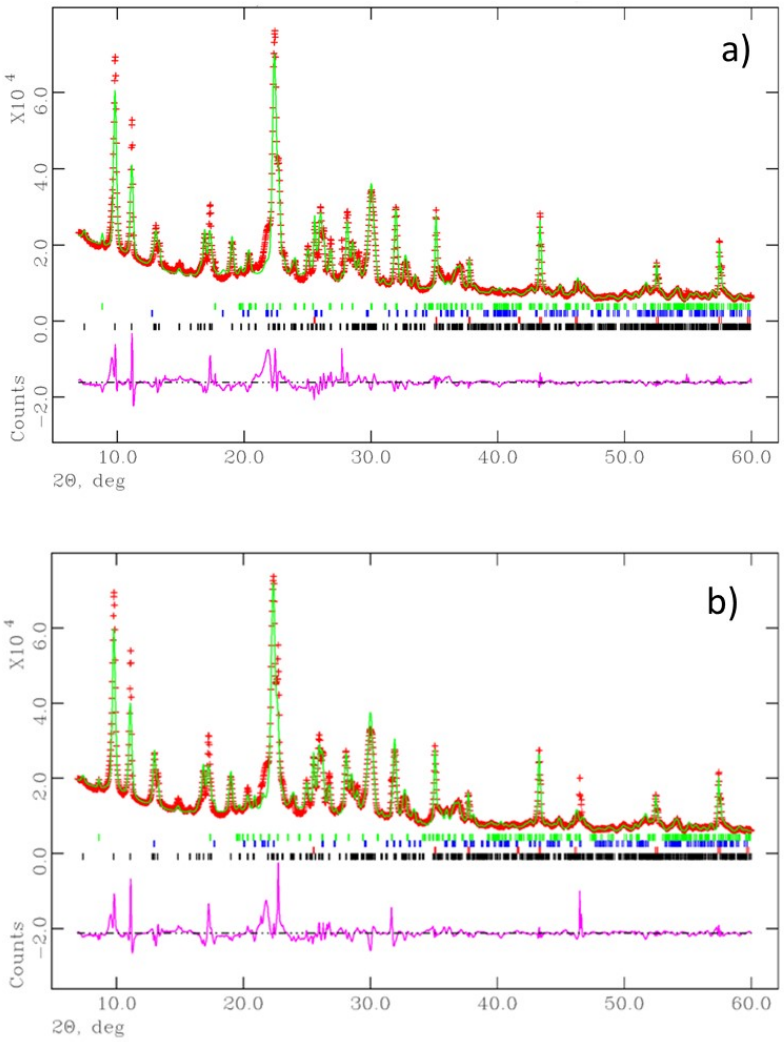

Figure 2-3. Observed (red dash marks) and calculated (green line) diffraction patterns and final difference curve (purple line) from Rietveld refinements of pristine clinoptilolite sample (a) and Na-exchanged sample (b).

2.3.2 Adsorption breakthrough curves

The results achieved from the adsorption tests on Na-Clino, Ca-Clino and untreated clinoptilolite samples, as well as zeolite 13X, at 293 K are presented in **Figure 2-4 (A)**. As can be noticed the cation exchange modification of Clino with Na^+ showed to improve the CO_2 adsorption capacity as compared to the pure Clino. However, for cation exchange with Ca^{2+}, no significant increase in the adsorption performance of the sorbent has been observed. Here, the impact of diverse cations on the CO_2 adsorption uptake can be explained by the position of cations in the zeolite framework. Indeed, the location of the cations can attribute to CO_2 diffusion limitation into the zeolite porous structure [64]. Different studies on the adsorption properties of clinoptilolite have reported that the Na^+ is mainly located in the ten-membered ring (channel A) while Ca^{2+} is principally positioning in the eight-member ring (channel B). The occupation of channel B (as a smaller channel comparing to channel A) with Ca^{2+} can be the cause of channel blockage and diffusional restriction to CO_2. It has been also noted that the majority of Na^+ cations in Na-Clino are substituted with the larger cations of presents in the structure of Clino including K^+ and Mg^{2+} which open up channel A and facilitate the CO_2 adsorption [62]. The dimension of channels and the cation distributions on the Clino structure are reported in **Table** 2-4 .The superior CO_2 adsorption of Clino respecting Ca-Clino can be attributed to the cationic variability of Clino leading to increased surface charge heterogeneity and stronger electrostatic interactions [66]. The CO_2 loading capacities of all samples are calculated and reported in **Figure 2-4 (B)** in the term of mmol CO_2/ g sorbent.

In this regard, similar studies have indicated the beneficial effect of ion-exchange with cations carrying high charge density [35,36]. Their research presented the influence of alkali and alkaline earth metal cations on the CO_2 adsorption capacity of Clino that is changing respectively as following $Li^+ \approx Na^+ > K^+ > Rb^+ > Cs^+$ and $Ba^{2+} > Sr^{2+} >> Be^{2+} \approx Mg^{2+} > Ca^{2+}$. [32].

Table 2-4. The dimension of channels and the position of cations in the structure of clinoptilolite.

Channel	Cahnnel Dimension [A°]	Cation Position	Exchangeble Cations
A	7.2 x 4.4	M (1)	Na^+ and partially Ca^{2+}
		M (4)	Mg^{2+}
B	4.7 x 4.1	M (2)	Ca^{2+} and partially Na^+
C	5.5 x 4.0	M (3)	K^+

Comparing to Clino, zeolite 13X presented superior CO_2 adsorption uptake of almost 2 times larger than Clino at the same operating conditions. The difference in their CO_2 adsorption uptake contributed to the presence of different influencing factors including the pore size, cation distribution and CO_2 diffusion mechanism. Regarding the CO_2 mass transfer, zeolite 13X has been proved to be controlled by macropores [80]. Here, to understand the effect of mass transfer on the adsorption properties of Clino, the CO_2 adsorption breakthrough curves are measured for two different gas flow rates of 40 and 80 mL/min at 293 K (with 10 vol% CO_2 in N_2). As shown in **Figure 2-5** at higher gas flow rate a shift in the breakthrough curve to shorter times is detected while the amount of CO_2 holds up in the adsorption bed remained equivalent to the one at a lower gas flow rate (adsorption capacity ~ 0.9 mmol/g). The identical CO_2 adsorption uptake, as well as the similar shape of breakthrough fronts, indicated the absence of surface or diffusion limit for the CO_2 transport into the sorbent porous structure. Such adsorption behavior seen in Clino demonstrated its equilibrium-controlled CO_2 adsorption kinetic.

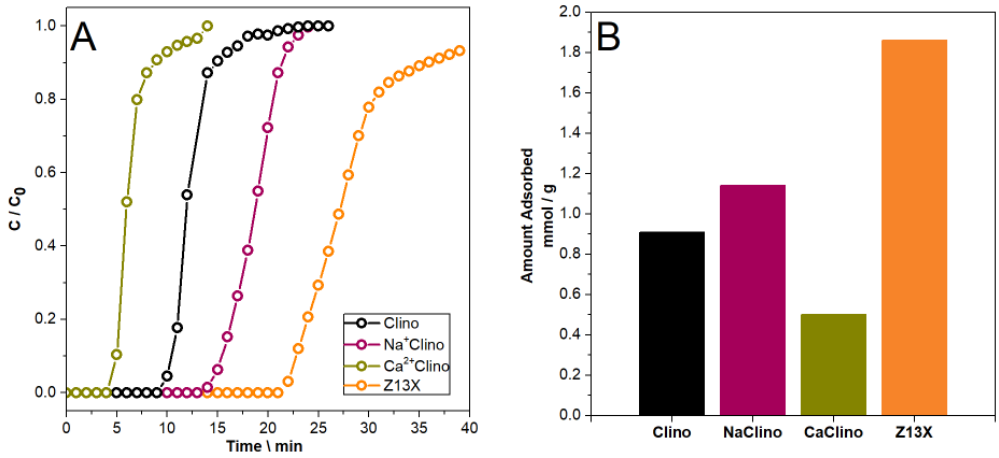

Figure 2-4. (A) Adsorption breakthrough curves of CO_2 for the Na^+ and Ca^{+2} exchanged clinoptilolite, natural clinoptilolite and zeolite 13X at 293 K. A gas flowrate equal to 40 mL/min composed of 10 vol % CO_2 in N_2 is used. (B) the CO_2 adsorption capacity of the modified and untreated clinoptilolite calculated from their adsorption breakthrough curves.

Furthermore, the effect of temperature on CO_2 adsorption capacity of Na-Clino, Clino and zeolite 13X are investigated. Indeed the high-temperature tests are performed only on Na^+ modified clinoptilolite as it owns better CO_2 sorption performance as compared to Ca-Clino. The CO_2 breakthrough curves are measured at 293 K, 308 K, 323 K and 338 K with a partial pressure of 0.1 bar. Here, due to the exothermic nature of the adsorption process, the temperature increase has resulted in a decrease in the adsorption capacities of all the samples. As shown in **Figure 2-6 (C)** the effect of temperature rise on the breakthrough curves of zeolite 13X is significantly indicated by the reduction in its breakthrough time. Whereas, Clino showed a more stable adsorption behavior in the stated range of temperature (293 - 338 K) and established a better adsorption performance **Figure 2-6 (A)** at higher temperatures (>323 K) as compared to the commercial zeolite 13X. The relevant CO_2 loading capacity of all samples as indicated in **Figure 2-6 (D)**, presenting an elevated adsorption capacity for Clino and Na-Clino at temperatures > 323 K. Such a behavior makes Clino and Na-Clino preferable for flue gas treatment applications within temperature <373 K. Here, the lower CO_2 uptake of

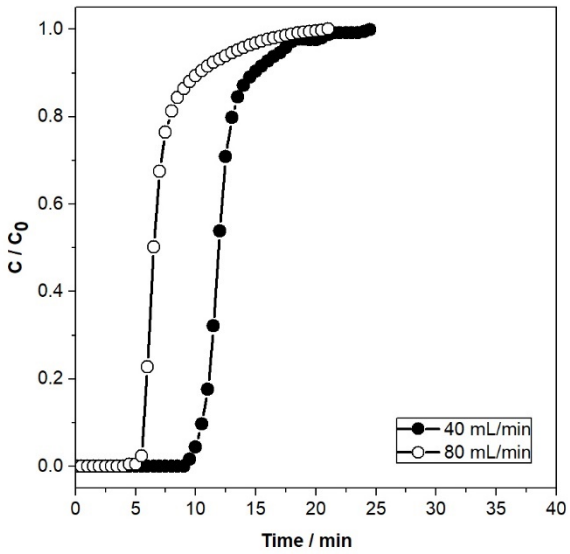

Figure 2-5. Effect of flow rate on the adsorption breakthrough curves for natural clinoptilolite.

zeolite 13X at higher temperatures could be attributed to its high heat of adsorption. The steep shape of the breakthrough curve of zeolite 13X at the high temperature indicated the heat limited mechanism of the adsorption. It should be specified that for lower temperature, 293 K, due to lack of temperature control and its slight variation during the process the breakthrough slope is even less sharp and it takes more time for the breakthrough front to achieve saturation.

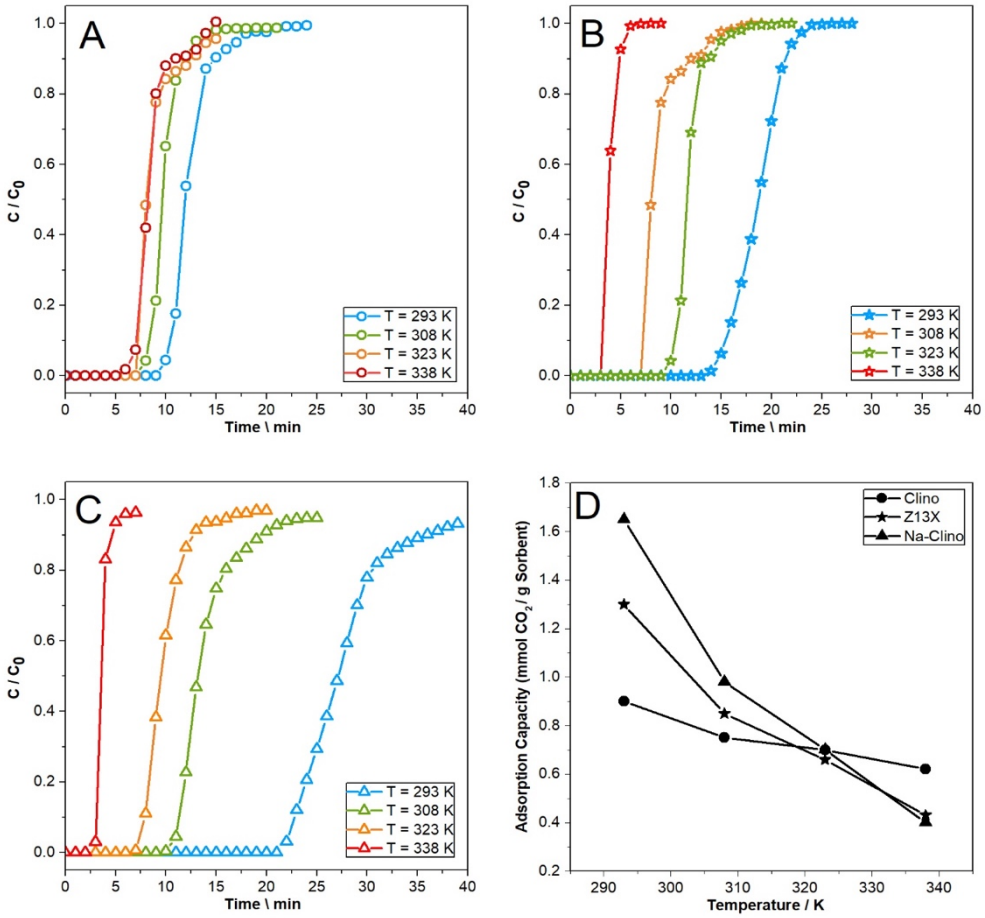

Figure 2-6. Adsorption breakthrough curves measured (A) for Clino; (B) Na-Clino; (C) Z13X at temperatures of 293 K, 308 K, 323 K and 338 K. The adsorption tests were performed with a gas composed of 10 vol% CO_2 in N_2 (40 mL/min) and 1 bar. (C) The Comparison between the adsorption capacity of 13X, Clino and Na-Clino, as measured from the breakthrough curves at 293, 308, 323 and 338 K.

2.3.3 CO_2 adsorption isotherms and isosteric heat of adsorption

Figure 2-7 shows the CO_2 adsorption isotherms at 283 K (left side) and 303 K (right side) on 13X, Clino and Na-Clino outgassed at 573 K. In order to verify the possible presence of irreversibly adsorbed CO_2, after the first adsorption run the samples were outgassed for 2 h, and subsequently underwent a second adsorption run. The largest total amount of adsorbed CO_2 (*i.e.* at the maximum equilibrium pressure) in the first run was observed with zeolite 13X, *i.e.* 5.48 (at 283 K) and 4.80 mmol g^{-1} (at 303 K). A negligible amount of irreversibly adsorbed CO_2 was measured (*i.e.* 0.06 mmol g-1), the second run curve being almost superimposed to the first run one. Accordingly, Jacobs et al. [81] reported that after outgassing at room temperature, less than 3 CO_2 molecules per unit cell remain adsorbed in NaX zeolite.

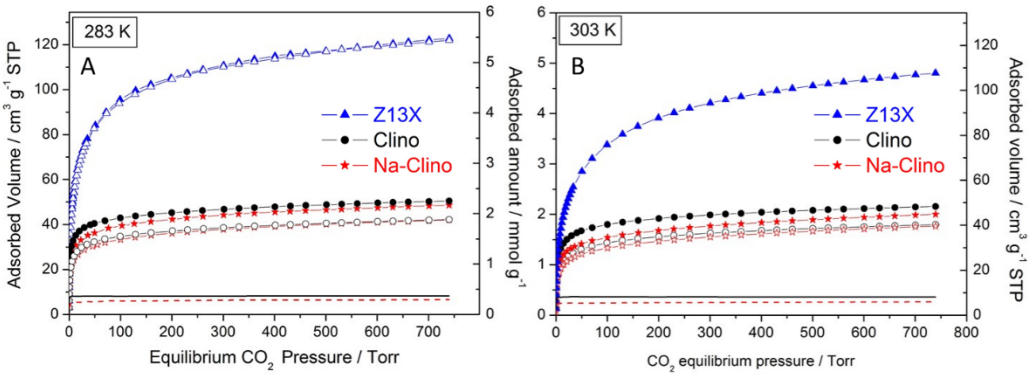

Figure 2-7. CO_2 adsorption isotherms at 283 (left side) and 303 K (right side) on 13X (blue triangles), Clino (black circles), and Na-Clino (red stars) outgassed at 573 K. Full and empty symbols refer to first and second run (i.e. after 2 h outgassing at room temperature) adsorption measurements, respectively. Difference-isotherms (as obtained by subtracting the second run curve from the first run ones) on Clino (solid lines) and Na-Clino (dashed lines) are also reported.

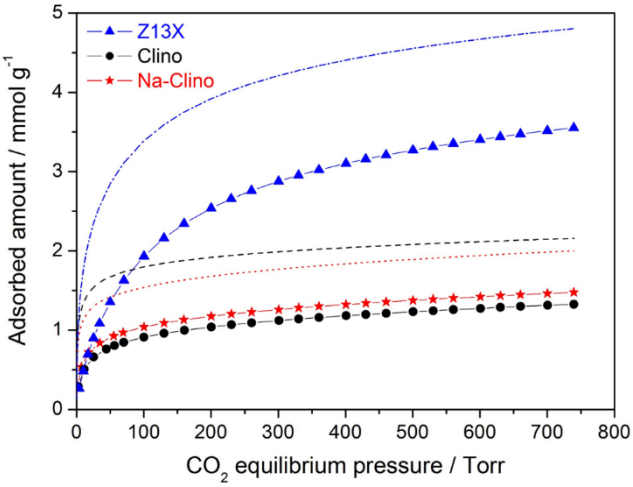

Figure 2-8. CO_2 adsorption isotherms at 303 K on 13X (blue triangles), Clino (black circles), and Na-Clino (red stars) outgassed at 373 K. To highlight the effect of the outgassing temperature, the curves are shown in Figure 6 (right side) are also reported (blue dash-dot for 13X; black dash for Clino; red dot for Na-Clino).

As a general trend, the total amount of CO_2 adsorbed in all the isotherms largely exceeds that observed in the breakthrough curves. Such a difference is likely due to the different experimental set-up (one working under a flow of N_2-CO_2 mixture, the other working at under equilibrium conditions with pure CO_2) and to the adopted outgassing temperature (373 K for breakthrough curves and 573 K for isotherms). The effect of the latter parameter is investigated by measuring also adsorption isotherms at 303 K on samples outgassed at 373 K (**Figure 2-8**). With sample 13X,

the lower outgassing temperature resulted in a 26% decrease of the total adsorbed CO_2 (3.55 mmol g^{-1}), likely due to the coordination of water molecules to Na^+ adsorption sites [23].

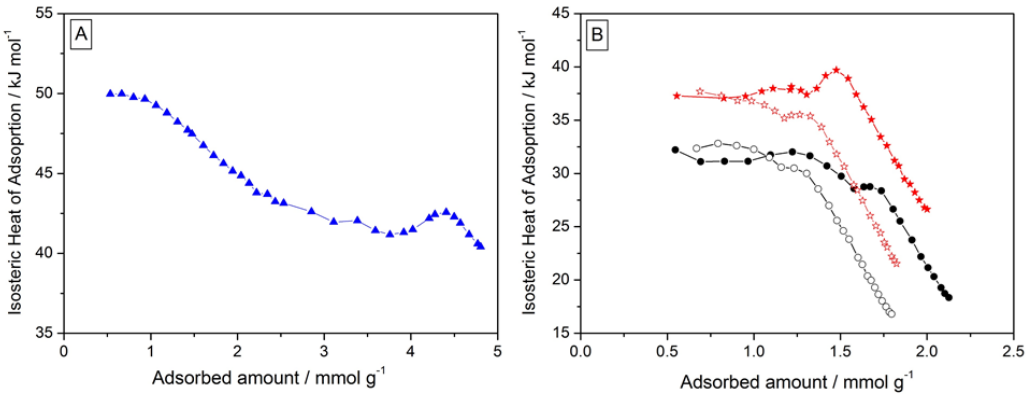

Figure 2-9. Isosteric Heats of adsorption measured on 13X (blue triangles), Clino (black circles), and Na-Clino (red stars). Empty symbols in section B refer to q_{iso} calculated from second run adsorption measurements.

With respect to zeolite 13X, the definitely lower total adsorbed amount was observed with Clino (2.25 and 2.16 mmol g^{-1}, at 283 and 303 K, respectively) and Na-Clino (2.17 and 2.00 mmol g^{-1}, at 283 and 303 K, respectively). With both samples, the occurrence of irreversibly adsorbed CO_2 was observed, *i.e.* 0.36 and 0.27 mmol g^{-1}, with Clino and Na-Clino, respectively. The difference-curves between the first and second run show a markedly Langmuir-type shape, the plateau is reached at very low equilibrium pressures (*ca.* 10 Torr), as expected by the interaction of CO_2 with the strongest sites. This finding is consistent with the IR spectroscopy of adsorbed CO_2 (vide infra). In contrast to adsorption capacity as measured from breakthrough curves (Figure 2-4), Clino adsorbed a slightly larger CO_2 amount than Na-Clino in the overall isotherm pressure range. This is likely due to the different outgassing temperature of the measurements. Indeed, isotherms obtained on samples outgassed at 373 K (Figure 2-9) showed higher adsorption capacity for Na-Clino (*i.e.* 1.48 mmol g^{-1}, compared to 1.32 mmol g^{-1} for Clino). Among the three samples, Clino seems to be the one most affected by a decrease in the outgassing temperature (- 38% of total adsorbed volume).

The different cations contents of the two samples are most probably the main cause of such difference. In particular, the strongly polarizing Mg^{2+} (and Ca^{2+}) cations, more abundant in Clino (**Table 2-1**), could give strong interactions with water molecules, thus being available for CO_2 adsorption only after outgassing at high temperature. As a final remark concerning the differences observed between adsorption capacities as measured by breakthrough curves and volumetric isotherms, zeolite 13X seems to be the sample that behaves most differently in the two types of measurement, even when the same outgassing temperature is adopted. Actually, selectivity towards N_2 and CO_2 may also play a role in the capacities determined by breakthrough curves. Indeed, N_2 has a larger kinetic diameter (3.64

Å) than CO_2 (3.30 Å) [69] and its diffusion into the narrower porosity of the clinoptilolite structure could be hindered. A second explanation could be that the heat of adsorption, which is higher with 13X (vide infra), induces a temperature gradient within the reactor, with higher temperatures in the center of the sorbent bed leading to locally reduced adsorbed amounts [82].

The isotherms shown in **Figure 2-7** were used to calculate the isosteric heats of CO_2 adsorption (q_{iso}), as reported in **Figure 2-9**. The highest q_{iso} was observed with zeolite 13X, showing a q_{iso} of 50 kJ/mol in the low coverage region. This value matches the zero-coverage heat (q_{iso}) n=0 determined in previous studies [22,83–85]. As the coverage increases, the q_{iso} of 13X decreases and reaches a value of 42 kJ/mol. Then, after a slight increase observed in the 4.0 - 4.5 mmol g^{-1} coverage range (corresponding to CO_2/Na^+ ratio of ca. 0.9), q_{iso} decreases again. It is worth noting that only some Na^+ cations in Na-FAU are accessible for the CO_2 molecules (i.e. sites I and I' are not accessible) [86]. Hence, the CO_2/Na^+ ratio reached maximum coverage does not necessarily imply that each Na^+ ion host less than one CO_2 molecule. The nature and strength of the different species forming between Na^+ ions and CO_2 will be discussed in detail in the following section.

Na-Clino shows a rather constant value of q_{iso} (i.e. ca. 37 kJ/mol) up to ca. 1.5 mmol g^{-1} coverage, then a sharply q_{iso} decrease is observed, dropping to ca 26 kJ/mol. The presence of a flat region could be related to the cations content, the Na^+ ions content largely exceeding that of other cations. The observed steep decrease in q_{iso} is likely due to saturation of the cationic sites and to the establishment of unspecific dispersion forces. Accordingly, the slight q_{iso} increase occurring immediately before the steep decrease could due to adsorbate-adsorbate interactions, the contribution of which is maximum near the monolayer completion [87].

With respect to Na-Clino, lower q_{iso} is observed with Clino in the entire investigated coverage range. On the other hand, the extrapolation to zero-coverage seems to lead to $(q_{iso})_{n=0}$ similar to that of Na-Clino, suggesting that for smaller CO_2 doses q_{iso} could be significantly greater than 32 kJ mol^{-1}. Actually, additional information on the strength of sites adsorbing CO_2 at very low coverage was provided by IR spectroscopy (as discussed in the following section), definitely supporting this picture.

Finally, we also calculated $(q_{iso})_{REV}$ form second run adsorption measurements. With both Clino and Na-Clino, curve shapes similar to those obtained from first-run isotherms were obtained, the steep decrease in $(q_{iso})_{REV}$ being observed at lower coverage. As expected, the extent of the curve shift towards lower coverage fairly matches the total amount of irreversibly adsorbed CO_2 calculated from the two isotherm runs.

As a whole, the obtained q_{iso} values are in good agreement with the different behavior observed in the breakthrough curves obtained at different temperatures, since the greater the q_{iso}, the less favored is the adsorption at high temperature.

2.3.4 IR spectroscopy of adsorbed CO_2

In order to investigate the nature of the species contributing to the observed q_{iso}, IR spectroscopy of adsorbed CO_2 was carried out. The spectra were collected at the beam temperature (B.T.), by dosing increasing amounts of CO_2 ($7.5*10^{-3}$ – 112.5 Torr equilibrium pressure range) on samples outgassed at 573 K. Although the coverages obtained at the investigated equilibrium pressures may be slightly lower than the corresponding ones in isotherms at 303 K (B.T. being estimated ca. 308-313 K [88]), some semi-quantitative considerations can be obtained by comparing of volumetric and spectroscopic results. In this regard, the coverage obtained with Clino and Na-Clino in the volumetric isotherms at 112.5 Torr (i.e the maximum pCO_2 used in the IR measurements) is ca. 1.82 and 1.56 mmol g^{-1}, respectively. Looking at **Figure 2-9**, it comes that the pCO_2 range used in IR measurements corresponds to coverages up to the steep decrease in q_{iso}.

As an acidic probe, CO_2 allows the study of basic sites, by the formation of carbonate-like species with characteristic IR bands in the 1800–1200 cm^{-1} range [23,89–92]. The same molecule may act as a basic probe, by interacting through with Lewis sites (metal cations) forming linear adducts [23,92–94]. CO_2 has four fundamental modes: the symmetric stretching (ν_1), the doubly degenerate bending vibration (ν_2), and the asymmetric stretching vibration (ν_3). For symmetry reasons, the ν_2 and ν_3 modes are infrared active and appear at 667.3 cm^{-1} (ν_2) and 2349.3 cm^{-1} (ν_3) in the free molecule. The ν_1 mode is only Raman active and occurs at 1388.3 cm^{-1} in the free molecule. Formation of the aforementioned linear adducts leads to *i)* the activation of the symmetric stretch (ν_1 mode) of CO_2, absorbing at ca. 1380 cm^{-1} and *ii)* an upward shift in the position of the ν_3 mode (the greater the polarizing power of the cation, the higher the ν_3 frequency). To this respect, the correct reference for the position of the ν_3 band is not the free gas, but the molecule interacting with an all-silica microporous adsorbent (*i.e.* silicalite), in which CO_2 gives rise to a band at 2341 cm^{-1} [94]. **Figure 2-10 (A)** reports the IR spectra of CO_2 adsorbed on 13X in the 2500–1250 cm^{-1} range. The first CO_2 dosage (p_{eq} = $7.5*10^{-3}$ Torr) led to the formation of two pairs of IR absorptions at 1711 – 1364 cm^{-1} (weaker), and at 1488 – 1431 cm^{-1}. According to the literature [23,89,95], the intensity of the former pair increases progressively with coverage, while that of the latter reaches a maximum (at about p_{eq} = 0.2 Torr), and then decreases. Both pairs of bands are due to carbonate-like species and arise from the splitting $\Delta\nu$ of the E' mode of free carbonate ion. The larger the splitting, the larger the distortion from the D3h symmetry of the fully symmetric CO_3^{2-} ion. The observed intensity variation with coverage is generally ascribed to the conversion of high symmetric carbonates to less symmetric ones [23,89,91,96], although different structures have been proposed for the two species. Early works [96,97] indicated that sites III' located in the large cavities at four-membered ring [98] and containing the less-shielded cations are probably involved in carbonate-like formation.

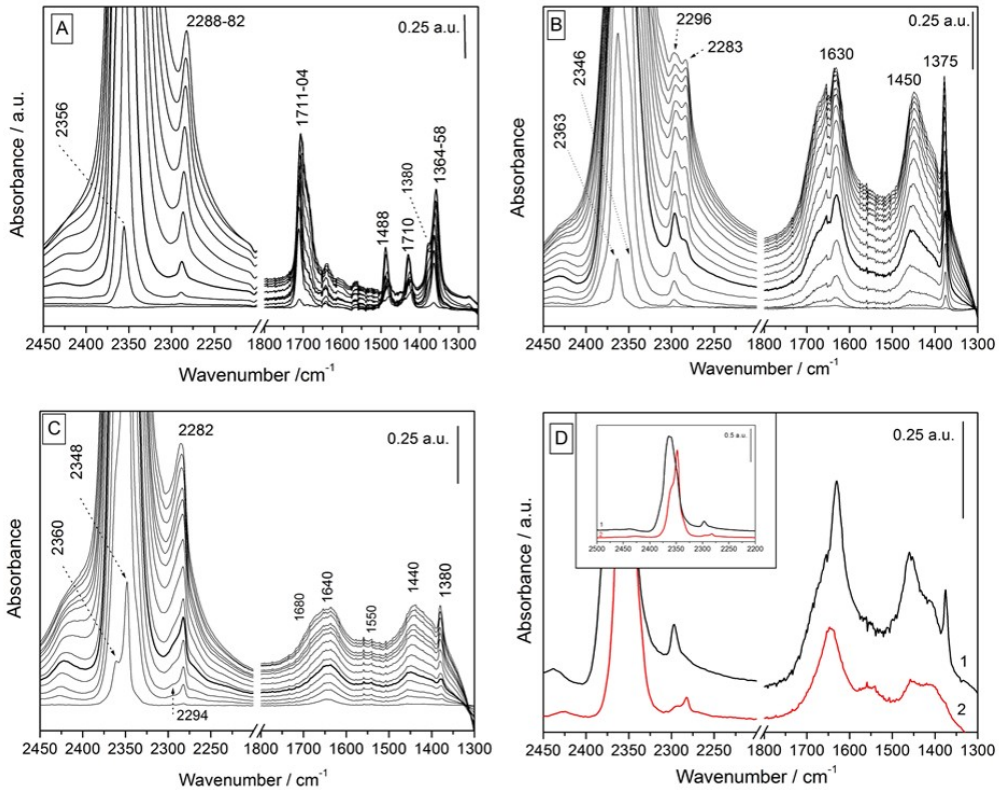

Figure 2-10. IR spectra of CO_2 adsorbed at increasing equilibrium pressure (7.5*10-3- 112.5 Torr) on zeolite 13X (section A), Clino (section B), and Na-Clino (section C). Bold curves in sections A, B and C refer to spectra taken at a CO_2 equilibrium pressure corresponding to ca. 0.5 mmol g-1 coverage (as determined from isotherms at 303 K reported in **Figure 2-7**, right side), i.e. corresponding to the first point of qiso plots. Section D compares spectra take on Clino (curve 1) and Na-Clino (curve 2) after 2 h outgassing at breakthrough time.

The conversion process is reversed upon outgassing at B.T. for few minutes (**Figure 2-10**) since bands at 1488 – 1431 cm^{-1} are restored, whereas bands at 1711 – 1364 cm^{-1} decrease in intensity, and are almost depleted after prolonged outgassing. Formation of stable carbonate-like species likely accounts for the high q_{iso} observed at low coverage.

The position of bands at 1711 – 1364 cm^{-1} does not change up to ca. 2 Torr p_{CO2}, while a shift towards lower wavenumber is observed for higher equilibrium pressures (reaching 1704 – 1358 cm^{-1} at p_{MAX} = 112.5 Torr CO_2). Interestingly, the coverage obtained at an equilibrium pressure of 2 Torr in volumetric isotherm at 303 K (ca. 1 mmol g^{-1}) fairly matches the beginning of the descending part of q_{iso} plot. The constancy of the band splitting indicates that the observed shift is not due to changes in the symmetry of the species. Rather, solvation effects, probably related to the adsorption of large amounts of CO_2 also in the form of linear adducts, could account for the observed shift. Accordingly, the initial band's position is readily restored in the early stages of outgassing, together with the disappearance

of absorptions due to linear adducts. The formation of the latter is evidenced by *i)* the strong absorption in the ν_3 spectral region and *ii)* the activation of the (Raman-active) ν_1 mode at 1380 cm^{-1}. After the second CO_2 dosage (p_{eq} = 0.04 Torr), a sharp band at 2356 cm^{-1} appears, being assigned to the ν_3 mode of $Na^+\cdots O{=}C{=}O$ linear adducts, whereas relatively higher p_{CO2} are required to appreciably observe the ν_1 mode. Due to its high molar absorption coefficient, the ν_3 mode rapidly saturates upon increasing p_{CO2}. However, the formation of the adduct can be followed by monitoring the band at 2288 cm^{-1}, which corresponds to similar adducts involving $^{13}CO_2$ (natural abundance of about 1%). Bands at frequencies higher than ca. 2400 cm^{-1} are also observed, but not considered in the present work being due to combination modes (due to coupling of framework modes and adsorbate vibrations) thoroughly discussed in ref.[85].

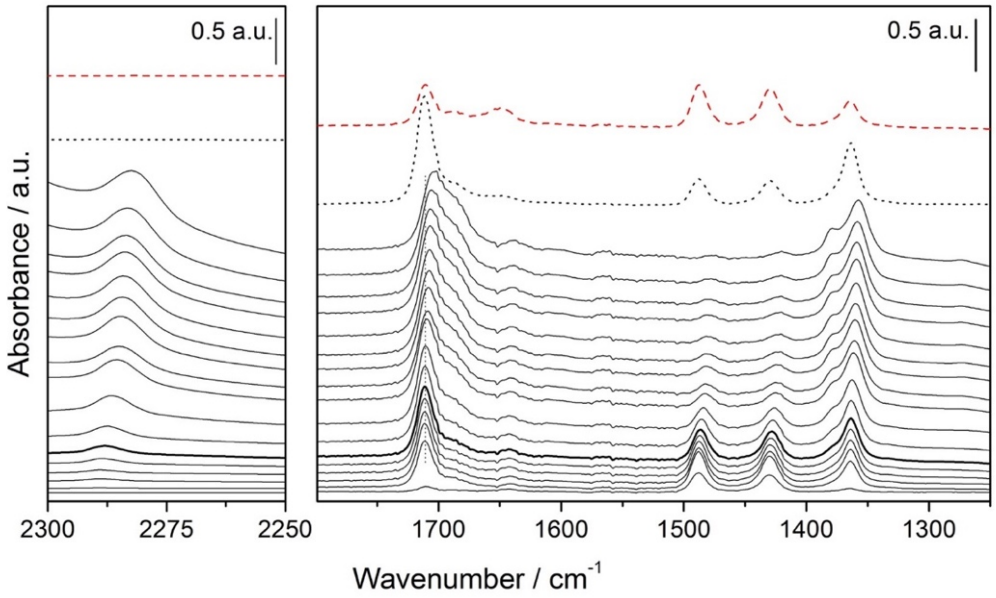

Figure 2-11. IR spectra of CO_2 adsorbed at increasing equilibrium pressure (7.5*10-3- 112.5 Torr – solid curve from bottom to top) on zeolite 13 X. Spectra are shifted vertically upward for a better understanding of the adsorption processes. Spectra are taken after 2 min (black dot) and 2 h (red dash) outgassing shows reversibility of conversion process involving the two carbonate species.

The lower stability of the linear adducts with respect to carbonate-like species is evidenced by the much more rapid disappearance of the corresponding adsorptions upon outgassing and by the (slightly) higher p_{CO2} at which they form.

A progressive shift towards lower frequency (up to 2282 cm^{-1}) is observed upon increasing pCO_2, indicating a weakening of the interaction with coverage, which can also account for the observed decrease in q_{iso}. The observed shift could be due to variations in the CO_2/Na^+ ratio (e.g. 1:2, 1:1, 1:2) of the linear adducts. On the one hand, stable bridged adsorption complexes on dual cation sites (*i.e.* $Na^+\cdots O{=}C{=}O\cdots Na^+$) were found in simulations of CO_2 adsorption on NaX [85].

On the other hand, the occurrence of a stepwise adsorption process where a Na^+ initially coordinated to one CO_2 molecule accepts a second ligand, so forming 2:1 adducts (e.g. $Na^+\cdots(CO_2)_2$) was observed with different zeolite structures [33,63,99]. When two adsorbed molecules share the same Na^+ site, each of them should undergo a weaker interaction with the cation.

Compared to 13X, the assignment of bands raising from CO_2 adsorption on Clino and Na-Clino is not straightforward, the two main reasons being *i)* the co-presence of different extraframework cations, and *ii)* the lack of literature data on IR spectroscopy of CO_2 adsorption on HEU framework type. Thus, the main purpose of this study is to evaluate the strength of CO_2 interaction simply on the basis of *i)* the position of the ν_3 mode and the activation of ν_1 mode, both depending on the polarizing power of the cation, and *ii)* the species stability upon outgassing at B.T. **Figure 2-10 (B)** reports the IR spectra of CO_2 adsorbed on Clino in the 2500–2200 and 1800-1250 cm^{-1} ranges. The early stages of CO_2 adsorption (p_{eq} = $7.5*10^{-3}$ - $2.5*10^{-1}$ Torr) show the formation of a peak at 2363 cm^{-1}, the corresponding ν_3 modes due to $^{13}CO_2$ being located at 2296 cm^{-1}, and, subsequently, the appearance of shoulders at 2348 and 2282 cm^{-1}. Closer inspection of the low coverage spectra also reveals the possible presence of a second shoulder at 2373 cm^{-1} probably due to CO_2 interacting with extraframework Al^{3+} ions [92]. Thus, CO_2 linear adducts form onto (at least) two distinct Lewis sites with different polarizing power. On the basis of both sample composition (K^+ and Mg^{2+} being the most abundant cations) and the frequencies reported in the literature for CO_2 interaction with K^+ [95,100–102] and Mg^{2+} [89,103] in different zeolite structures, we tentatively assign the two components to linear adducts on Mg^{2+} (2363 and 2296 cm^{-1}) and K^+ (2348 and 2282 cm^{-1}). The relative intensity of the two bands clearly changes with coverage and, for high equilibrium pressures, the two bands show similar intensity, suggesting a larger availability of the cation with lower polarizing power. Finally, no appreciable shift in the band's position is observed with increasing equilibrium pressure.

The 1800 – 1300 cm^{-1} spectral region shows a complex band envelope with maxima at 1640 and 1440 cm^{-1} and shoulders at ca. 1689, 1550 and 1405 cm^{-1}, likely due to different types of carbonates and bicarbonates [91]. Moreover, strong activation of the ν_1 mode is evidenced by the sharp and intense absorption at 1375 cm^{-1}, clearly visible even at very low coverage. This is somehow an expected feature, given the strong polarizing power of Mg^{2+} ion (due to its small radius and the two positive charges).

The corresponding spectra of CO_2 adsorbed on Na-Clino are reported in Figure 2-10 (C). For the lowest CO_2 dose (p_{eq} = $1.5*10^{-2}$ Torr), two adsorptions are seen in the ν_3 region, at 2349 and 2360 cm^{-1} (weaker). The corresponding ν_3 modes due to $^{13}CO_2$ are located at 2282 and *ca*. 2293 cm^{-1} (shoulder), whereas activation of the ν_1 mode gives rise to the band, appreciably visible only at relatively high equilibrium pressures, at 1380 cm^{-1}, with a shoulder at 1376 cm^{-1}. The increase in equilibrium pressure does not result in an appreciable shift of the 2282 cm^{-1} band. Rather, a band broadening leading to a single asymmetric peak occurs for relatively low p_{CO2}. Then, for higher p_{CO2}, the band shape does not change significantly. This

feature well correlates the flat region observed in q_{iso} plot for coverage higher than *ca*. 0.5 mmol g^{-1}. Finally, a complex band envelope similar to that observed with Clino, although definitely less intense, is seen in the carbonate spectral region (vide infra). We have reason to believe that, even though located at similar frequencies, the ν_3 modes observed with Clino and Na-Clino are due to different species. The first obvious reason is the cations content, with a large abundance of Na^+ ions (and a halved content of K and Mg) in Na-Clino. Secondly, the ν_1 mode showed different positions and relative intensity. Third, different stability of the linear adducts upon outgassing at B.T. for 2 h was observed, as shown in **Figure 2-10 (D)**.

With Clino, the fraction of irreversibly adsorbed CO_2 mainly consists of *i)* part of the linear adducts formed onto Mg^{2+}, as evidenced by the persistence of both ν_3 (2362 – 2296 cm^{-1}) and ν_1 (1375 cm^{-1}) modes, and *ii)* some carbonate (1550 – 1405 cm^{-1}) and bicarbonate (1640 – 1455 cm^{-1}) species. On the other hand, with Na-, bands at 2349 and 2282 cm^{-1}, with shoulders at 2360 and 2293 cm^{-1}, respectively, are Clino observed along with absorptions due to carbonate and bicarbonates. In contrast, the ν_1 mode is completely depleted. Based on these observations, we tentatively assign both the absorption at 2349 ($^{13}CO_2$ at 2282) and 2360 ($^{13}CO_2$ at 2293) cm^{-1} to linear adducts formed onto Na^+ ions located in different extraframework cation sites, probably differing in the magnitude of the electric field polarizing the CO_2 molecules. However, this interpretation leaves an open question, *i.e.* what is the actual origin of the higher q_{iso} of Na-Clino compared to Clino. In this regard, it is worth noting that the low extent of ν_1 activation observed with Na-Clino could be due to the formation of energetically favorable bridged adsorption complexes on dual cation sites ($Na^+\cdots O=C=O\cdots Na^+$), for which the symmetry lowering occurs in a less extent with respect to single-site complexes ($Na^+\cdots O=C=O$). Accordingly, it was shown that CO_2 adsorption complexes formed between a pair of Na^+ cations in Na-A zeolite were characterized by an IR band centered at 2360 cm^{-1} [104].

As a final remark on the larger extent of carbonates formation on Clino with respect to Na-Clino, we ascribe the higher basicity of Clino to its larger content in alkaline-earth-metal cations. It was previously proposed that residual water molecules play a role in carbonate formation, especially when divalent cations are involved [89,105]. The presence of residual water in our samples outgassed at 573 K was evidenced by weak absorption at 1648 cm^{-1} (*i.e.* δ(O-H) bending mode of H_2O). If in Al-rich basic zeolites (*e.g.* Na-X and Na-A) the basic oxygen atoms are (mainly) those of the framework, in the present case they could be (also) provided by residual water molecule coordinated to the extraframework cations (Mg^{2+} or Ca^{2+}), following a process similar to that described in ref. [89,105]:

$$M^{2+}(H_2O)_x + CO_2 \rightarrow M^{2+}(CO_3)^{2-} + (H_2O)^{x-1} + 2H^+ \qquad (2\text{-}7)$$

A closer inspection of the spectra reveals indeed a negative band at 1648 cm^{-1} due to consumption of water molecules, and a positive peak at 1630 cm^{-1} (overlapping the broad absorption in the 1700 – 1600 cm^{-1}) due to Brønsted acid groups formed upon dissociation of water.

If the presence of a small water amount favors carbonates formation in Clino, larger water contents were shown to hinder CO_2 adsorption capacity, likely due to saturation of cationic sites. Further IR studies to unveil the role of pre-adsorbed water on CO_2 adsorption are in progress.

2.4 Conclusions

In this study, the use of natural Clinoptilolite as a solid sorbent for CO_2 separation from flue gases at moderate temperatures (293 – 338 K) was investigated. The CO_2 adsorption capacities of bare and ion-exchanged Clinoptilolite were measured under both dynamic (i.e. in a fixed-bed reactor operating under CO_2/N_2 mixture flow) and equilibrium (i.e. by measuring single component adsorption isotherms) conditions, and compared to those of state-of-the-art Z13X.

The adsorption capacity as measured from the breakthrough curve of CO_2/N_2 (10:90 vol.) mixture at 293 K is Z13X > Na-Clino > Clino > Ca-Clino, thus showing a moderate beneficial effect of the exchange with Na^+ (and a detrimental one with Ca^{2+}) on the adsorption capacity of Clino. Notably, at slightly higher temperatures (i.e. 338 K), the highest CO_2 uptake was obtained with Clino, whereas Z13X and Na-Clino showed similar performances.

On the other hand, CO_2 adsorption isotherms were used to measure the isosteric heat of adsorption (q_{iso}) of Clino, Na-Clino and Z13X, and to investigate the effect of pre-treatment temperature. So measured on Z13X (i.e. 50 – 42 kJ/mol) is responsible for the drastic decrease in CO_2 adsorption capacity of this material with the temperature increase. In contrast, Na-Clino showed a smaller and rather constant value of q_{iso} (i.e. 37 kJ/mol) up to ca. 1.5 mmol g^{-1} coverage, whereas an even lower q_{iso} was observed with Clino over the entire investigated coverage range. The obtained q_{iso} values are in agreement with the CO_2 breakthrough curves obtained at different temperatures, since the greater the q_{iso}, the less favored is the adsorption at high temperature.

The nature and the strength of the surface species contributing to the observed q_{iso} were investigated by means of FTIR spectroscopy of adsorbed CO_2. With bare Clino, CO_2 forms linear adducts onto K^+ and (less abundant) Mg^{2+} cations, and carbonate-like species onto basic sites, all the species being only partially reversible at beam temperature. The exchange with Na^+ ions led to a decrease in surface basicity, and to the formation of both single (Na+···O=C=O) and dual (Na+···O=C=O···Na+) cationic sites, available for linear adducts formation.

From a practical point of view, the improved adsorption capacity of Clinoptilolite at high temperatures (over 323 K) versus the state-of-the-art zeolite Z13X makes it a potential sorbent for CO_2 removal from flue gases by minimizing the input energy required to the system. Moreover, this work presents experimental evidences indicating that a strategy to improve the adsorption capacity of natural Clinoptilolite could be to control the water content of the adsorbent material.

Chapter 3

3 Measurement of CO_2 Adsorption Equilibrium on Clinoptilolite by Zero Length Column (ZLC) Technique

The research work presented in this chapter is carried out during 6 months visiting research period at the University of Edinburgh (Carbon Capture Group) under supervision of Prof. Stefano Brandani and Dr. Enzo Mangano. The experimental part are executed at the Adsoprtion Laboratories using Zero-lenghth Column Systems.

Abstract

In this study, a zero-length column (ZLC) is used to investigate the CO_2 diffusion mechanism into the porous structure of natural clinoptilolite and to measure the CO_2 adsorption loading capacity of both untreated and alkali exchanged cations (Na^+, K^+ and Cs^+) clinoptilolite. The adsorption tests are performed at 35 °C, 55 °C and 75 °C with CO_2 partial pressure of 0.1 bar. The ZLC technique enables rapid monitoring of the kinetic and equilibrium properties of the samples using only a small amount (<15mg). Moreover, kinetic evaluation and CO_2 adsorption isotherms are measured with volumetric methods at the same operating conditions. Such analysis provides information on the isosteric heat of adsorption and allows a comparison between the adsorption capacities obtained by the two methods. From the ZLC results, the CO_2 adsorption nature of all samples is recognized to be equilibrium-controlled. Whereas the CO_2 uptake capacity for the different samples changes in the following order K-Clino > Na-Clino > Clino > Cs-Clino, confirming the beneficial effect of K^+ and Na^+ cations. By repeating the

adsorption tests in different cycles, it is observed that the sample capacity is reproducible only after the 2nd cycle. To understand the nature of the irreversible CO_2 adsorbed, Temperature Programmed Desorption analysis (TPD) is performed on all samples at 300 °C.

3.1 Introduction

Synthetic and natural zeolites are among the most promising adsorbents utilized for CO_2 treatment applications from industrial flue gas. The most significant properties of these zeolites that are affecting their CO_2 adsorption capacities are their cations distribution, charge densities [69,106,107] and the ratio of Si/Al. In this regard, several studies have investigated the application of synthetic zeolites and have shown that those belonging to type X, A and Y are presenting notable CO_2 uptake [17,18,101,102]. Other adsorption studies performed on natural zeolites are reported the CO_2 adsorption performance of mainly two types including chabazite and clinoptilolite [31,63,64,69,106–108]. These studies have discussed the possibility of enhancing the CO_2 adsorption potential of natural zeolites by tailoring their structure and introducing extra-framework cations into their matrix. For instance, the cation exchange process performed on chabazite using Li^+, Na^+, K^+ and alkaline-earth cations Mg^{2+}, Ca^{2+}, Ba^{2+} presented the competitive adsorption performance for Na^+ and Ca^{2+} exchanged chabazite at high temperature [106]. A similar study was performed on the cation exchanged clinoptilolite over a pressure range of 0 to 8 atm at 303 K. Their results achieved are presenting favorable adsorption characteristics and high selectivity which makes the natural clinoptilolite suitable for pressure swing adsorption applications [32]. The main aspects discussed in these works are including the kinetic separation of CO_2 from N_2 and CH_4, the linearity and non-linearity of CO_2 adsorption isotherms and the CO_2 adsorption rate for different gases through utilizing volumetric [68,82,92,109] and gravimetric techniques [63]. Among the other potential methods for fast monitoring of the CO_2 adsorption kinetics is the zero-length column (ZLC) technique. This method has been used for estimating the gas diffusion mechanism in the porous structure of adsorbent materials mainly synthetic zeolites [24,80,110]. However, none of the literature reviews have reported the use of the ZLC method for evaluating the mass transfer mechanism of natural zeolites.

In this chapter, the ZLC technique is applied to assess the CO_2 adsorption properties of cation-exchanged clinoptilolite with alkali metal cations of Na^+, K^+ and Cs^+. The adsorption experiments are carried out in the following conditions: CO_2 partial pressure of 0.1 bar and temperatures of 35 °C, 55 °C and 75 °C. Here, the reversibility of the adsorption process is analyzed during the temperature-programmed desorption (TPD) investigation by running the adsorption measurements in three consecutive cycles. The results achieved showed the effect of different cations on the CO_2 adsorption capacity of clinoptilolite. The CO_2 uptake of the exchanged clinoptilolites is confirmed to be varied in this order Cs-Clin > K-Clin > Na-Clin > Clin. Insight to the presence of strong sites on the framework of

clinoptilolite is verified by the results obtained from TPD analysis showing a partially strong interaction of CO_2 with basic sites of clinoptilolite. The strongly adsorbed CO_2 is removed from the sorbent during a TPD with a set temperature of 110 °C and a temperature ramp of 1 °C/min. However, a big portion of CO_2 which is weakly adsorbed to the sorbent can be removed easily at the same adsorption operating condition.

Furthermore, the CO_2 diffusion mechanism in modified clinoptilolites related to the location of exchangeable cations and channel blockage is investigated. The results indicate that the CO_2 mass transfer in all samples is equilibrium controlled . The CO_2 uptake rates vary in different samples due to the effect of different cations location (K, Na, Mg, Ca, Cs). The Henry law constant and the adsorption equilibrium isotherms are calculated by examining the frequency response attained from the ZLC technique. These isotherms are showing lower adsorption uptake as compared with data found from the volumetric method due to the formation of strongly adsorbed CO_2 on the adsorbent surface. Indeed, the isotherm and Henry law constant obtained from the ZLC method are only reporting the physically adsorbed CO_2. Later, the isosteric heat of adsorption is estimated by measuring CO_2 isotherms at different temperatures by using the van Hoff relation.

3.2 Experimental

3.2.1 Sample preparation

The Clinoptilolite (obtained from Zeolado) used is in the form of powder with particle sizes range of 250 μ - 500 μ [70]. The cation-exchange samples are prepared by using an aqueous solution of sodium chloride (NaCl), potassium chloride (KCl) and cesium chloride (CsCl). Initially, clinoptilolite (Clino) is washed with deionized water, filtered and dried at 80 °C overnight. The cation-exchanged samples are prepared using 1 g of clinoptilolite in a 250 mL of 0.6 N cation salt solution. During this process the solution is mixed for 2 h at the temperature of 50 °C, afterward, it is washed, centrifuged three times and dried in the oven at 80 °C for 24 h. Finally, the prepared samples are calcinated at 300 °C.

3.2.2 Kinetic measurements

A schematic diagram of a ZLC system reported from ref. [111] is shown in **Figure 3-1**.

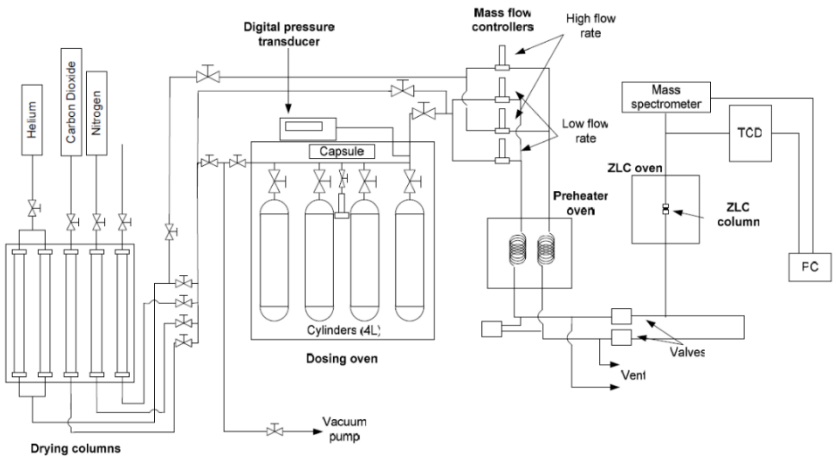

Figure 3-1. ZLC schematic diagram.

For the kinetic measurements, the column used is a Swagelok 1/8" reducing union as demonstrated in **Figure 3-2** packed with the 15 mg of sample. Normally, the amount of sample used in the ZLC measurement is in the range of 1 mg - 5 mg, however, here a larger amount of sample is used due to the lower capacity of samples as compared to commercial zeolite 13X. The detail of the ZLC apparatus used in our work is described completely in a work done by X. Hu and S. Brandani [112].

Figure 3-2. A semi-automated zero-length column apparatus used in this study. (A) the dosing oven; (B) ZLC apparatus; (C, D) ZLC column.

The ZLC system is composed of a SANYO 212 dosing oven that is used in our work for the mixture preparation of 10 vol% CO_2 in He. The mixture needs to rest for at least 3 h after preparation to be perfectly mixed. The ZLC column itself is placed in an oven connected to the mass spectrometer (AMETEK benchtop quadrupole). The frequency response from the mass spectrometer is analyzed to understand the adsorption behavior of our samples. In this method, the desorption curves are studied rather than the adsorption curves due to the better signal to noise ratio. The ZLC system is behaving like a continuous stirred tank reactor (CSTR) due to its short length [110].

For the measurements initially, the packed column is regenerated with a stream of inert gas (He) at a low flow rate (3 cc/min) with a temperature ramp of 1°C/min.

The regeneration temperature is set at 110 °C for 2 h, increased to 300 °C for 6 h and finally cooled down to the operating temperature. For evaluating correctly the sample's saturation time, firstly several tests are performed using a single flow rate and different saturation times of 5, 10 and 20 mins. Once the saturation time is known, the adsorption and desorption tests are carried out by varying the flow rate. Indeed, by performing tests at low flow rates the adsorption is moving toward equilibrium while, by increasing the flow rate it tends to be kinetically limited. Here, the desorption response provides insight into the mass transfer kinetics. In fact, the desorption is carried out at identically same adsorption rate which at high flow rates yield to the diffusion time constant (D_c/r_c) where D_c is the diffusivity in the micropores and r_c is the crystal radius and at low flow rates yield the Henry's constant [113].

The dead volume of the system including the cell, the piping from the dosing oven up to the ZLC and the piping between the switching valves and the gas spectrometer is calculated by carrying out blank tests prior to the adsorption tests. The blank test response has been considered to be a function of gas flow rate whereas the effect of temperature is supposed to be significantly small.

3.2.3 Adsorption breakthrough curves and TPD analysis

The second part of the ZLC measurements is aimed at evaluating the adsorption capacities of all samples (Clino, Na-Clino, K-Clino and Cs-Clino) by analyzing their adsorption breakthrough curves. The difference between dynamic and kinetics measurements (as discussed before) is the length of the ZLC column used, which in this case is a Swalgelock 1/4" reducing union packed with a 3 times larger amount of zeolite (50 mg). The gas mixture preparation and the sample pretreatment steps are identical to the ZLC kinetics experiments. The operating conditions for these experiments are flow rates of 5 and 10 cc/min; temperatures of 35, 55, 75 °C; and partial pressure of 0.1 bar. By integrating the adsorption breakthrough curves relevant to each sample, its CO_2 uptake capacity is estimated. Whereas, the desorption curves are used to investigate the stability and the reproducibility of the adsorbent capacity by repeating the tests in three different cycles. At the end of the last cycle, the sample temperature is increased up to 300 °C via a TPD analysis to explore the possibility of carbonate formation due to chemically adsorbed CO_2 to the sorbent strong sites. The TPD program is set to 110 °C for 2 h and 300 °C for 6 h with a ramp of 1 °C/min.

In this set of experiments, the TPD measurements temperature was remained constant at 300 °C and not reduced to the operating condition at the end of 6 h to assure no water traces in the system. For this reason, the blank tests here are measured at 300 °C.

3.2.4 Volumetric Method

The adsorption isotherms are measured using a volumetric system composed of a Quantochrome Autosorb iQ as shown in Figure 3-3.

Figure 3-3. Autosorb volumetric system.

Here, a known amount of sample (~ 0.5 g) is inserted into a 9 mm measuring cell. The sample weight in the cell is measured before and after the sample outgassing occurred in a two steps temperature rise process; 110 °C for 2 h and increased to 300 °C for 6 h under vacuum condition. The temperature program used for the volumetric method is identical to the one used during the ZLC measurements. In this stage, the liquid nitrogen is used to trap the moisture released from the sample. The isotherm measurements are performed with pure CO_2 dosing to the system several times until reaching the desired equilibrium pressure. Each experiment includes adsorption isotherm measurements up to 1 bar and desorption back to 0.05 bar. A Julabo F-25 circulator is used to run the tests at the preferred temperatures of 35 °C, 55 °C and 75 °C. Along with the CO_2 isotherm experiments, the N_2 isotherms were also measured at 20 °C providing information on the pore distribution, surface area and dimension of the adsorbent.

3.3 Theory

3.3.1 ZLC Measurement Theory

The zero-length column technique is a chromatographic method for measuring the diffusion coefficient of pure gases in microporous materials. This method can be used to evaluate the intra-crystalline diffusion of small particles and to solve the problem associated with the high-pressure drops and high contribution of the axial diffusivity [114]. By using low adsorbate concentration, a very small amount of adsorbent and high carrier gas flow rates for the desorption the ZLC method is capable of removing the heat and mass transfer resistances [80,115]. The ZLC theory is developed based on the pore diffusion control mechanism rather than the

external mass transfer resistance. The operating conditions for performing ZLC tests are defined in order to operate in Henry's law region which eventually requires the linearity of the isotherms [114]. Instead, for the strongly adsorbed species with non-linear isotherms, the ZLC theory was modified by introducing a non-linear coefficient [116].

The ZLC column is assumed to work as a CSTR due to a very small amount of adsorbent and the short length of the column. Therefore, a CSTR model is used to describe the adsorption behavior of the adsorbent in a ZLC apparatus. The mass balance is given by **Equation (3-1)**.

$$V_s \frac{dq}{dt} + V_g \frac{dc}{dt} + Fc = 0 \tag{3-1}$$

In this equation: Vs is the volume of solids in the ZLC;
Vg is the volume of gas in the ZLC;
q is the average adsorbed phase concentration;
c is the sorbate concentration in the gas phase;
F is the flow rate of carrier gas.

During the adsorption tests, the gas phase concentration is measured and the carrier flow rate is assumed to be constant. Vg is estimated by running blank tests with different gas flow rates.

The initial and boundary condition are as follows:

$$c(0) = c_0 \tag{3-2}$$

$$q(r,0) = q_0 = Kc_0 \tag{3-3}$$

$$\frac{\partial q}{\partial r}|r_0 = 0 \tag{3-4}$$

$$q(R,t) = Kc_t\,; \quad K = H\ (Henry\ law\ constant) \tag{3-5}$$

The analytical solution for the ZLC assuming Fickian diffusion in spherical particles developed by S. Brandani and D. Ruthven [117] is as follows:

$$\frac{c(t)}{c_0} = \sum_{n=1}^{\infty} \frac{2L}{\beta_n^2 + (L-1-\gamma\beta_n^2)^2 + L - 1 + \gamma\beta_n^2} \exp\left(-\frac{\beta_n^2 Dt}{R^2}\right) \tag{3-6}$$

Where β_n are given by the roots of:

$$\beta_n \cot\beta_n + L - 1 - \gamma\,\beta_n^2 = 0 \tag{3-7}$$

$$L = \frac{FR^2}{3KV_sD} \tag{3-8}$$

$$\gamma = \frac{V_g}{3KV_s} \tag{3-9}$$

The dimensionless parameter L is a measure to understand how far is the system from equilibrium. It is defined as the ratio between the diffusional time constant (D/R_2) and the washout time of solid (F/KV_s). To understand the controlling mechanism of the system experiments at different flow rates needs to be carried out. At high purge flow rate the desorption is controlled by the diffusion inside the particle while at low purge flow rate the controlling system is convection [113]. This means that for L>>1 the system is controlled under the kinetics regime and for L<1 the system is under equilibrium control. The parameter γ is defined as a ratio between the hold up in the fluid phase and accumulation in the solid phase. The γ is very small for the gaseous system, however, for weak adsorption, its value can be significant [118].

3.3.2 Kinetic control analysis

When working in a diffusion regime the **Equation (3-10)** is reduced to:

$$\frac{c(t)}{c_0} = \frac{2L}{\beta_n^2 + (L - 1 - \gamma\beta_n^2)^2 + L - 1 + \gamma\beta_n^2} \exp\left(-\frac{\beta_n^2 Dt}{R^2}\right) \tag{3-10}$$

In a plot of c/c_0 vs. t, the long-time asymptote approaches a straight line from which the parameter L (slope) and D/R^2 (intercept) can be extracted. To validate the diffusional time constant obtained it is necessary to perform experiments with different flow rates. The resulting responses will be characterized by the same slope of L and different intercepts.

3.3.3 Equilibrium control analysis

At a low purge flow rate, the diffusional time constant is smaller than the contact time and though the system approaches equilibrium (L is approaching zero). The response solution for this curve reduces to the following equation [119]:

$$\ln\frac{c}{c_0} = \frac{Ft}{KV_s + V_g} \tag{3-11}$$

In a semi-log plot, c/c_0 vs. Ft is a straight line with the slope of $1/(KV_s+V_g)$ invariant with the flow rate. Therefore, in the equilibrium-controlled regime varying the purge flow rate does not make any change in the semi-log plot. This characteristic of the Ft plot can be used to recognize the equilibrium-controlled systems. In this regime, Henry's law constant can be obtained from the slope of this

plot when $KV_s >> V_g$ (for strongly adsorbed species). However, for weakly adsorbed components, the value of KV_s is of the same order of magnitude as V_g, where V_g is calculated by running a blank test. The semi-log plot, c/c_0 vs. Ft yields the value of V_g.

3.3.4 CO_2 isotherm calculation

The ZLC analysis can be used as a breakthrough experiment to evaluate the adsorbed amount of CO_2 in the column. The main assumption considered in the analysis of ZLC breakthrough curves is that the flow rate of the carrier gas remains constant (as an inert gas). In this way, it is possible to calculate the outlet flow rate of the gas exiting the column approximated by:

$$Fy_{out} = \frac{F_{in}}{1-y} y_{out} \tag{3-12}$$

Where y is the mole fraction of the adsorbed species obtained from:

$$\frac{c}{c_0} = \frac{y}{y_0} \tag{3-13}$$

The mass balance can be written in as:

$$v_s \frac{d_q}{d_t} + v_g C \frac{d_y}{d_t} + F_{in} C \frac{y}{1-y} = 0 \tag{3-14}$$

Under equilibrium condition it is possible to achieve the equilibrium isotherm by using the desorption curve which will be later integrated to extract the equilibrium data as follows:

$$q^* = \int_0^\infty \frac{Fc_y}{v_s} dt - \int_0^t \frac{Fc_y}{v_s} dt - \frac{v_g c}{v_s} y \tag{3-15}$$

This equation can be rearranged as follows by substituting the F (not constant) with Fc (flow rate of the purge).

$$q^* = \frac{F_c}{v_s} \int_0^\infty \frac{c_y}{1-y} dt - \frac{F_c}{v_s} \int_0^t \frac{c_y}{1-y} dt - \frac{v_g c}{v_s} y \tag{3-16}$$

Equation (3-16) can be normalized by plotting c/c_0 vs. F_t/V_s to compare different samples. The area under the curve is proportional to the amount of gas adsorbed.

3.3.5 Analysis of CO_2 breakthrough curves

$$\left[\varepsilon\frac{dc}{dt}+(1-\varepsilon)\frac{dq}{dt}\right]V=(Fc)_{IN}-(Fc)_{OUT} \tag{3-17}$$

Considering the gas and the solid phases are at equilibrium and the ideal gas consideration the above equation can be written as follows:

$$(\varepsilon+(1-\varepsilon)K)V\frac{dy}{dt}=(F_{corr}\frac{y}{1-y})_{IN}-(F_{corr}\frac{y}{1-y})_{OUT} \tag{3-18}$$

$$K=\frac{q_1-q_0}{c_1-c_0} \tag{3-19}$$

The mass balance for the carrier gas can be written as:

$$-[\varepsilon+(1-\varepsilon)K_{corr}]V\frac{dy}{dt}=(F_{corr})_{IN}-(F_{corr})_{OUT}=\Delta F_{corr} \tag{3-20}$$

With the consideration of constant carrier gas flow rate this equation can be considered as:

$$\Delta F_{corr}=\Delta V_{corr}\ \frac{y-y_1}{\int_0^\infty(y-y_1)dt} \tag{3-21}$$

The equilibrium isotherm can be obtained from the breakthrough curve for adsorption and desorption respectively by the following equations:

$$\varepsilon+(1-\varepsilon)K=\frac{F_{corr}}{(y_1-y_0)V}\int_0^\infty\left[\frac{y_1}{(y_1-y_0)}-\left(\frac{y_1}{(y_1-y_0)}\right)\left(\frac{y}{1-y}\right)\right]dt \tag{3-22}$$

$$\varepsilon+(1-\varepsilon)K=\frac{F_{corr}}{y_1V}\int_0^\infty\left[\frac{y_1}{(y_1-y_0)}-\left(1+\frac{\Delta F_{corr}}{\mathrm{F}_{corr}}\right)\left(\frac{y}{1-y}\right)\right]dt \tag{3-23}$$

3.4 Results and discussion

In this section, the results of ZLC tests on the alkali metal cation exchanged zeolite of clinoptilolite (Clino), Na-Clino, K-Clino and Cs-Clino are presented and discussed. Comprehensive information on the textural structure and characteristics of Clino are described in **Chapter 2**. In this chapter, the results obtained from ZLC measurements regarding the equilibrium and kinetics behavior of the adsorbent and the breakthrough curves are discussed.

3.4.1 ZLC data analysis

The preliminary results attained indicates the samples saturation time as shown in **Figure 3-4** for Clino. The results revealed that the time necessary for the sample to be fully saturated is 10 min. The same value has been noticed for other samples.

To understand the kinetics behavior of different samples several ZLC tests are performed at different flow rates. As discussed before by presenting the desorption results in a semi-log plot of c/c0 vs. Ft it is possible to evaluate the kinetics or equilibrium regime of the sorbent. The overlapping of the desorption curves at different flow rates in an Ft plot is the evidence of an equilibrium-controlled system. To guarantee a correct interpretation of ZLC desorption curves, some experiments are carried out by applying a range of different flow rates and temperatures. By increasing the adsorption rates or the L value in a kinetically controlled system, the desorption curves cross each other at a point. Only for the equilibrium control regime, the desorption curves overlap [120]. However, lowering the adsorption temperature or increasing the gas flow rate helps to detect better the diffusivity mechanism of CO_2 molecules inside the sample's pores.

The ZLC results for Clino, Na-Clino, K-Clino and Cs-Clino indicated an equilibrium controlled mechanism for CO_2 adsorption on all samples. **Figure 3-5** presented the results for Clino at 35 °C with flow rates of 5, 10 and 20 cc/min. Here, to assure that the adsorption mechanism is fully equilibrium controlled the same measurements are carried out at -10 °C.

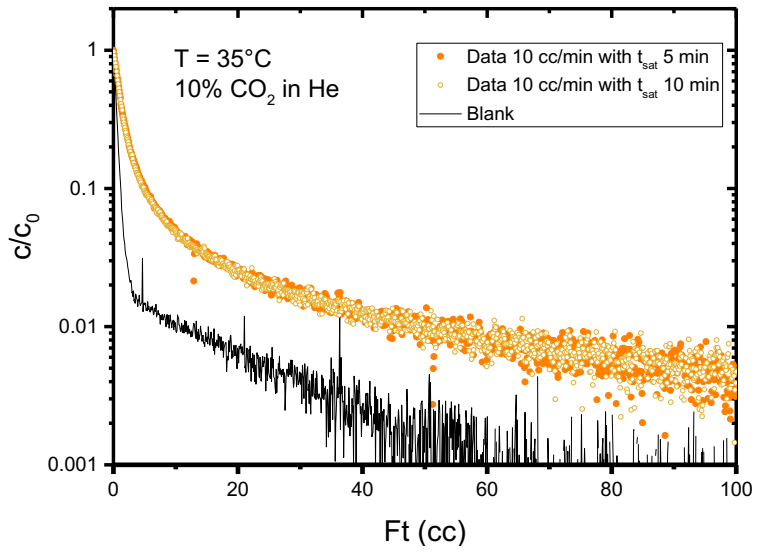

Figure 3-4. ZLC curves for Clino with different saturation time. Using a mixture of 10 vol% CO_2 in He with a flow rate of 10 cc/min at 5 and 10 min saturation time.

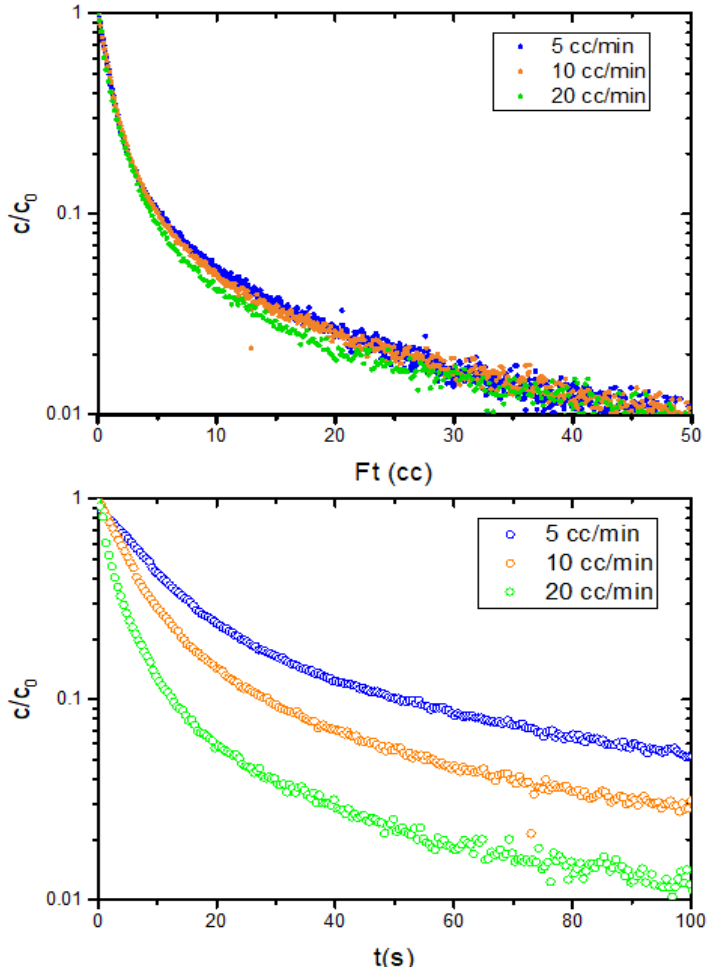

Figure 3-5. ZLC response curves for Clino plotted as (A) ln(c/c0) vs.Ft; (B) ln(c/c0) vs.t at 35 °C showing lack of dependency on the flow rate.

Identical tests performed on all other samples proved similar equilibrium controlled mechanisms as for Clino. The ZLC results gained for Na-Clino, K-Clino and Cs-Clino are exhibited in Figure 3-6. The ZLC desorption analysis confirmed the equilibrium controlled regime for all the samples.

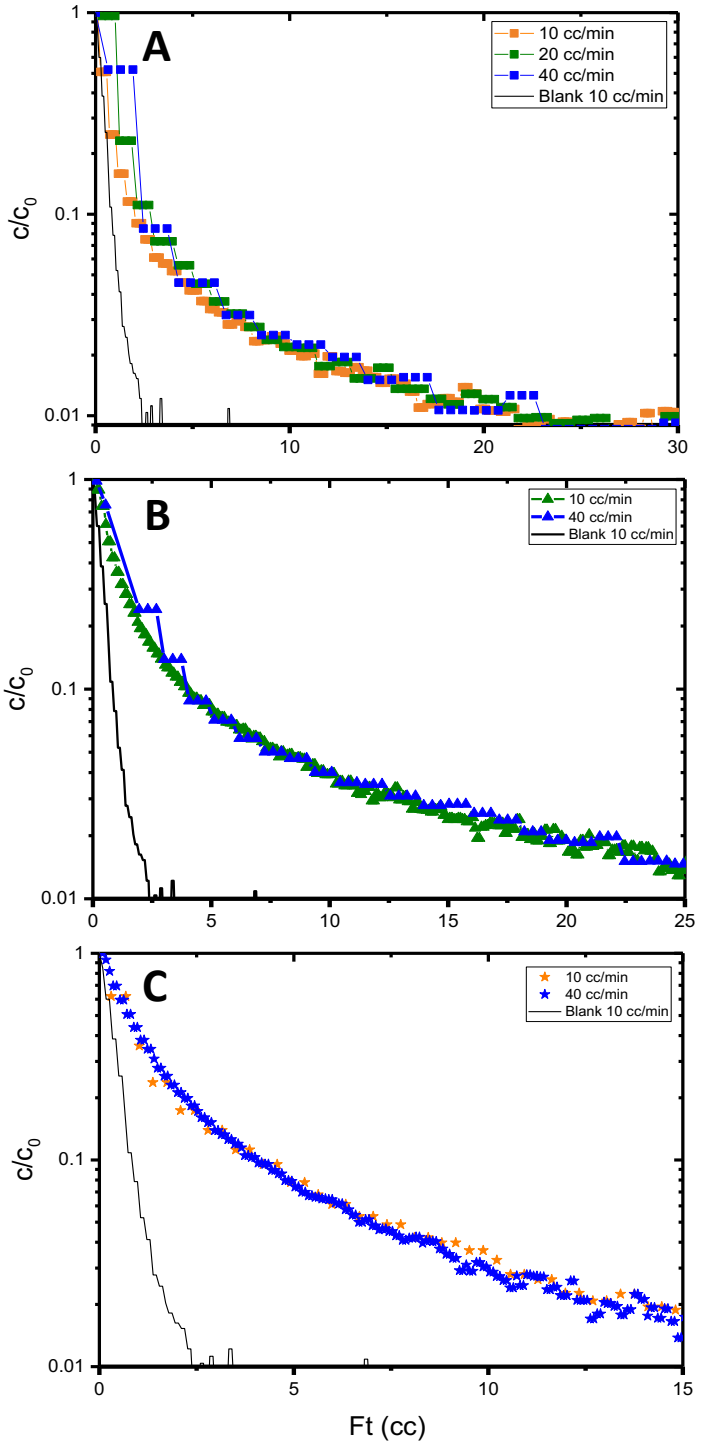

Figure 3-6. ZLC response curves for plotted as ln(c/c0) vs.Ft (A) Na-Clino; (B) K-Clino; (C) Cs-Clino.

The ZLC response curves of different samples presented linear and independent flow rate behavior as explained by **Equation (3-11)**. The small non-linearity at the initial region can be explained by the small delay in the gas sampling [119].

As explained previously under equilibrium conditions, in the long-time region the ZLC response curve in the c/c_0 vs. t plot approaches a linear asymptote with the

of slope 1/(KVs + Vg). The Henry constant can be extracted from the slope of the linear asymptote where K is the dimensionless Henry's law constant, Vg is the dead volume of the system obtained by performing blank experiments and Vs is the volume of solid inside the ZLC column. Indeed, the Henry law constant for all the samples at 35 °C is calculated from the linear asymptote as shown in **Figure 3-7**.

The observed Henry constants at 35 °C are reported in **Table 3-1** considering the blank volume equal to 1 cc and the solid volume of 23×10^{-3} cc. The larger Henry's constant indicates stronger interaction between the CO_2 molecules and the adsorbent surface. As shown in **Table 3-1** the value of the Henry's constant changes in the following order K-Clino > Na-Clino > Cs-Clino ≈ Clino. The higher amount of Henry constant belonging to K-Clino and Na-Clino is attributed to the presence of stronger cations on the sorbent surface. Indeed the smaller ionic radius and the bigger charge density of the K^+ and Na^+ induce an increase in the surface heterogeneity of the sorbent. Eventually, this contributed to the higher adsorption capacity for K-Clino and Na-Clino.

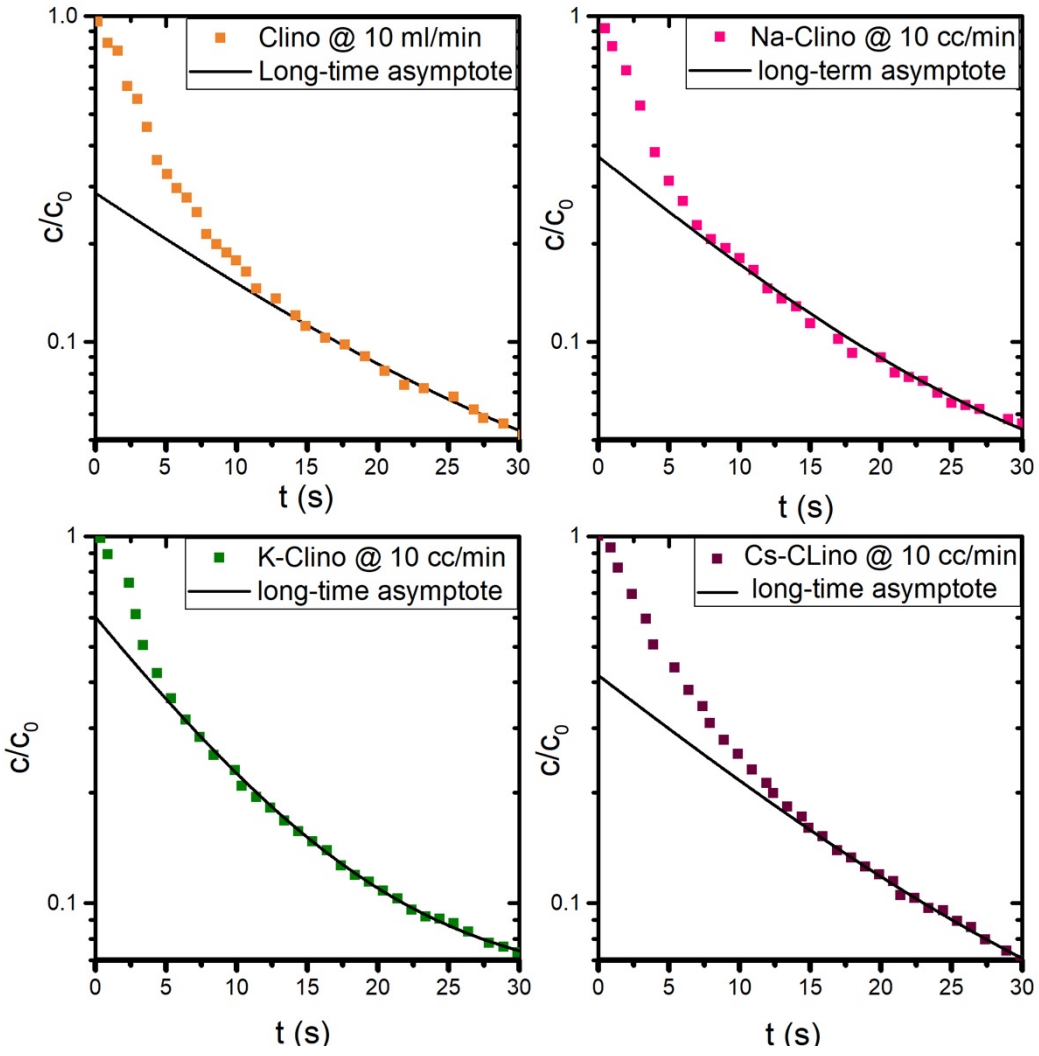

Figure 3-7. ZLC desorption curves of Clino, Na-Clino, K-Clino and Cs-Clino. The fitted curves show the long-time asymptotes which were used to calculate the Henry constants.

Table 3-1. The Henry constants calculated for Clino, Na-Clion, K-Clino and Cs-Clino at 35 °C.

Adsorbent	Dimensionless Henry's Law Constant
Clino	4.03×10^3
Na-Clino	5.06×10^3
K-Clino	6.04×10^3
Cs-Clino	4.20×10^3

3.4.2 Breakthrough analysis

The adsorption capacities of all the samples are measured using a ZLC with a long-column packed with almost 50 mg of sample. The analysis is carried out at temperatures of 35 °C, 55 °C and 75 °C at a partial pressure of 0.1 bar. The tests are repeated in different cycles to check the reproducibility of the adsorption capacities. The samples with the highest content of K and Na cations showed better CO_2 uptake. The results achieved from the adsorption breakthrough curves for different samples are presented in the following subsections.

3.4.2.1 Clinoptilolite

As discussed in Chapter 3, Clino is a natural zeolite with a porous structure composed of 8 and 10 membered rings. An important parameter in tailoring the adsorption performance of the Clino apart from the pore dimension is the distribution of cations on its structure. The XRD analysis of clinoptilolite (as discussed in Chapter 3) showed the main cations on the clinoptilolite structure to be Mg^{2+}, K^+ and Ca^{2+} while the number of other cations including Na^+ and Fe^{2+} is comparably lower. The effective ionic radius and the charge to ionic radius ratio of all the extra-framework cations on its building are shown in **Table 3-2**. The cationic variability causes an increase in the surface charge heterogeneity induces stronger electrostatic interactions and, in some cases, higher adsorption capacity. For instance, Fe-Clino showed the lowest CO_2 capacity although being the smallest cation with the biggest charge density among all other studied cations [66].

Table 3-2. Physical properties of cations present in the structure of Clino [66].

Cations	**Effective Ionic Radius (Å)**	**Charge to Ionic Radius**
Fe^{2+}	0.55	5.45
Mg^{2+}	0.72	2.78
Ca^{2+}	1	2
Na^+	1.02	0.98
K^+	1.38	0.72
Cs^+	1.67	0.59

The measured adsorption breakthrough curves for Clino are exhibited in an Ft plot during three adsorption and desorption cycles as can be seen in **Figure 3-8**.

The desorption step has occurred under the same condition as for the adsorption with a stream of pure He. At the end of the 3rd cycle, a TPD analysis is performed at 300 °C to check the amount of CO_2 which was adsorbed strongly to the sites. From the breakthrough curves, the adsorption capacities during the 2nd and 3rd cycles are reduced compared to the 1st cycle. These results provide insight into the interaction mechanism of CO_2 with the zeolite framework and bring evidence on the presence of strong adsorption sites. The TPD analysis showed that all the CO_2 adsorbed is released by increasing the temperature up to 110 °C. The amount of CO_2 released during the first desorption run is considered to be weakly adsorbed, while the CO_2 desorbed in the TPD step is believed to be strongly adsorbed CO_2 forming carbonate-like species. This is in accordance with the results obtained from the FTIR as presented in **Chapter 2**, where the fraction of irreversibly adsorbed CO_2 is related to the linear adducts forms onto the Mg^{2+} and the absorption due to carbonate and bicarbonate formation.

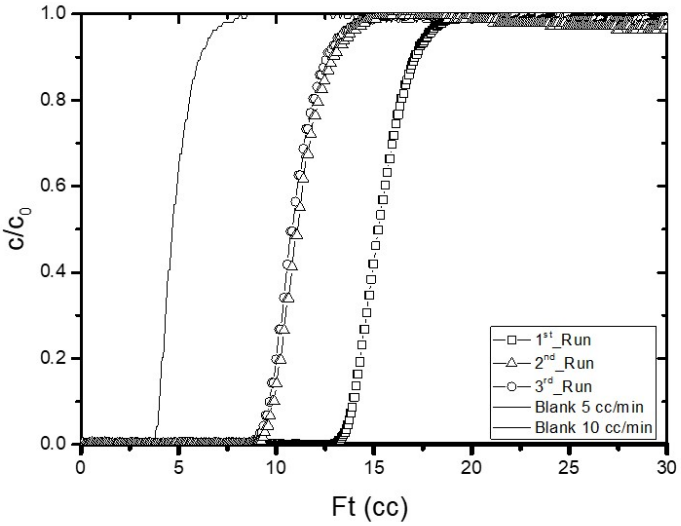

Figure 3-8. Adsorption breakthrough curves for Clino during 3 cycles plotted as c/c0 vs. Ft.

The calculated adsorption capacities during each cycle are reported in **Table 3-3**. The weight of clinoptilolite lost due to the presence of water adsorbed in the sample is calculated during a TGA analysis. The real weight of the samples is corrected, and the adsorption capacities of the sorbent are calculated considering the mass of the sample loss which is about 14 wt% as shown in **Figure 3-9**.

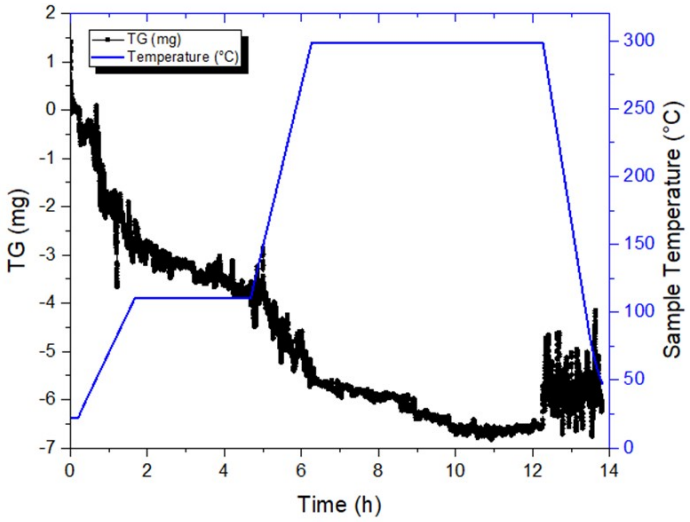

Figure 3-9. TGA analysis of Clino measured by increasing the temperature up to 300 °C.

Table 3-3. The adsorption capacities of Clino at different temperatures during three cycles and a TPD stage.

Temperature (°C)	N. Cycles	Adsorption	Desorption
		Capacity (mol/kg)	
35	1st Run	0.93	0.63
	2nd Run	0.54	0.54
	3rd Run	0.50	0.49
300	TPD	-	0.35
55	1st Run	0.53	0.34
	2nd Run	0.23	0.1
300	TPD	-	0.2
75	1st Run	0.45	0.36
	2nd Run	0.35	0.30

Furthermore, to see the effect of temperature the breakthrough analysis was repeated at 35 °C, 55 °C and 75 °C. The results of which are presented in **Figure 3-10** for both adsorption and desorption. The results from TPD analysis are shown in **Figure 3-11**.

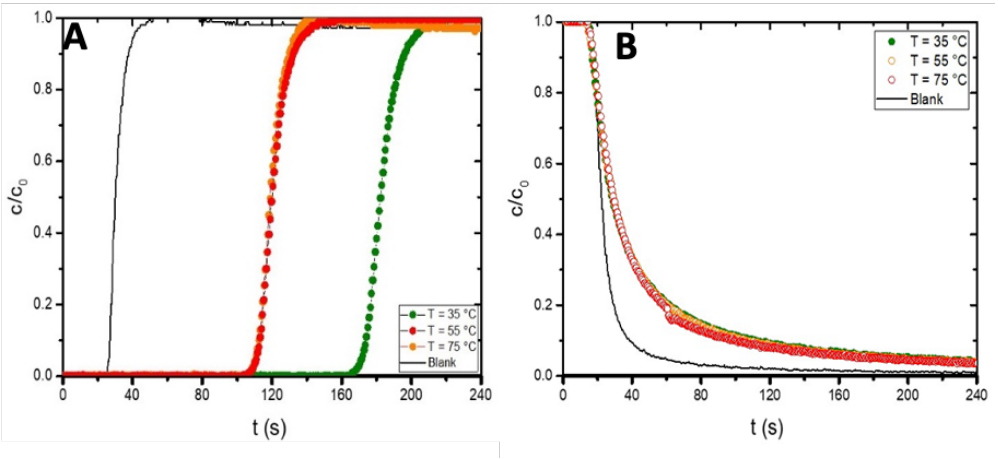

Figure 3-10. (A) Adsorption and (B) Desorption breakthrough curves for Clino at 35 °C, 55 °C and 75 °C.

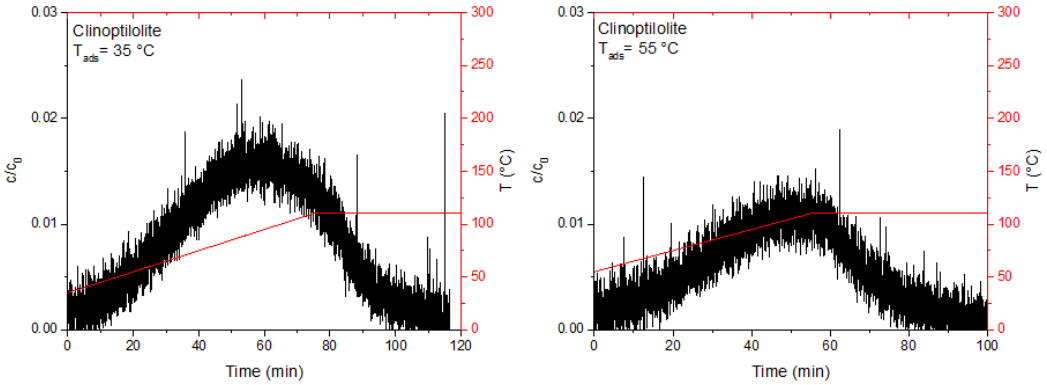

Figure 3-11. TPD analysis for Clino at 300 °C performed after desperation tests (at 35 °C and 55 °C).

3.4.2.2 Na-Clino

The cation exchange process of Clino with Na^+ shown to improve the CO_2 adsorption capacity mainly due to the increased electrostatic interactions as indicated in **Chapter 1**. Indeed, the smaller radius of Na^+ and its higher electrostatic charge density is leading to higher surface potential. Similar CO_2 uptake experiments are performed on Na-Clino samples using the ZLC column, which provides information on the sample's adsorption capacity. The tests are carried out during different cycles to investigate the stability and regenability of the sample. Furthermore, several adsorption tests at different temperatures are performed to understand the effect of temperature change on the material adsorption performance. The results of all of these tests are presented in **Figure 3-12**, **Figure 3-13** and

Table 3-4. As indicated in **Figure 3-12** the adsorption loading capacity of the sample is reduced during the 2nd cycle as compared to the 1st one. This confirmed that a part of the CO_2 adsorbed is not released after degassing. The TPD analysis

performed following the 3rd adsorption cycle confirmed that part of the CO_2 is strongly adsorbed on the strong zeolitic sites.

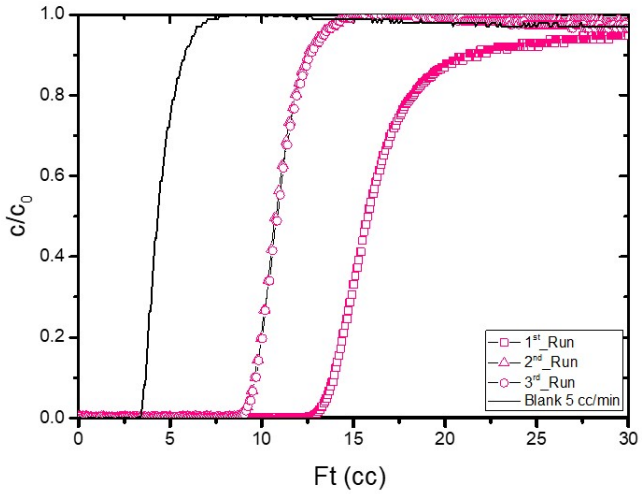

Figure 3-12. Adsorption breakthrough curves for Clinoptilolite during 3 cycles as plotted in c/c0 vs. Ft.

Table 3-4. The adsorption capacities of Na-Clino at different temperatures during three cycles and a TPD stage.

Temperature (°C)	N. Cycles	Adsorption	Desorption
		Capacity (mol/kg)	
35	1st Run	1.13	0.81
	2nd Run	0.80	0.78
	3rd Run	0.80	0.78
300	TPD	-	0.34
55	1st Run	0.92	0.80
300	TPD	-	0.11
75	1st Run	0.68	0.64
300	2nd Run	-	0.01

The amount of CO_2 adsorbed and desorbed in each cycle is reported in **Table** 3-4**.** The values calculated are indicating that the part of adsorbed CO_2 which was not released from the sample during the 1st cycle is completely desorbed during the TPD analysis. During the 2nd and 3rd cycle almost all of the CO_2 is escaped. Examining the results at 75 °C it is evident that all of the CO_2 trapped during the 1st cycle is released in the desorption stage. This provides evidence that at the higher temperatures the possibility for the formation of carbonate-like species during the interaction between the CO_2 and Na-Clino is lower than for the case of the Clino. This behavior of the material makes it a more stable and sustainable adsorbent for CO_2 adsorption applications at high temperatures, although it needs to be taken into account the decrease in the CO_2 adsorption capacity at such temperatures. Referring to the results obtained in **Chapter 3**, **Section 2.3.4** the IR spectroscopy confirmed the formation of linear adducts on the Na-Clino (single

(Na+···O=C=O) and dual (Na+···O=C=O···Na+) cationic sites). The carbonate species are less likely to be formed on Na-Clino due to decrease in the surface basicity. The main reason attributed to the difference between the amount of carbonate formation on Clino as compared to Na-Clino is its larger content in alkaline-earth-metal cations.

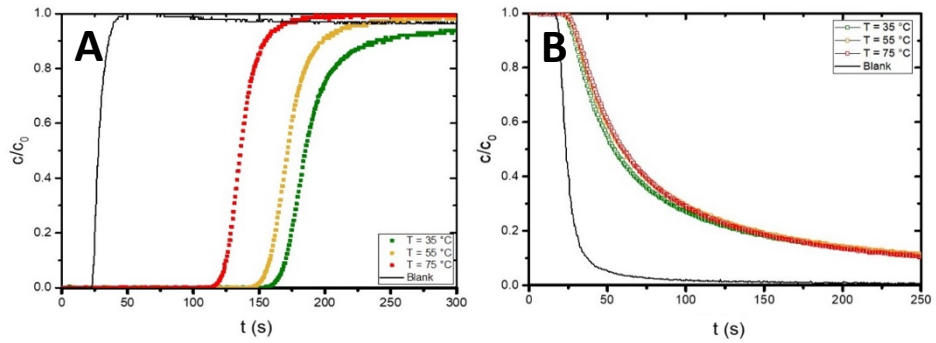

Figure 3-13. (A) Adsorption and (B) Desorption breakthrough curves for Na-Clino at 35 °C, 55 °C and 75 °C.

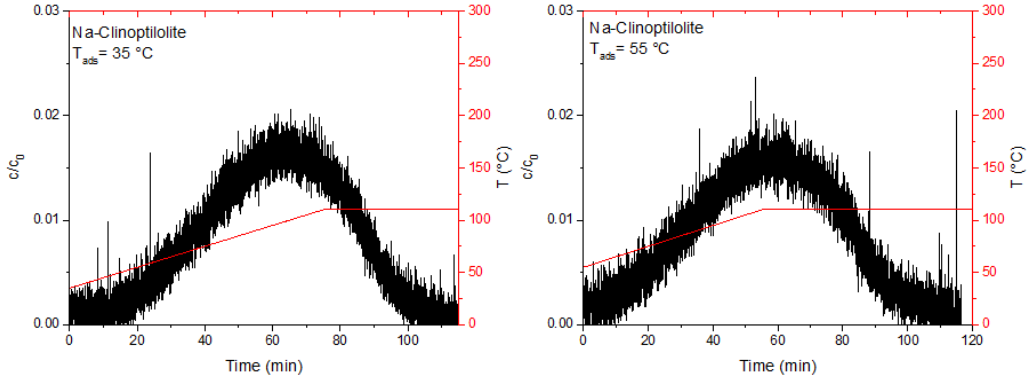

Figure 3-14. TPD analysis for Na-Clino at 300 °C performed after desperation tests (at 35 °C and 55 °C).

Table 3-5. The adsorption capacities of Na-Clino at different temperatures during three cycles and a TPD stage.

Temperature (°C)	N. Cycles	Adsorption	Desorption
		Capacity (mol/kg)	
35	1st Run	1.13	0.81
	2nd Run	0.80	0.78
	3rd Run	0.80	0.78
300	TPD	-	0.34
55	1st Run	0.92	0.80
300	TPD	-	0.11
75	1st Run	0.68	0.64
300	2nd Run	-	0.01

3.4.2.3 K-Clino

The CO_2 adsorption performance of cation exchanged Clino, as discussed before, are affected by the dimension and charge density of cations. Among the alkali metal cations the ionic radius of cation are changing in this order $Li^+ > Na^+ > K^+ > Cs^+$. Here the CO_2 adsorption capacity of K-Clino has shown to be the largest among all other alkali metal exchanged Clino. The results obtained from the ZLC analysis are reported in **Figure 3-16**, **Figure 3-15** and **Table 3-6**. This unveiled that along with the electrical charge density and size of cations their distribution on the Clino framework has an important impact on their CO_2 uptake. Therefore, the larger CO_2 capacity of the K-Clino comparing to Na-Clino can be induced by the complete exchange of K^+ with the clinoptilolite framework since one of the dominant cations presents in the clinoptilolite before cation modification was K^+. As compared to the results obtained in **Chapter 2** the alkali methal cations tested here including K^+ and Na^+ are presenting higher adsorption capacity respecting to Ca^{2+} exchanged Clino.

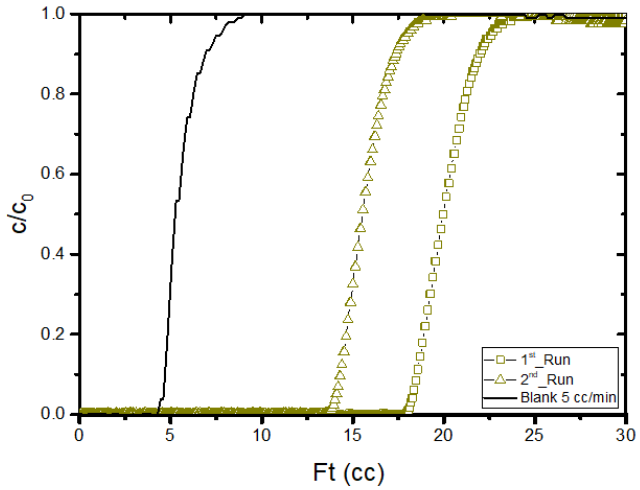

Figure 3-16. Adsorption breakthrough curves for K-Clino during 3 cycles as plotted in c/c0 vs. Ft.

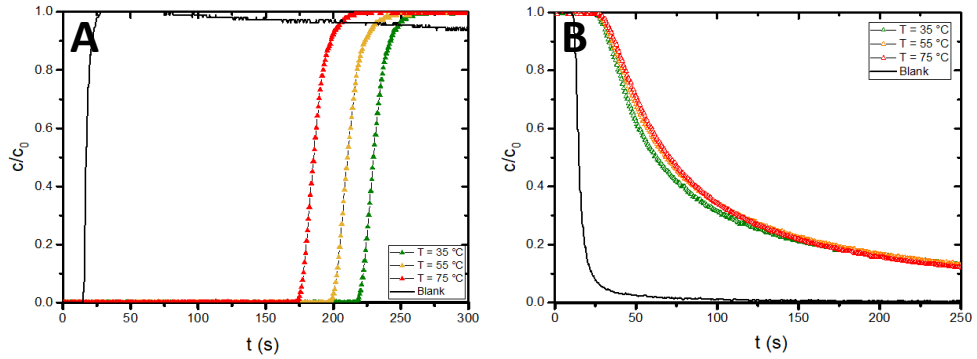

Figure 3-15. (A) Adsorption and (B) Desorption breakthrough curves for K-Clino at 35 °C, 55 °C and 75 °C.

Table 3-6. The adsorption capacities of K-Clino at different temperatures during three cycles and a TPD stage.

Temperature (°C)	N. Cycles	Adsorption	Desorption
		Capacity (mol/kg)	
35	1st Run	1.25	1.05
	2nd Run	0.95	0.94
	3rd Run	0.91	0.89
300	TPD	-	0.21
55	1st Run	1.14	0.97
300	TPD	-	0.13
75	1st Run	1.00	0.89
300	2nd Run	-	0.10

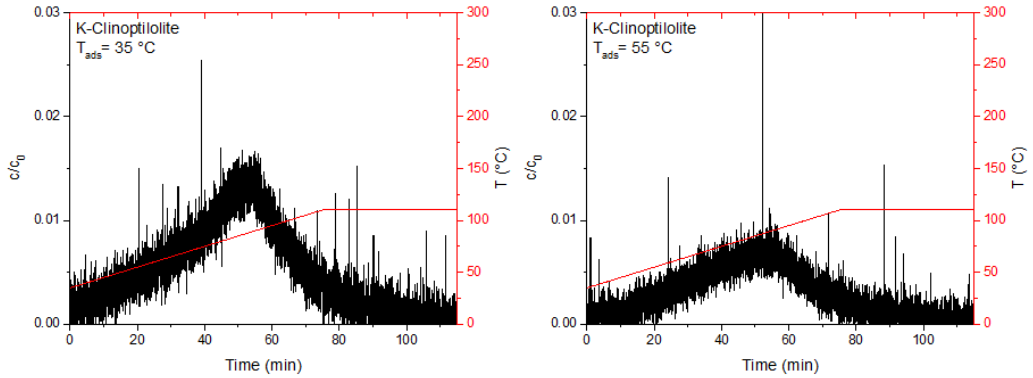

Figure 3-17. TPD analysis for K-Clino at 300 °C performed after desperation tests (at 35 °C and 55 °C).

3.4.2.4 Cs-Clino

The overall adsorption capacity of CO_2 on the Cs-Clino is the lowest among the cation-exchanged samples (i.e. it is lower than in Na-Clino and K-Clino). This can be explained by the larger size of Cs^+ ions and its lower charge density that affects the overall CO_2 uptake by limiting the accessibility of CO_2 molecules to the pore channels of the Cs-Clino. The relevant CO_2 adsorption and desorption breakthrough curves of Cs-Clino during different cycles and at various temperatures are presented in **Figure 3-18**, **Figure 3-19** and **Table 3-7**. These results indicate that a high portion of the CO_2 is adsorbed via physically weak bonds. In fact, by referring to the data reported in **Table 3-7**, it is evident that most of the CO_2 adsorbed during the 1st cycle is released. At the temperatures of 55 °C and 75 °C almost all the CO_2 is removed during the desorption run. Thus, in the TPD analysis, no CO_2 peak is observed.

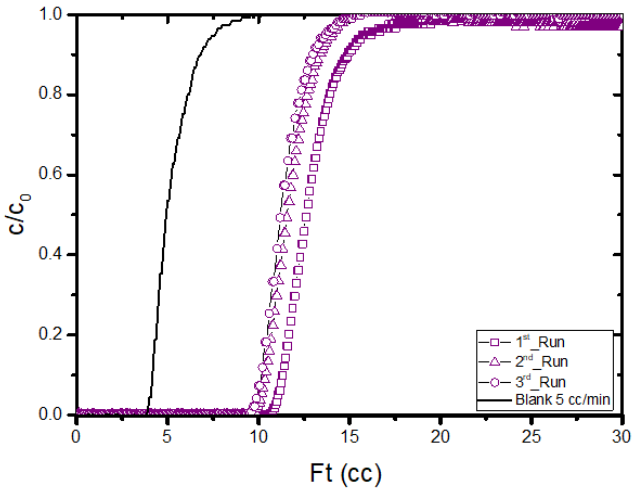

Figure 3-18. Adsorption breakthrough curves for Cs-Clino during 3 cycles as plotted in c/c0 vs. Ft.

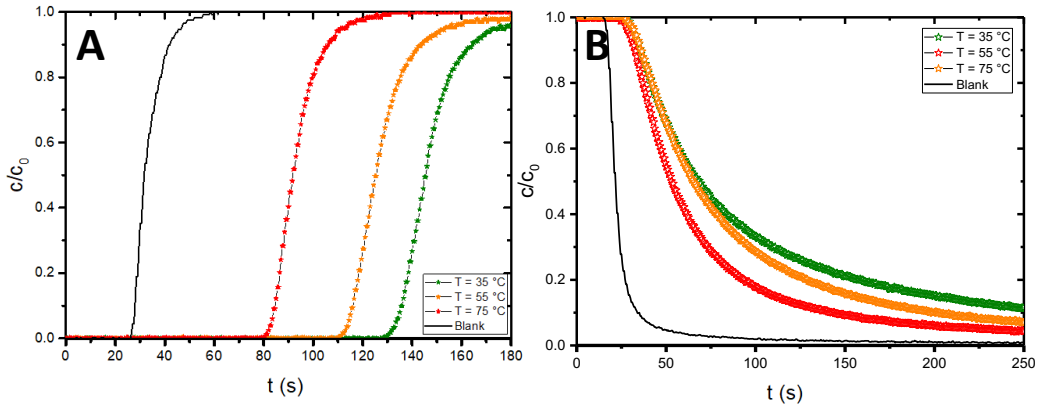

Figure 3-19. (A) Adsorption and (B) Desorption breakthrough curves for K-Clino at 35 °C, 55 °C and 75 °C.

Table 3-7. The adsorption capacities of K-Clino at different temperatures during three cycles and a TPD stage.

Temperature (°C)	N. Cycles	Adsorption	Desorption
	Capacity (mol/kg)		
35	1st Run	0.67	0.63
	2nd Run	0.57	0.56
	3rd Run	0.57	0.56
300	TPD	-	0.092
55	1st Run	0.54	0.49
300	TPD	-	0.01
75	1st Run	0.31	0.30
300	2nd Run	-	0.01

3.4.3 Conclusion

The CO_2 uptake measurements and kinetics analysis were carried out for Clino, Na-Clino, K-Clino and Cs-Clino using the ZLC column. The response curves of CO_2 interaction with all the samples plotted in terms of Ft plot showing that the the mass transfer mechanism can be approximated by an equilibrium controlled behavior. However, the adsorption capacity is varying as follows: K-Clino > Na-Clino > Clino > Cs-Clino. This verifies the effect of the cation charge density and its distribution on the sorbent on the adsorption capacity; indeed, the alkaline cations (K^+ and Na^+) carrying higher electrostatic charges reported the higher CO_2 adsorption caapcity. The Henry Law constant was obtained from the ZLC results which is changing in the following order K-Clino > Na-Clino > Cs-Clino ≈ Clino. The larger amount of Henry Constant related to K-Clino and Na-Clino is coresponding to the presence of strong cations of K^+ and Na^+ on the sorbent surface. The smaller ionic radius and the bigger charge density of the K^+ and Na^+ induce an increase in the surface heterogeneity of the sorbent. Eventually, this contributed to the higher adsorption capacity for K-Clino and Na-Clino.

The stability and reproducibility of the adsorption capacities were tested by repeating the tests in three cycles. These experiments confirmed that the CO_2 is partly adsorbed via physical interaction, which can form linear adducts. The nature of such adsorbed CO_2 depends on the strength of the adsorption sites presence on the structure of the sorbent. The other part of CO_2 is adsorbed as carbonate-like species that are mostly formed at basic sites. The presence of the strongly adsorbed CO_2 on the sorbent was verified by performing TPD analysis. Hence, the amount of CO_2 adsorbed at the higher temperature of 75 ^oC was shown to be mostly due to the weak interactions. This reduces the energy input for the regeneration of the samples and increases the sorbent adsorption stability, giving promising results for the application of Clino, Na-Clino and K-Clino for removal of CO_2 from hot flue gases.

Chapter 4

4 From Biogas to Biomethane: Modelling a Fixed-Bed Adsorber for CO_2 Removal

Some part of this chapter of the thesis has been published in the 18th European Control Conference (ECC) with the following description:

L. Bisone, S. Bittanti, S. Canavese, E. Davarpanah, A. De Marco, M. Notaro and V. Prandoni, Model-based Design of a Control System for the Upgrade of Biogas with Zeolite Sorbent Reactors, DOI: 10.23919/ECC.2019.8795932.

Abstract

The upgrade process of biogas to biomethane, by CO_2 removal from CH_4 in a fixed-bed reactor packed with zeolite 13X pellets is investigated. The experimental results are obtained from a pilot-plant installed in an industrial landfill producing biogas from domestic waste disposal. The experiments are analyzed during three stages of adsorption, regeneration and cooling. The adsorption phase is carried out at a low temperature of 20 °C, due to the exothermic nature of the process, to attain a high efficiency. Following the adsorption stage, the regeneration takes place in a TSA configuration by heating the system up to 85 C° and depressurizing it to 100 - 500 mbar under low purge flux of N_2. A mathematical model is developed for interpreting the experimental data and predicting the dynamic behaviors of all three process stages. The operability of each phase is exploited by means of a one-dimensional model using mass, energy and momentum balances. To solve these equations the equilibrium isotherms for pure CO_2 are also measured and validated

by the Toth model isotherm. Model parameters are optimized by validating the model with the experimental data.

Keywords: Post-combustion CO_2 capture, Biogas upgrading, Zeolite 13X, Process modeling, Breakthrough curves.

4.1 Introduction

The emerging renewable energies are aimed to replace fossil fuels as the main cause of greenhouse gas emission and climate change. Among such energies, one sustainable source is biomethane recovered from biogas which is produced by landfill or anaerobic digestion of waste disposal. Biogas cleaning and upgrading to biomethane occur through the removal of any gas contaminants and separation of CO_2 from CH_4 [122]. Such a process is similar to post-combustion CO_2 capture methods, though the existing technologies developed for CO_2 separation from industrial streams can be implemented for biogas treatment. The post-combustion capture technologies up to date are thermal [123] or pressure swing adsorptions [124], solvent scrubbing, physical adsorption, membrane and cryogenic separation [125,126]. However, the absorption process with the solvent suffers from a high energy penalty which makes this technique less economic. Alternatively, adsorption processes due to their low regeneration energy and high CO_2 capture efficiency are considered a cost-effective CO_2 separation method [127]. Conventional solid sorbents applied for CO_2 adsorption are activated carbons, zeolites, metal oxides, mesoporous silicate and amine-based frameworks among which zeolite 13X, zeolite 5A and activated carbon have been extensively examined for CO_2 capture purposes. Apart from the sorbent selection, the choice of optimized adsorption process is to be made considering the maximum CO_2 capture efficiency. The adsorption processes implemented in industrial-scale are classified into temperature (TSA), pressure (PSA) or vacuum (VSA) swing adsorption according to their regeneration method [128]. Nevertheless, for the applications in which the adsorbent strongly interacts with the sorbent structure, TSA is preferred over PSA-based methods due to operational cost for pressure variation. Hence, TSA adsorption is also suffered from high-temperature loads and long regeneration cycles. A combination of TSA/PSA is a good choice for overcoming the drawbacks of each particular TSA and PSA processes.

Most studies on adsorption processes are focused on numerical modeling and experimental analysis to achieve an effective design and to improve the energy consumption of the system [129]. Such numerical models after being validated by experimental results are expected to be capable to predict the dynamic behavior of adsorption for different sorbents, configurations and operational conditions at low cost [130]. Although several studies are established for simulating the PSA system [131], few studies have investigated the TSA model for single and binary mixtures [132] or the combination of the two methods.

To simulate the adsorption process for a TSA configuration of a pilot-scale, a full characterization of the CO_2 /CH_4 or/and CO_2/N_2 equilibrium data on the sorbent zeolite 13X is required. The equilibrium data for different components present in this work are taken from studies performed previously on zeolite 13X [133]. Some of these works have discussed the CO_2 molecular mass transfer on zeolite 13X, which verified the macro-pore diffusion control behavior of the sorbent [80]. Moreover, for determining the dynamic performance of the system the mass and heat transfer phenomenon has to be defined properly.

In this work, a mathematical model for the adsorption process is developed by using equilibrium equation and mass, heat and momentum balances for each component and the whole system. Experimental data regarding breakthrough curves and gas temperature profiles are used to validate the model and to determine the mass and heat transfer parameters. Such information is obtained by using a fixed-bed reactor with a rectangular cross-section and filled with zeolite pellets during three phases including adsorption, desorption and cooling. Here the regeneration stage is performed in a combined TSA mode through the system heating up to 85 °C.

4.2 Experimental Section

4.2.1 Experimental setup

The pilot-scale reactor used in this work for adsorption/desorption tests is a fixed-bed reactor with a rectangular cross-section area, which was described previously in [134] and is shown in **Figure 4-1**. The reactor is made up of 4 separate modules each of them composed of 8 independent channels. The cooling and heating of the reactor during the adsorption and regeneration phases are controlled by tubes passing through both reactor external wall and internal section to guarantee an effective heat exchange between the sorbent and the gas stream. This type of heat exchanger assures a homogeneous temperature distribution along the reactor, both axially and radially. Each channel is packed with the porous pellets of zeolite 13X. The dimension of the reactor along with the properties of the sorbent are reported in **Table 4-1**. The reactor is designed to treat a biogas flowrate of 1 Nm^3/h. Biogas stream before entering the adsorption column is passing through a pre-treatment column filled with activated carbon to dehumidify the gas and to clean it from any traces of H_2S or any other contaminants. In the adsorption column, the temperature of the gas stream is monitored by several thermocouples located in every channel at the entrance, in the middle and at the end of the reactor. The gas outlet composition is measured by an ABB Gas analyzer able to monitor CO_2 and CH_4 gas. The system can operate in automated, semi-automated and manual modes for switching between different phases.

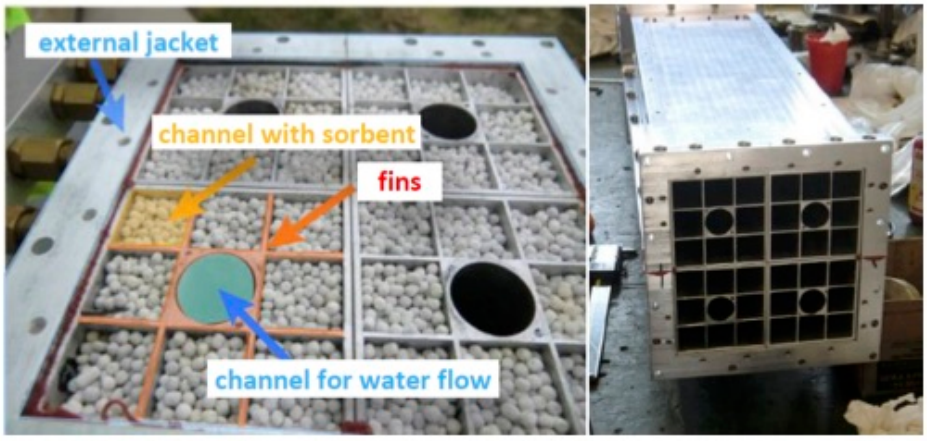

Figure 4-1. Fixed-bed reactor for adsorption with a rectangular cross-section filled with zeolite 13X.

4.2.2 Breakthrough experiments: Adsorption, Desorption and Cooling phases

The three stages of the process as discussed before are adsorption, regeneration and cooling as presented in **Figure 4-2**. During the adsorption step, the column temperature is maintained constant at the desired operating temperature using a thermal fluid pumped by a circular bath (Julabo chiller). The CO_2 and CH_4 outlet concentrations are recorded, once the CO_2 concentration in the outlet arrived at 1% of its inlet concentration, the column is switched to the desorption phase. Here, the adsorption tests are performed at 25 °C.

The desorption stage is configured to work as a temperature swing process in which the column temperature is increased gradually to 85-90 °C with a ramp of 1 °C/min. The column is purged continuously during this stage using N_2 gas with a low flowrate (almost 0.1 Nm^3/h). The heating/cooling thermal fluid is circulating in the column with a flow rate of 1.3-1.5 m^3/h. Desorption time for the column is 1 h, and there is no transition time between the adsorption and desorption phases.

Finally, the cooling step is initiated by cooling down the column to the adsorption temperature and pressurizing the system to 1 bar. Similarly, in this phase, no transition time is considered relative to the former one. The initial composition of biogas and its properties are reported in **Table 4-1**.

Table 4-1. Setup dimension and properties of zeolite 13X used as an adsorbent.

Sorbent zeolite 13X	Symbol	Value	Unit
pellet diameter	D_p	0.001	[m]
particle density	ρ_p	1358	[kg/m^3]
particle porosity	ε_p	0.4	-
heat capacity of sorbent	C_s	1200	[J/ (K kg)]
sorbent mass	M_s	6.835	[kg]
Experimental setup			
column length	L	1	[m]
channel width	R_i	0.018	[m]
number of modules	-	4	-
number of channels	-	8	-
wall thickness	t_w	0.002	[m]
bulk density	ρ_b	630	[kg/m^3]
bulk porosity	ε_b	0.55	-
Total porosity	ε_t		-
heat capacity of wall	C_w	920	[J/ (K kg)]
Biogas			
CO_2 molar fraction	y_{CO2}	0.65	-
CH_4 molar fraction	y_{CH4}	0.35	-
density	ρ_{biogas}	1.05	Kg/m^3
heat capacity biogas	C_p	1360	[J/ (kg K)]
biogas viscosity	∂	1.32e-5	Pa.s

4.3 Numerical Model

To model the adsorption process, the mass, momentum and heat transfer equations coupled with the kinetic equation are solved. These equations are written

as partial differential and algebraic equations (PDAE) for the gas phase (adsorbent) and the solid phase (adsorbate). Finally, the initial and boundary conditions have to be chosen properly to define correctly the dynamic response of the system in terms of gas outlet concentration and temperature profiles. Several assumptions are considered for developing this model including:

- The biogas is considered to be composed of only CO_2 and CH_4 molecules and is treated as an ideal gas;
- The concentration, temperature and velocity gradient is neglected in the radial coordination;
- The Linear Driving Force (LDF) model is used to identify the mass transfer resistance between the gas phase and the adsorbent;
- The isosteric heat of adsorption is considered to be constant.

For the kinetic equation, different works have applied the LDF model to the gas mass transfer into the porous adsorbent [132,135]. Such works showed that the LDF model satisfies the mass transfer conditions and makes the calculation computationally less complicated. The main equations for the numerical model of the process based on these assumptions are described in the following sections.

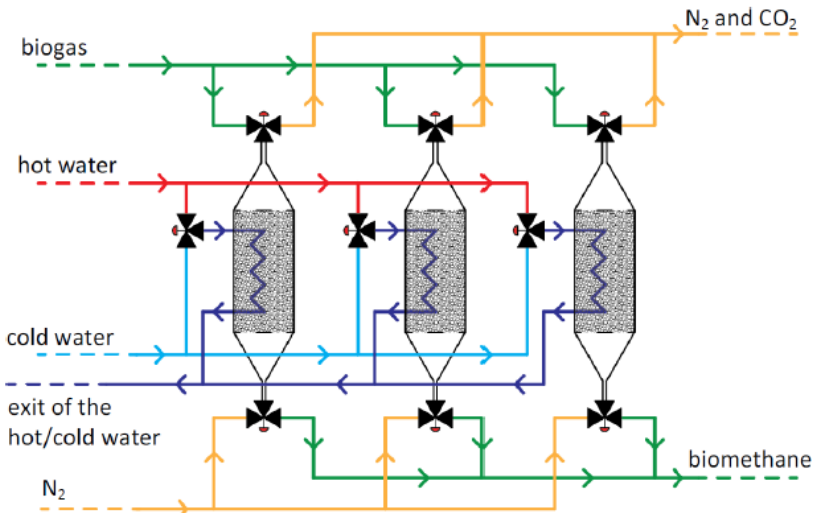

Figure 4-2. The cyclic configuration of the three stages of the process including the adsorption, desorption and cooling.

4.3.1 Mass Balance

The mass balance for each component describes as:

$$\varepsilon \frac{\partial c_i}{\partial t} + \varepsilon \frac{\partial (u_{avg} c_i)}{\partial z} + (1-\varepsilon)\rho_p \sum_{i=0}^{j} \frac{\partial \bar{q}_i}{\partial t} - \varepsilon \mathrm{D} \frac{\partial^2 c_i}{\partial z^2} \qquad (4\text{-}1)$$

In this formula, the effect of axial dispersion has been neglected. While the total mass balance is the sum of all component's mass balance written as:

$$\mathcal{E}\frac{\partial c_{tot}}{\partial t} + \mathcal{E}\frac{\partial\left(u_{avg}c_{tot}\right)}{\partial z} + (1-\mathcal{E})\rho_p \sum_{i=0}^{j} \frac{\partial \bar{q}_i}{\partial t} = 0 \tag{4-2}$$

To satisfy the mass continuity condition the total concentration is equal to the sum of component concentration ($C_{tot} = \Sigma C_i$ = constant). Therefore, **Equation (4-2)** can be simplified to **Equation (4-3)** [136].

$$\mathcal{E}c_{tot}\frac{\partial\left(u_{avg}\right)}{\partial z} + (1-\mathcal{E})\rho_p \sum_{i=0}^{j} \frac{\partial \bar{q}_i}{\partial t} = 0 \tag{4-3}$$

The first term $\mathcal{E}\frac{\partial c_{tot}}{\partial t}$ sets to zero due to the fact that the total concentration or pressure of the ideal gas does not change with time at a particular grid point. However, $\mathcal{E}\frac{\partial c_{tot}}{\partial z}$ being zero means that the concentration or pressure of the ideal gas does not change along the length of the reactor at any given time.

Where the gas is considered to behave as an ideal gas. The behavior of which can be presented by the Equation of States as follows:

$$y_i P = \frac{c_i}{RT} \tag{4-4}$$

The gas velocity in the column is calculated as a function of the pressure gradient in the column using the Ergun equation.

$$\frac{\partial P}{\partial z} = \frac{150\mu(1-\varepsilon)^2}{\varepsilon^3 {d_p}^2}\mathrm{u} - \frac{1.75(1-\varepsilon)\rho}{\varepsilon^3 {d_p}^2}|u|\mathrm{u} \tag{4-5}$$

where ρ is the fluid density; μ is the dynamic viscosity and dp is the particle diameter.

The mass transfer rate between the gas and the adsorbent surface proportional to the LDF model is written for the solid phase as:

$$\frac{\partial \bar{q}_i}{\partial t} = k_{LDF}\left(q_i^{eq} - q_i^t\right) \tag{4-6}$$

Here, k_i is the mass transfer coefficient and q_i^{eq} is the concentration of the adsorbed phase at equilibrium. The LDF model assumes a lump coefficient for all mass transfer coefficients including the film resistance at the surface of the adsorbent and macropore or micropore resistances for the adsorbate inside the particles. The LDF model has been successfully applied to describe the dynamic

behavior of the adsorption column for different types of adsorbent transfer into the particle pores.

4.3.2 Energy balance

The energy balance for the gas phase in thermal equilibrium with the solid phase and the adsorbed phase can be described as:

$$\varepsilon_t \rho_g C_g + (1-\varepsilon_t)\rho_p (C_s + C_{ads})\frac{\partial \mathrm{T}}{\partial t} - (1-\varepsilon)\rho_p \sum_{i=0}^{i} (-\Delta H_i)\frac{\partial \bar{q}_i}{\partial t} + \mathrm{u}\rho_g C_g \frac{\partial \mathrm{T}}{\partial z} + \frac{2h_b}{R_{in}}(\mathrm{T} - T_w) = K_T \frac{\partial^2 \mathrm{T}}{\partial z^2} \tag{4-7}$$

Where the parameters are inside the equation are h_b is the heat transfer coefficient between the adsorbent bed and the wall; ΔH is the isosteric heat of adsorption which is considered constant; Cg, Cs and Cads are respectively the specific heat of the gas phase, adsorbent bed and the adsorbed phase and K_T is the thermal conductivity coefficient of the bed.

The energy balance corresponding the temperature of the column wall is described as:

$$\frac{\partial T_w}{\partial t} = \frac{2}{C_w(R_{out}^2 - R_{in}^2)}\left(h_b R_{in}(T - T_w) - h_w R_{out}(T_w - T_f)\right) + K_T \frac{\partial^2 \mathrm{T}}{\partial z^2} \tag{4-8}$$

The wall is exchanging heat with the adsorbent bed and the fluid circulating in the reactor jacket. While the energy balance for the thermostatic fluid in the reactor jacket is stated as:

$$\frac{\partial T_f}{\partial t} = \frac{2h_f R_{out}(T_w - T_f)}{C_f(R_{out}^2 - R_{in}^2)} + V_f \frac{\partial T_f}{\partial z} \tag{4-9}$$

The temperature of the fluid circulating in the reactor jacket is evaluated by solving all the heat and mass balance equations together.

4.3.3 Boundary and initial conditions

The boundary conditions reflect the inlet and outlet conditions of the gas stream. Here, the Danckwerts boundary conditions are implemented which is applicable to the finite difference discretization scheme. The boundary condition for the inlet and outlet flow is expressed as:

$$uc_{i\,z=0} - D\frac{\partial c_i}{\partial z}|_{z=0} = uc_{i\,IN} \tag{4-10}$$

$$D\frac{\partial c_i}{\partial z}|_{z=0} = 0 \tag{4-11}$$

The Danckwerts boundary condition for the temperature is written as follows:

$$uc_g T_{i\,z=0} - k_T\frac{\partial T_i}{\partial z}|_{z=0} = uc_g T_{i\,IN} \tag{4-12}$$

$$uC_g\frac{\partial T_i}{\partial z}|_{z=0} = 0 \tag{4-13}$$

The initial condition is written as

$$C_i(z,0) = C_0\ ;\ q_i(z,0) = 0;\ \ T_i(z,0) = T_0\ ;\ T_w(z,0) = T_\infty \tag{4-14}$$

4.4 Results and Discussions

4.4.1 Solving procedure and parameter identification

The finite difference method is used to solve the one-dimensional Partial Differential Equations (PDEs) by discretizing the reactor length (L) into N strips of constant width Δz = L/N as shown in **Figure 4-3**. In each strip, the sorbent and the gas behavior are described by ODEs obtained by integrating the PDE along the reactor length. The numerical solution for the mathematical model is compiled by using the MATLAB function of ode 15s able to solve a set of ODEs. The complete process is simulated considering a unique column for each step until arriving at the steady-state, where the outlet concentration and temperature of each column remain constant.

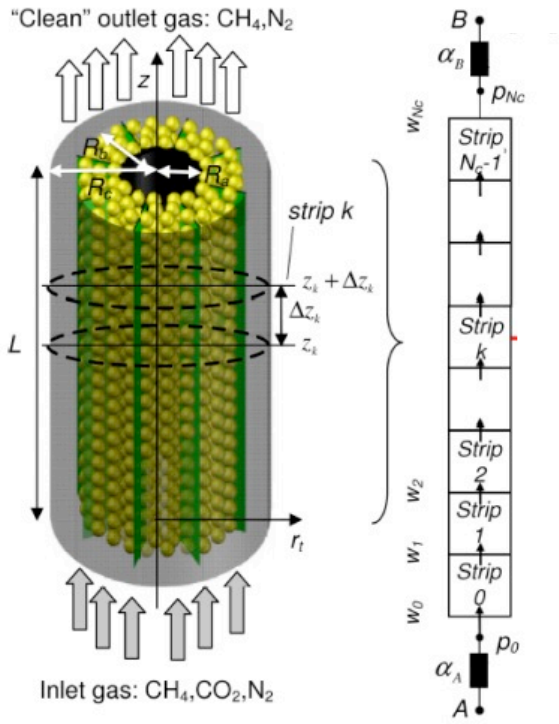

Figure 4-3. The discretization scheme of the reactor in which the reactor is divided into N number of strips of length Δz. For each strip, the gas and the adsorbent behavior is described by a set of PDEs.

4.4.2 Adsorption equilibrium model: parameter identification

To govern a rigorous numerical model for the adsorption process the equilibrium isotherm and kinetic data are required. The adsorption equilibrium data provides information on the adsorption behavior of pure CO_2 and CH_4. The relevant isotherms are taken from the study done on the adsorption equilibrium of CO_2, CH_4 and N_2 on zeolite 13X by S. Caventai et al [25]. In their work, the adsorption equilibrium data are measured by a magnetic suspension microbalance and fitted with different isotherm models. Here the data obtained from the multisite Langmuir isotherm are used. The corresponding equation of the model is as follows:

$$\frac{q_i}{q_{mi}} = \theta = K_i P \left(1 - \frac{q_i}{q_{mi}}\right)^{ai} \tag{4-15}$$

$$K_i = K_i^0 \exp\left(-\frac{\Delta Hi}{RT}\right) \tag{4-16}$$

In this model, the isosteric heat of adsorption is considered constant. The parameters explaining the model are: a_i that is the number of sites occupied by each component and K_i that is the equilibrium constant (as a function of temperature). The corresponding multisite Langmuir model parameters at 298 K are given in **Table 4-2** [25].

Table 4-2. Multisite Langmuir Isotherm parameters of the studied adsorption systems [25].

Gas	Q_{mi} (mol kg^{-1})	K_i^0 (MPa^{-1})	ΔH_i (kJ mol^{-1})	a_i
CO_2	17.9	3.20×10^{-8}	54.73	13.12
CH_4	28.8	4.34×10^{-4}	15.67	8.14

4.4.3 Parameter Identification

The estimation of the model parameters is done by comparing the experimental data with the simulation data. The parameters to be compared are the concentration of the CH_4 and CO_2 in the reactor outlet and the temperature of the bed at the inlet and the outlet of the reactor. The kinetics and heat transfer coefficients to be estimated are respectively K_{CO2}, K_{CH4} and h_L. To do so the routine optimization toolbox fmincon of MATLAB is used which gets the closest solution to the experimental data by the following equation:

$$min \sum_{n=1}^{ni} [y_{exp,i} - y_{sim,i}(X)]^2 < \delta \tag{4-17}$$

Where X is the K_{CO2}, K_{CH4} and h_L; ni is the total number of experimental data at the test operational conditions. This function optimized the simulation parameters by minimizing the sum of the squares of the errors between the experimental and modeled data. One of the constraints for this function is obtaining the steady-state condition where the concentration of each component in the outlet is less than 1% of the feed's concentration.

The mass transport of CH_4 and CO_2 into the pores is confirmed to be controlled by molecular diffusion in the macropores [80]. Therefore, the mass transfer coefficient in the LDF model can be experimentally assumed with the following expression:

$$\text{Ki} = \frac{15\varepsilon_p Di_{eff}}{{r_p}^2} \frac{C_i}{q_i^*} \tag{4-18}$$

Where ε_p and r_p are respectively the particle porosity and radius, while Di_{eff} is the effective macropore diffusivity. The Di_{eff}/ r_p^2 is the diffusion time constant [s^{-1}] where the Di_{eff} parameter corresponds to the:

$$Di_{eff} = \frac{\varepsilon_p D_p}{\varepsilon_p + (1 - \varepsilon_p) K_i} \tag{4-19}$$

Here, k_i is the equilibrium constant as expressed in **Equation (4-16)**, which is shown to be a strong function of temperature [137]. Moreover, the heat transfer coefficient of h_L can be assessed by using the following correlations [138]:

$$Nu = \frac{h_L 2R_i}{K_L} = 0.813Re^{0.9}\exp\left(-\frac{6D_p}{2R_i}\right) \quad (4\text{-}20)$$

$$Re = \frac{\rho_g u D_R}{\mu_g} \quad (4\text{-}21)$$

Ri is the radius of the column, Dp is the diameter of the particle and K_L is the axial thermal conductivity. The initial value used for h_L is calculated using the **Equation (4-20)** which is a function of fluid Reynold number. The axial thermal conductivity is calculated by the following relationships [137]:

$$K_L = D_L C_g \quad (4\text{-}22)$$

$$D_L = \gamma_1 D_m + \gamma_2 d_p \frac{u}{\varepsilon} \quad (4\text{-}23)$$

Where D_L is the dispersion coefficient calculated as a function of molecular diffusivity and turbulent mixing. The values for the γ_1=0.7 and γ_2=0.5 are the tortuosity and turbulent mixing taken from Ruthven [137]. The related parameters obtained for the

4.4.4 Model validation for one column

The essential parameters for the model including the physical properties of the fluid and the adsorbent as long as the equilibrium data are reported respectively in **Table 4-1** and **Table 4-2**. The initial estimates for K_{CO2}, K_{CH4} and h_L parameters are calculated using the empirical correlations summarized in **Section 4.4.3**. The model validation is performed comparing the transient time obtained from the model and the experimental data at 20 °C with a CO_2 molar fraction of 20 %. The experimental variables to be modeled are the outlet CO_2 molar fraction, the sorbent temperature in the initial section and the sorbent temperature at the final section of the adsorption column.

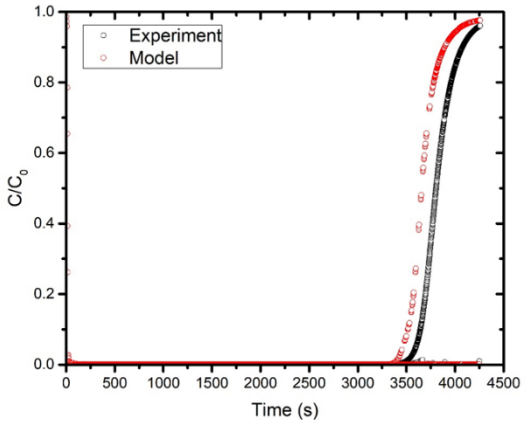

Figure 4-4. Model validation: comparison of the molar fraction of CO_2 at the reactor outlet from the experimental measurements and the model simulation.

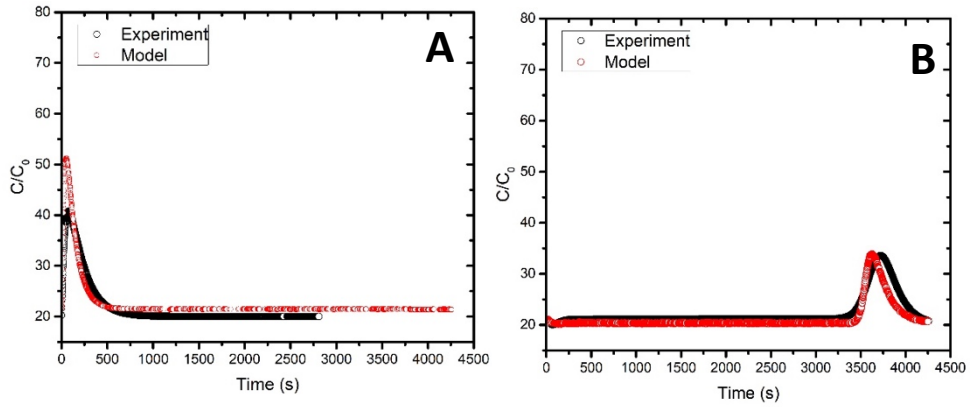

Figure 4-5. Model validation: comparison of the experimental measurements and the model simulation for (A) temperature at the reactor's initial section; the (B) temperature at the reactor's outlet (20 °C and 1 bar).

The values for K_{CO2} and h_L are calculated via correlations and by the fitting of the model with the experimental data. However, the parameter of K_{CH4} is obtained only by the empirical correlation to make the model less complex. This assumption is made based on the experimental data where it indicated that the CH_4 curve front breaks through with a transition time (τ_d) of 150 s. This value is much smaller compared with the breakthrough time for the CO_2 at the same condition which is at 1500 s. The corresponding values estimated are summarized in

Table 4-3. Estimated and fitted mass and heat transfer coefficients.

	K_{CO2} [s^{-1}]	K_{CH4} [s^{-1}]	h_L [W m^{-2} K^{-1}]
Empirical Correlation	0.10	0.002	8.8
Experimental Fitting	0.06	-	12

4.4.5 Interpretation of breakthrough analysis

The parameter identification and the model calibration are carried out using the results of a single experiment at 20 °C with a CO_2 molar fraction of 20 %. Such a model is used to predict all the data obtained from the other tests with CO_2 and CH_4 molar fractions of 40 vol% and 60 vol%, respectively, at temperatures of 20 °C, 40 °C and 80 °C. The results are represented the composition and temperature profiles of all the tests in **Figure 4-6**, **Figure 4-7** and **Figure 4-8**.

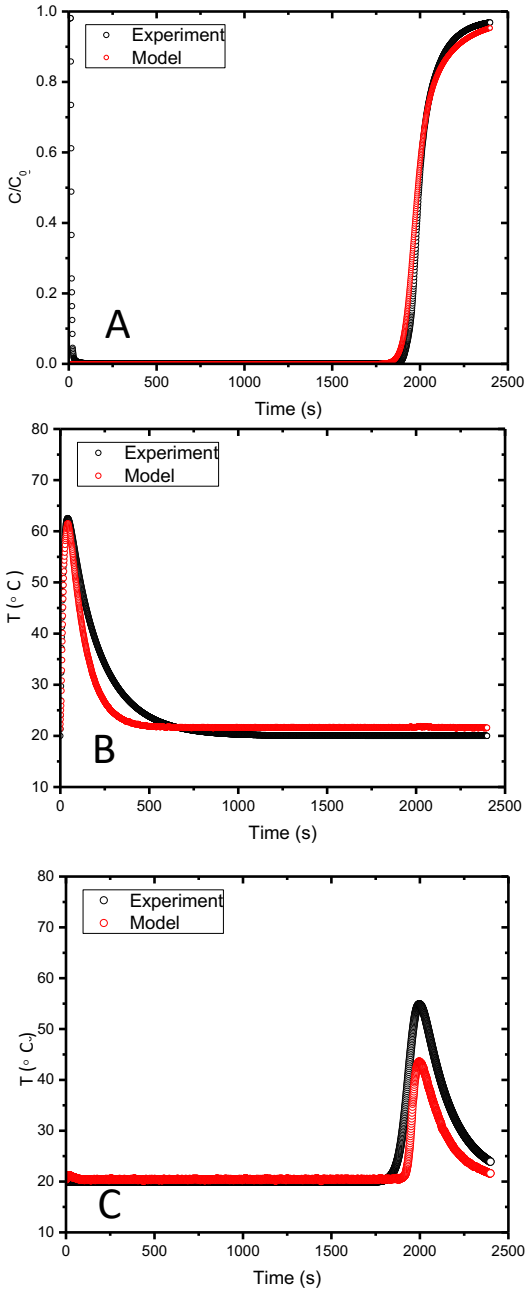

Figure 4-6. Comparison of the experimental data and simulated data for breakthrough and temperatures. (A) Exit profile of CO_2; (B) Inlet profile of temperature; (C) outlet profile of temperature. The experimental condition of CO_2/CH_4 mixtures of 40/60 v/v at 20 °C and 1 bar.

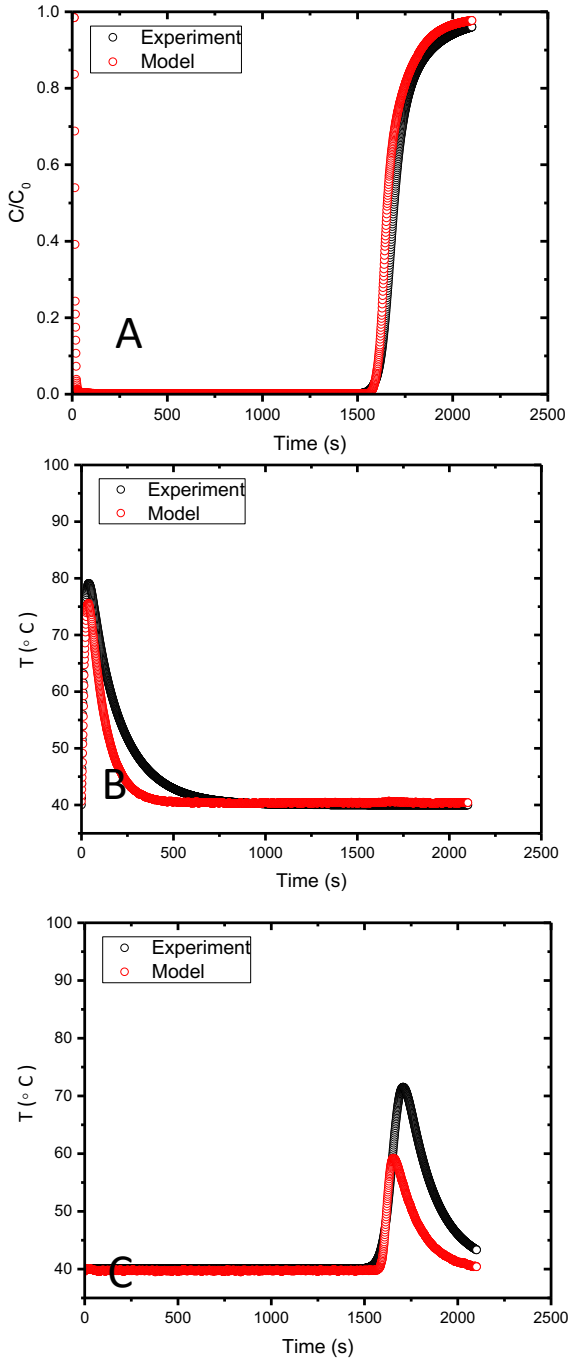

Figure 4-7. Comparison of the experimental data and simulated data for breakthrough and temperatures. (A) Exit profile of CO_2; (B) Inlet profile of temperature; (C) outlet profile of temperature. The experimental condition of CO_2/CH_4 mixtures of 40/60 v/v at 40 °C and 1 bar.

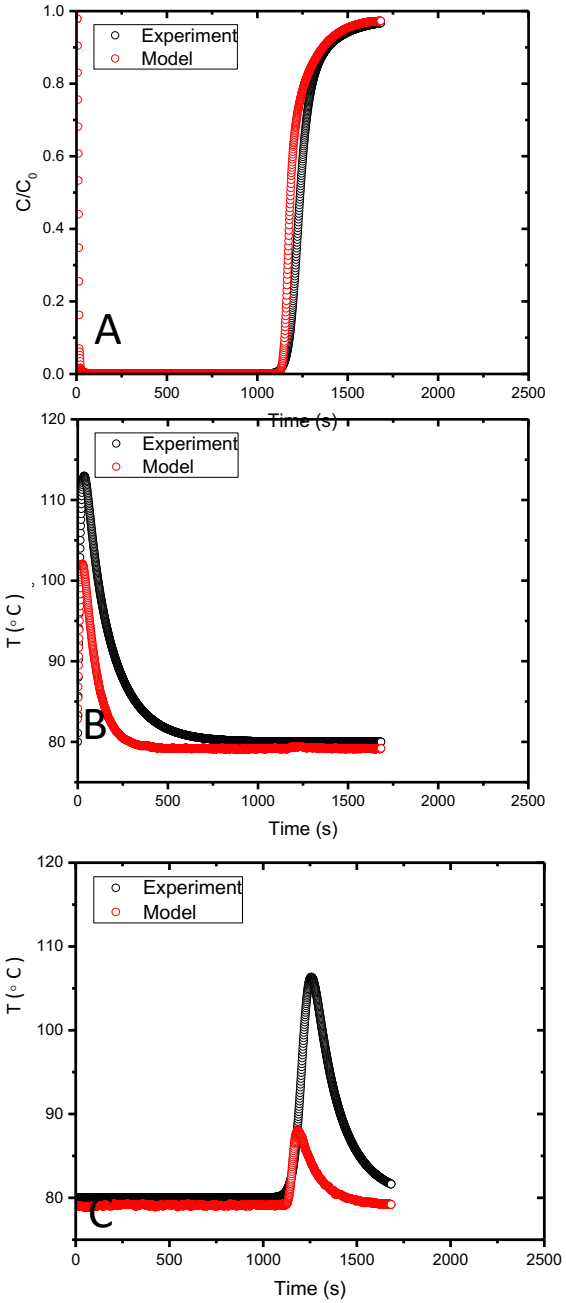

Figure 4-8. Comparison of the experimental data and simulated data for breakthrough and temperatures. (A) Exit profile of CO_2; (B) Inlet profile of temperature; (C) outlet profile of temperature. The experimental condition of CO_2/CH_4 mixtures of 40/60 v/v at 80 °C and 1 bar.

The results obtained showed a good interpretation of experimental data by the model over the entire range of temperatures. The CO_2 breakthrough curve is completely in agreement with the simulated data, which reveals that the overall pressure of the column is stable over the whole process. The difference between the experimental and simulated temperatures data can be attributed to several simplificatons used in the model: parameters such as the adsorption isosteric heat was also considered constant while it was observed to vary as a function of the CO_2

coverage (see Chapter 2), as well as the radial temperature profile in the column was neglected. Hence, the deviation between the experimental and the modelled data at the reference value of 20 °C **(Figure 4-5** and **Figure 4-6**) is smaller than the results found for the tests performed at different temperatures. This effect is strongly linked to the changes in the gas velocity associated with the gas adsorption along the fixed be column.

As can be seen in **Figure 4-5**, **Figure 4-6**, **Figure 4-7** and **Figure 4-8** the temperature in the column increases significantly with the movement of the CO_2 breakthough front due to the exothermic nature of the adsorption process. A large temperature peak corresponding to the CO_2 breakthrough front is observed, which at initial increased sharply; whereas after arriving at a peak's maximum value decreases slowly when the adsorbption bed became saturated. Indeed, the sharp initial increase indicates a fast mass transfer and the smooth tail implies the slow heat transfer from the sorbent to the reactor wall and then from the wall to the fluid circulating in the column jacket [138].

4.5 Conclusions

In this work, the behavior of a fixed-bed reactor packed with commercial zeolites 13X is reported for the upgrading of a biogas (CO_2 and CH_4) mixture. The experiments and simulations are done at a range of temperatures including 20 °C, 40 °C and 80 °C with a CO_2/CH_4 molar fraction of 20 and 40 vol%. The mathematical model is developed using the material, energy and momentum balances together with the kinetics and equilibrium equations. To estimate the parameters regarding the mass and heat transfer a single experiment is used as a reference. These validated parameters are used later to predict the adsorption behavior of the system at other process conditions. The estimated parameters are K_{CO2}, K_{CH4} and h_L which are respectively the kinetics coefficients for CO_2 and CH_4 and the heat transfer coefficient of the gas mixture. These parameters are firstly introduced in the model using empirical correlation and later been corrected through comparison with the experimental data by applying optimization methods.

Moreover, the isosteric heat of adsorption is reported from the literature work by s. Cavenati et al. [25]. Here, the heat of adsorption is considered to be constant during the whole adsorption process while in principle it is a function of both temperature and loading. This assumption makes the model numerical solution less complex.

The mathematical model developed in this work showed satisfactory results depending on the operating conditions. The simulated data for the gas molar fractions are in agreement with the experimental data. As we mentioned before the adsorption capacity of zeolite 13X for CO_2 as compared with CH_4 is much larger. This contributes to the fact that the CH_4 fronts appear after around 150 s. The match between the simulated and experimental breakthrough curves indicated the stable pressure gradient inside the column.

However, the temperature behaviors found by the model at different conditions are showing different consistency with the experimental data. The tests performed at operational conditions similar to the reference experiment exhibits better agreement. Whereas at higher temperature conditions, there a higher deviation of the temperature profiles at the inlet and outlet of the adsorption system. This demonstrates the importance of several features such as the feed velocity and the adsorption heat.

This model is used to predict the cyclic behavior of the adsorption process. The model gives insight into the issues in studying the adsorption process in a fixed bed reactor. The desorption and cooling stages can be included into the model by adding their corresponding equations. Here, it is worthy to optimize the model by using supplementary information to tune the model variables and control strategies of the system. In perspective, this type of model can be used to simulate the scale-up of new adsorbent materials such as Clino.

Chapter 5

5 Enhanced CO_2 absorption in organic solutions of Bio-based ionic liquids

This chapter of the thesis has been published in the Journal of Advanced Sustainable system with the following description:

E. Davarpanah, S. Hernàndez, G. Latini and S. Bocchini*, Enhanced CO_2 Absorption in Organic Solutions of Biobased Ionic Liquids, Adv. Sustainable Syst. 2020, 4, 1900067, DOI: 10.1002/adsu.201900067.*

Abstract

Solutions of bio-based ionic liquids (ILs) for recovering CO_2 from industrial flue gas are investigated. Four choline-based amino acids ([Cho][AA]): Alanine, Glycine, Proline, and Serine, which are task-specific for this purpose are tested. The drawbacks related to the high viscosity of these ILs were limited by applying DMSO as a solvent, which is chosen because it is a polar aprotic liquid with low toxicity, low vapor pressure, and relatively low price.

The choline-based amino acids synthesized in this study present aspiring absorption capacities (~ 0.3 mol CO_2/mol IL, with only 12.5 wt% IL in DMSO) and represent the best performing of task-specific ILs solutions at the state-of-art. These solutions are potentially competitive due to their low cost, low environmental impact, easy processability (due to their low viscosity) and good regenerability for the production and storage of highly pure CO_2.

5.1 Introduction

Climate change has been correlated with a strong increase in anthropogenic CO_2 emissions over the last century.[139] Thus, many research projects aim to limit these emissions by different processes. The first step often consists of the separation of CO_2 from the source stream, e.g. flue gases, to concentrate and purify it for further processing. Hence, CO_2 separation has a prominent role in the field of climate change mitigation.[140]

CO_2 separation is applied in carbon capture and storage concepts (CCS) in Integrated Gasification Combined Cycle units (pre-combustion carbon capture), fossil fuel power plants [141–143] and in the field of biomass conversion. Future applications for CO_2 separation technologies are presumed to be within the so-called carbon capture and utilization (CCU) route.[144–146] The idea is to exploit CO_2 as a raw material for further chemical or industrial use and, thus, to valorize it by its recycling. In the long term, CCU aims the development of a circular economy concept with neutral carbon emissions.

Absorption is one of the main techniques used for CO_2 capture [147], it relies on either chemical or physical interactions between the solvent and the solute CO_2. In physical absorption, intermolecular forces, such as Coulomb, Van-der-Waals or other dispersion forces dominate the solute-solvent interactions. In chemical absorption, CO_2 chemically reacts with the solvent molecules and forms covalent bonds. Due to their stoichiometric reaction with CO_2, the CO_2 absorption capacity is very high, already at low CO_2 partial pressures. Chemical absorption is particularly appropriate if CO_2 is to be recovered from flue gas streams with relatively low concentrations. The major advantages of chemical absorption processes are the high selectivity for CO_2 and the high achievable gas product purity.

The most commonly used chemical absorbents are amines (15-60 wt%) in aqueous solutions (*i.e.* typical loading of 0.5 mol CO_2/mol amine for monoethanolamine, MEA). Amines have some drawbacks like a high corrosion rate at high concentrations, the outlet purified gas contains a high-water amount, the energy demand for their regeneration is high and they suffer from high evaporation losses.[148] Indeed, the reverse chemical reaction requires considerable activation energy that is commonly supplied by increasing the temperature of the absorbent. When a volatile absorbent is used, it must be either condensed from the purified gas stream or replenished with the consequent rise of operative costs. Therefore, improvement of the absorption medium e.g. decreasing the volatility without losing the high loading of the absorbent phase is the primary research interest in physical and chemical absorption technologies.

Since the 1990s, low-melting salts have gained increasing interest for application as alternative absorbents in a wide field of chemical processes. For salts with melting points below 100 °C, the term ionic liquid (IL) has been coined. As ILs are built up from an organic cation and an inorganic or organic anion, there is a vast variety of possible structures. Over the last years, a plethora of ILs and their mixtures have been investigated and many reviews have been published in the field.

Their major positive features are their tunability, stability and low vapor pressure.[38] Their stability and tunability allows ILs to be designed according to the specific needs of an application (task-specific ILs, TSILs) and hence make them more flexible than conventional absorbents. A second strong point is that ILs mostly exhibit very low to negligible vapor pressures thanks to their ionic nature. This renders ILs particularly attractive for applications where evaporation of the absorbent should be avoided, thus decreasing energy duties in the regeneration columns and in the downstream condenser.

Many studies aimed at improving the absorbent performance by systematically varying IL structures and analyzing the effect on CO_2 solubility and selectivity have been performed. Among those, ILs that have shown promising results are fluorinated, N-functionalized (amine-functionalized or amino acid-based), carboxylate-based, reversible and protic ILs. In general, functionalization of the anion is reported to have a greater influence on performance than of the cation. However, functionalization often brings about stronger intermolecular interactions resulting in a higher viscosity. This, in turn, leads to a fall of diffusion coefficient by one or two orders of magnitude and, hence, to an unfavorable mass transfer behavior.

To resolve the issues of high viscosity and absorbent evaporation losses, ILs have been used in solution with other liquids with a high boiling point (e.g. polyethylene glycol) [149] or supported on porous inert material.[150,151] This practice of mixing ILs with common industrial solvents reduces the cost of using ILs, which represent the ILs main drawback (*i.e.* their high price).Furthermore, ILs are generally referred to as “green solvents”, but the most common cations (e.g. imidazolium and pyridinium) and anions (that are often fluorine-based) do not show good biodegradability and biocompatibility.[150,151] Thus, ions derived from metabolic molecules are possible environmental-friendly alternatives, e.g. choline (a proved non-toxic and biocompatible cation) [152–154] and amino acids (AAs, renewable, biodegradable, biocompatible and naturally-abundant anions). Since every AA contains amine functionalities, AA based ILs (AAILs) are in principle optimal task-specific anions to produce ILs for CO_2 absorption.[155] As an example, our recent study proved that solution in dimethyl sulfoxide (DMSO) of choline glycinate [Cho][Gly] and prolinate [Cho][Pro] have high absorption capacity and molar efficiency at low relative pressure 0.2 bar.[156]

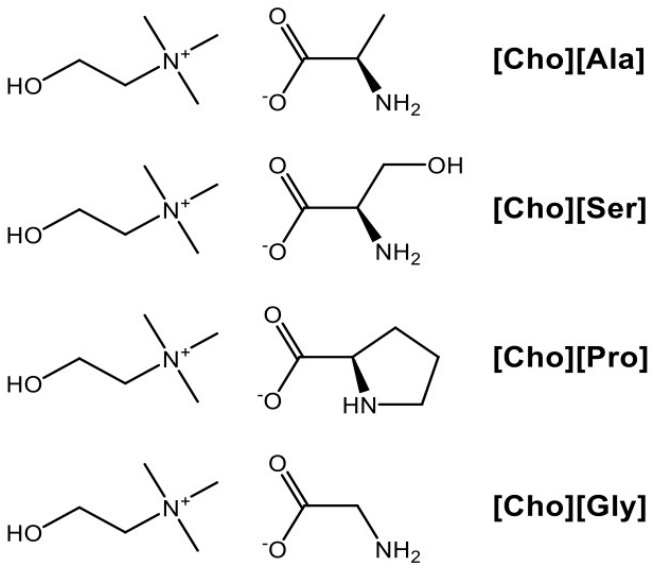

Scheme 5-1. Chemical structures of the four synthesized [Cho][AA] ILs.

In this study, the CO_2 absorption performance of four bio-based TSILs for industrial flue gas treatment was investigated. The four choline-based amino acids ([Cho][AA]) shown in **Scheme 5-1** were the TSILs tested for this purpose. An alternative to water, which has been employed as a solvent in most of the previous works, here we report the ILs application in solution with dimethyl sulfoxide (DMSO), a low vapor pressure organic solvent with a high boiling point (*i.e.* low volatility). DMSO was also chosen since it is a polar aprotic liquid, with low toxicity and a relatively low price. Due to those characteristics, DMSO is an advantageous solvent for ILs for maintaining low operative costs, energy duties and solvent losses during the regeneration process. The CO_2 absorption capacity of the [Cho][AA]s-DMSO solutions was calculated by monitoring the dynamic behavior of the system during the absorption process. The chemical interactions of such ILs and CO_2 were evaluated through IR analysis to identify which chemical species are formed and to explain the CO_2 desorption behavior of these systems. This study envisages how to address the regenerability of [Cho][AA]s ILs solutions, which is an important issue to face for industrial applications.

5.2 Experimental Section

5.2.1 Preparation of [Cho][AA]s solutions

The ILs were prepared using a previously developed methodology [16]. In a 250 mL flask, 0.5 mol of the chosen AA and an excess of potassium hydroxide (30.9 g, Carlo Erba, purity ≥85%) are mixed at RT in ethanol (200mL, supplied by Merck, purity ≥99.8%) under stirring. The potassium salt of the AA is formed, the suspension turned white while the excess of potassium salt precipitates. Once the potassium hydroxide pellets dissolved completely (c.ca 2 h), the choline chloride (69.8 g, supplied by Alfa Aesar, purity ≥98%) was added. The mixture was left under stirring for 4 h. The potassium salt dissolves and potassium chloride

precipitated as white powder leaving choline AA ILs in solution upon the exchange of K^+ by choline cations. The potassium chloride crystals were separated by centrifugation, and then ethanol and water produced during the reaction were removed using a rotary evaporator. The so obtained ILs (hereafter referred to as [Cho][AA]) are outgassed under dynamic vacuum at 30°C overnight to totally remove the possible residual ethanol and water. Four different amino acids were employed: L-Alanine, L-Proline, L-Serine, and Glycine. The success of the syntheses was confirmed by 1H-NMR and ATR-IR spectroscopy. The chemical structure of the four [Cho][AA] ILs is reported in **Scheme 1**.

Additionally, the ILs were degassed for 10 h by a vacuum pump under constant agitation to remove the dissolved gases and impurities. The [Cho][AA]s solutions were prepared by mixing ILs with DMSO using an electronic analytical balance at a weight ratio of 12.5 wt.%.

5.2.2 Characterization

ATR FT-IR spectroscopic measurement: pure ILs and IL-DMSO solution, before and after CO_2 absorption, were characterized using a Bruker Tensor II spectrophotometer equipped with DTGS detector and single-reflection Bruker Platinum ATR accessory with the diamond crystal. All the spectra were recorded at a resolution of 2 cm^{-1}, 32 scans in the spectral range 3800-600 cm^{-1}.

Density: densities of the IL-DMSO solutions were calculated using a Gay-Lussac pattern density bottle (volume ~5 mL). The volume of the empty density bottle was previously calculated using water. Then, the weight of the density bottle filled with [Cho][AA]-DMSO solution was measured using an analytical balance. All the measures were conducted at 20°C.

A Cannon-Fenske viscometer was employed to measure the viscosities of the different [Cho][AA]-DMSO solutions. Once the tube was filled with the proper amount of sample, it was placed in a constant temperature bath (bath temperature 20°C). After 10 minutes, so the sample and the tube reached the equilibrium temperature, the efflux time was measured by means of the chronometer in order to calculate the kinematic viscosities. Dynamic viscosities were calculated using the density values previously measured with the density bottle.

5.2.3 Experimental set-up

The experimental set-up used for the absorption and desorption measurements showed in **Figure 5-1** consists of a jacketed reactor, a magnetic stirrer, a gas chromatograph, and a circulating thermal bath. The quartz reactor has an internal diameter of 40 mm and a total volume of 125 cm^3. An external jacket with a thickness of 10 mm is used to maintain the temperature constant due to the exothermic nature of the absorption. The water passed through the jacket using a FALC SBF.15 circulating bath with a capacity of 15 L and an operating temperature

range of -30 - +100 °C. The reactor is sealed with a thick rubber cork stopper (40 mm thickness and 30 mm diameter). The cap has three holes, holding the thermocouple and gas inlet and outlet tubes. The gas is injected into the liquid phase through a stainless-steel tube with an outer diameter (O.D.) of 1/6" placed in the center of the cap. While the outlet gas is exit through a stainless-steel tube of 1/8" O.D.

The operating condition for temperature and pressure were monitored by a K type thermocouple and a pressure transducer connected to the outlet tube. The gas inlet flow rate is controlled by a Bronkhorst® mass flow controller. The system parameters of pressure in the headspace, temperature, flow rate of argon and flowrate of CO_2 are continuously monitored, and data are recorded by using software developed in the LABVIEW® platform. The CO_2 volume fraction expressed in ppm in the outlet gas is measured every minute by a micro-Gas Chromatograph (Varian 490-µGM). The GC is equipped with a PoraPLOT Q column of 10 m with a carrier gas of argon and a micro-TCD detector. The column temperature of the GC was kept at 80 °C. The analysis method uses an injection time of 40 ms.

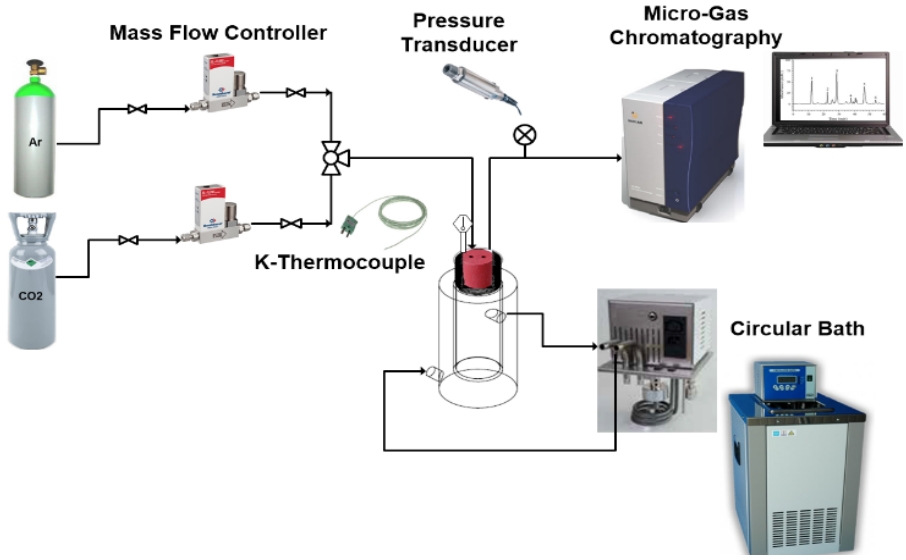

Figure 5-1. Laboratory test-bench for absorption and desorption measurements.

5.2.4 CO_2 absorption and desorption measurements tests

The absorption experiments are designed to evaluate the CO_2 loading capacity of ionic liquids [Cho][AA]s in the DMSO solution. The tests were carried out by bubbling a gas mixture with the composition of 17 vol% CO_2 and 83 vol.% Ar (considering flue gas composition) into the liquid phase consisted of 12.5 wt.% [Cho][AA]s in DMSO. The amount of solution used was 40 mL, filled half volume of the reactor. Therefore, the system response time due to the reactor headspace was calculated by monitoring the absorption profile of CO_2 in pure DMSO at the GC.

The complete process comprised of three consecutive operations absorption, desorption, and cooling. Before starting the tests, the system was inspected entirely for any gas leakage. During the test, the ILs solution was continuously stirred with a speed of 600 rpm to create uniformly disperse bubbles without forming any vortex. The total flow of the gas mixture used was 50 mL/min (CO_2 flow rate of ≈ 8 mL/min and the Ar flow rate of ≈ 42 mL/min). The CO_2 volume fraction in the outlet gas was analyzed by the GC until the CO_2 concentration of the gas at the inlet and outlet of reactor became equal or the solution converted to saturate. The operating conditions for both processes are reported in **Table 5-1**.

Furthermore, the regeneration process was investigated after the IL-DMSO solution was saturated, by heating and purging the system at 65 °C with a flux of pure Ar (100 mL/min). The rate of temperature change for heating was held at 1.3 °C/min until the system temperature reached the set point. The solution was maintained stirred with a speed of 600 rpm along the process. The absorption process was completed once the concentration of the CO_2 in the out-flowing gas measured by GC reached 1 vol% of the CO_2 concentration at the inlet. Finally, the solution was cooled down to an absorption operating temperature of 20 °C.

In addition, for realizing the viability of the IL-DMSO solution regeneration, which plays an important role in practical applications, the absorption and desorption process has been repeated for two additional cycles.

Table 5-1. Operating condition for absorption and absorption process.

Process	T (°C)	P (bar)	Flow Composition	Total Flowrate (mL/min)	CO_2 Concentration (vol%)
Absorption	20	1	CO_2 + Ar	50	17
Desorption	65	1	Ar	100	0

5.2.5 Absorption capacity theory

The absorbed amount of CO_2 in the solution of [Cho][AA]s and DMSO was calculated using the following equations [157]:

$$n_{CO2_{adsorbed}} = \int_{t0}^{tf} n_{CO2_{out}}(t).dt \quad (5\text{-}1)$$

$$n_{CO2_{out}(t)} = C_{CO2_{out}}(t).Q_{CO2_{out}}(t).(t-\Delta t) \quad (5\text{-}2)$$

Where: C_{CO2_out} (mol m^{-3}) is the concentration of the CO_2 recorded by GC at each time interval, Q_{CO2_out} (m^3 s^{-1}) is the volumetric flow rate of CO_2 at the reactor and Δt (s) is the time delay for GC. To understand the CO_2 absorption capacity of

pure [Cho][AA]s, the amount of absorbed CO_2 by DMSO was subtracted from **Equation (5-1)**.

$$n_{CO2_{absorbed}} = \int_{t0}^{tf} n_{CO2_{out}}(t).dt_{[Cho][AA]+DMSO} - \int_{t0}^{tf} n_{CO2_{out}}(t).dt_{DMSO} \quad (5\text{-}3)$$

For instance, the pure loading capacity of [Cho][Pro] is calculated, as shown **Figure 5-2** by integrating the absorption curve (orange curve) resulting from the difference between the CO_2 absorption test in DMSO (blue curve) and the CO_2 absorption test in the [Cho][Pro] (black curve). The integrated (gray) area will result in the amount of CO_2 absorbed by the [Cho][Pro].

Moreover, the molar CO_2 absorption capacities per moles of solution or moles of IL were, respectively, calculated by:

$$\alpha_{solution} = \frac{n_{CO2_{adsorbed}}}{n_{[Cho][AA]} + n_{DMSO}} \quad (5\text{-}4)$$

$$\alpha_{IL} = \frac{n_{CO2_{adsorbed}[Cho][AA]}}{n_{[Cho][AA]}} \quad (5\text{-}5)$$

5.2.6 Regeneration efficiency (η)

The regeneration efficiency expresses in **Equation (5-6)** shows the reversibility of the absorption process.

$$\eta = \frac{n_i}{n_0} \quad (5\text{-}6)$$

Where the n_0 is the moles of CO_2 absorbed in the fresh solution and n_i is the amount of CO_2 recovered in the absorption phase.

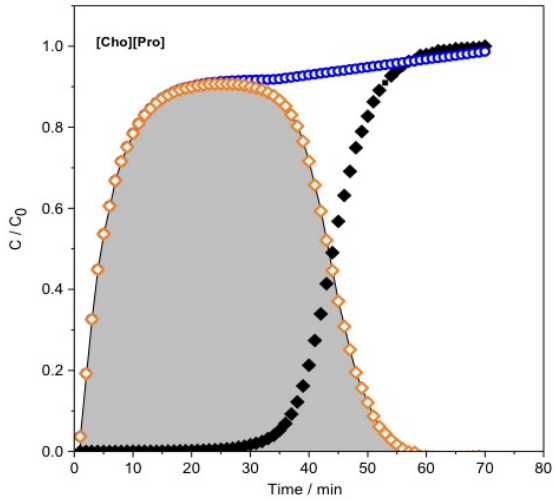

Figure 5-2. Absorbed CO_2 in pure [Cho][Pro] calculated by subtracting the DMSO absorption curve (Blue curve) from [Cho][Pro] in the solution curve.

5.3 Results and Discussion

5.3.1 Synthesis of the [Cho][AA] ILs

The synthesis of [Cho][AA] ILs usually relies on the water solution of choline hydroxide, [Cho][OH].[158–160] In fact, [Cho][OH] solution, which can be purchased or obtained from choline chloride [Cho][Cl] and AgO_2, is a convenient starting reagent for AAILs synthesis *via* acid-base titration. Such a synthesis method leads to the production of ILs with very high purity without any byproduct. However, the [Cho][OH] solution is corrosive, reactive and more expensive than plain [Cho][Cl] and its titration procedure is very long. To overcome these drawbacks and to achieve large-scale synthesis production for industrial applications, in this paper, a different synthetic approach was employed.[156] [Cho][AA] ILs were obtained *via* ionic metathesis between potassium AA salts and [Cho][Cl] in ethanol. More experimental details and the chemical characterizations (NMR, ATR-IR, TG) demonstrating the proper synthesis of the ILs are reported in **Scheme 5-2, Figure 5-3** and **Table 5-2.**

The good solubility of the ILs and the very scarce solubility of KCl [161] in the solvent was exploited to separate the IL from the byproduct, so obtaining a high purity. Moreover, the ionic metathesis methodology employs a cheap [Cho][Cl] reagent and can achieve high throughput, both aspects that are of main importance for industrial application.

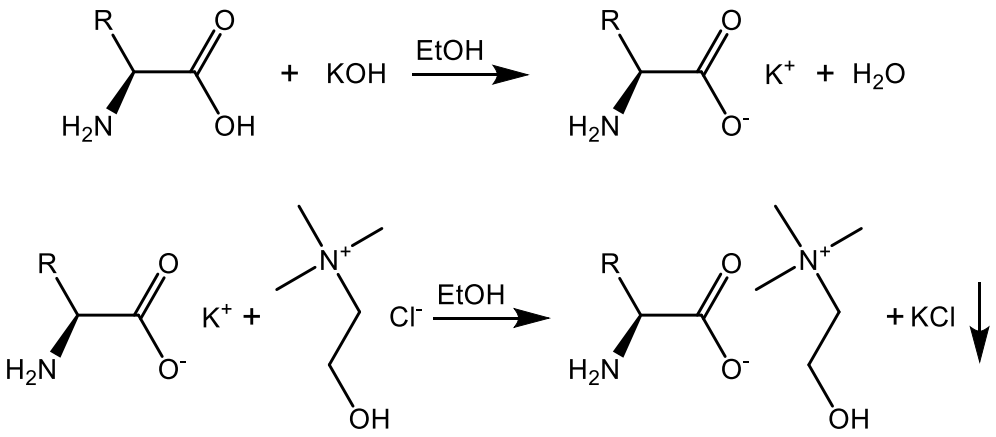

Scheme 5-2. Ionic metathesis synthetic path employed to produce [Cho][AA] ILs.

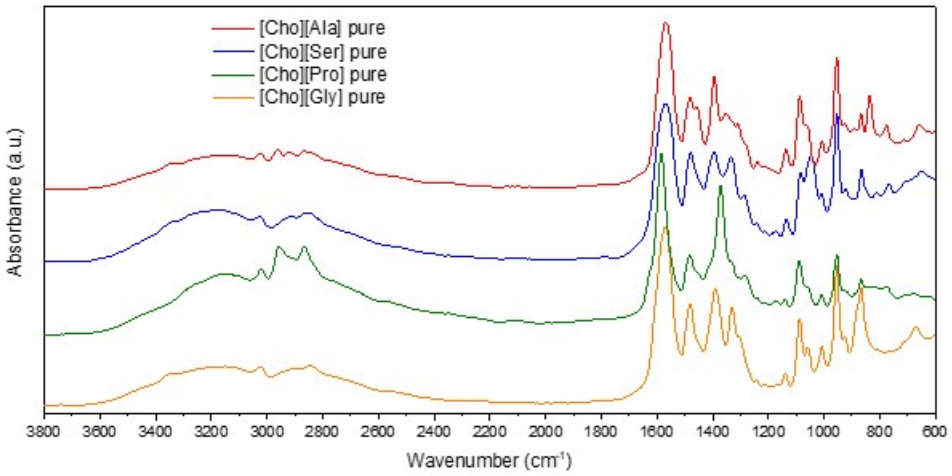

Figure 5-3. ATR-IR spectra of the pure [Cho][AA] ILs.

The TGA analyses were performed on the four [Cho][AA] ILs immediately after rotary evaporation and before the overnight vacuum treatment. All measurements were performed by means of a TG 209 F1 by NETZSCH Thermal Analysis. Approximately 10 mg of sample in alumina pans were heated from 30 to 800 °C (10 °C/min) under synthetic air and pure nitrogen (20 ml/min). In **Table 5-2** the degradation temperatures are reported as onset temperature of the different TG curves.

Table 5-2. Degradation temperature determined by Tonset from TG curves measured under air (O_2/N_2 20:80) and pure nitrogen.

Ionic Liquid	T_{onset} in air (°C)	T_{onset} in N_2 (°C)
[Cho][Ala]	187	186
[Cho][Pro]	171	171
[Cho][Ser]	183	190
[Cho][Gly]	174	186

5.3.2 Density and viscosity measurements

Different chemo-physical properties should be considered while testing new absorbents for CO_2 capture. Viscosity is one of the most important parameters from the practical viewpoint because it influences mass transport phenomena, *i.e.* CO_2 diffusion in the liquid, pressure drops for circulation of the liquid in the absorption plant and, consequently, energy consumption. [Cho][AA] ILs are notoriously very viscous [157], and consequently, CO_2 capture is not effective because of the poor gas diffusion into these liquids. Therefore, their dilution in a proper solvent is a strategy that can be employed to overcome the viscosity related issues.

With that purpose, in this work, we first evaluated the performance of a [Cho][AA] IL diluted in DMSO at different concentrations (see Section S5 in the SI). From those tests, we verified that the addition of DMSO improved the CO_2 absorption rate of ILs. The best performance was obtained with a 12.5 wt% solution of [Cho][Gly]. Thus, this concentration was used to evaluate the dynamic of the CO_2 absorption process in different [Cho][AA]-DMSO solutions. **Table 5-3** reports the density and viscosity values of the pure ILs and DMSO (reference values) at 20°C in comparison to the 12.5 wt% IL-DMSO solutions.

Table 5-3. Viscosity and density (at 20°C) of pure [Cho][AA] ILs and solutions of 12.5 wt.% [Cho][AA] ILs in DMSO.

	Pure substances		IL-DMSO 12.5%w/w	
	ρ (g/cm^3)	η (cP)	ρ (g/cm^3)	η (cP)
[Cho][Ala]	1.133 [a]	1051 [a]	1.106±0.036	3.76±0.12
[Cho][Ser]	1.204 [a]	21319 [a]	1.104±0.036	3.77±0.19
[Cho][Pro]	1.140 [a]	15298 [a]	1.110±0.036	3.89±0.13
[Cho][Gly]	1.158 [a]	2313 [a]	1.110±0.036	3.88±0.18
DMSO	1.098±0.035	2.01±0.15	-	-

[a] De Santis et al. [162]

Pure ILs exhibit density values in between 1.13 and 1.20 g/cm^3. As expected, the density (ρ) values are reduced after dilution in DMSO and settled at around 1.1 g/cm^3. However, the highest effect was observed for the viscosity (η) values that experienced a huge decrease upon dilution of the ILs in DMSO. Indeed, the IL-DMSO solutions display viscosity values in between 3.7 and 3.9 cP, not so far from pure that of DMSO (2 cP); whereas pure ILs show viscosities that are 3-4 orders of magnitude higher (10^3-10^4 cP) [155].

5.3.3 Absorption of CO_2 with a solution of [Cho][AA]s in DMSO

The breakthrough curves for the CO_2 absorption in the [Cho][Ala], [Cho][Ser], [Cho][Pro] and [Cho][Gly] solution DMSO were measured at a constant temperature of 20 °C and a pressure of 1 bar, by bubbling 17 vol% CO_2 in Ar in a CSTR absorption reactor. The gas was flowed into the system until arriving at the saturation point. Afterward, desorption behavior was evaluated by heating the IL solutions until 65 °C under a constant Ar flow (see experimental section). Such absorption and desorption processes were repeated to investigate the regenerability and efficiency of ILs solutions. The results of these experiments are presented in **Figure 5-4** for two sequential cycles of absorption (black data) and desorption (red data), showing the concentration of CO_2 in the reactor outlet normalized by its inlet concentration.

In the first absorption cycle the CO_2 absorption uptake of the ILs decreased in the order [Cho][Ala] > [Cho][Pro] > [Cho][Ser] > [Cho][Gly]. During the 2nd and 3rd cycles, the absorption performance of the [Cho][Ala] (that was the best IL in the 1st cycle) was conspicuously reduced (~67%) and then arrived at a steady-state value of ~0.29 mol CO_2/mol IL. For the other [Cho][AA] solutions, there was an absorption decrease from the 1st to the 2nd cycle of approximately 48%, 43% and 33% for the [Cho][Pro], [Cho][Ser] and [Cho][Gly], respectively. However, the latter IL-DMSO solutions revealed competitive performances as their absorption efficiency reported a few reductions (<12% variation) during the last two cycles and their absorption capacity was slightly superior to the [Cho][Ala] (0.30 to 0.33 molCO_2/mol IL).

The normalized CO_2 absorbed (Ads) and desorbed (Des) amounts from each [Cho][AA]s solution during the 1st and 2nd cycles are indicated in **Table5-4** in terms of mol CO_2/mol IL. These values were calculated by integrating the area under the CO_2 absorption-desorption curves of each [Cho][AA] IL. The absorption values calculated in mol CO_2/kg ILs are and their relevant desorption efficiencies were also calculated and are reported in **Table 5-5**.

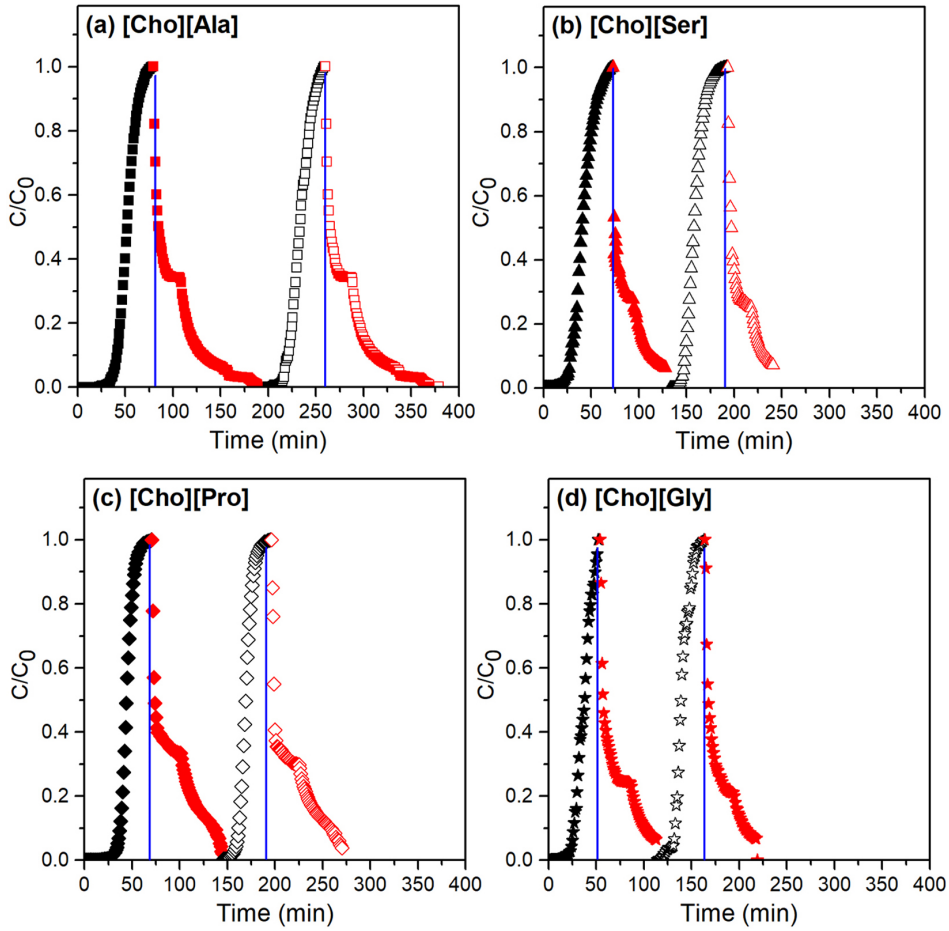

Figure 5-4. The breakthrough absorption curves (black) and desorption (red) profiles of CO_2 in the [Cho][AA]s ILs solutions in DMSO. The graph represents the corresponding data related to a) [Cho][Ala], b) [Cho][Ser], c) [Cho][Pro] and d) [Cho][Gly] during two complete cycles. The y-axis is showing the CO_2 concentration in the outlet normalized by its initial concentration.

Table5-4. Absorption capacities of [Cho][AA]s solutions through three cycles.

Absorption / Desorption Capacity (mol CO_2 / mol IL)					
	Cycle 1		Cycle 2		Cycle 3
	Ads	Des	Ads	Des	Ads
[Cho][Ala]	0.866	0.314	0.510	0.214	0.288
[Cho][Pro]	0.659	0.263	0.344	0.290	0.301
[Cho][Ser]	0.624	0.221	0.358	0.298	0.333
[Cho][Gly]	0.559	0.170	0.371	0.331	0.326

The physical state of all [Cho][AA] ILs was monitored before and after each absorption test. The presence of a white precipitate was evidenced for some of the amino acids after the CO_2 absorption, in particular for the [Cho][Ala] (see **Figure 5-5)**. The formation of a white precipitate in [Cho][Gly] and its absence in [Cho][Pro] was also observed, in agreement with previous observations from our group.[156] Hence, the significant CO_2 uptake variation during different absorption-desorption cycles can be explained by the formation of this white precipitate, after the 1st absorption cycle.

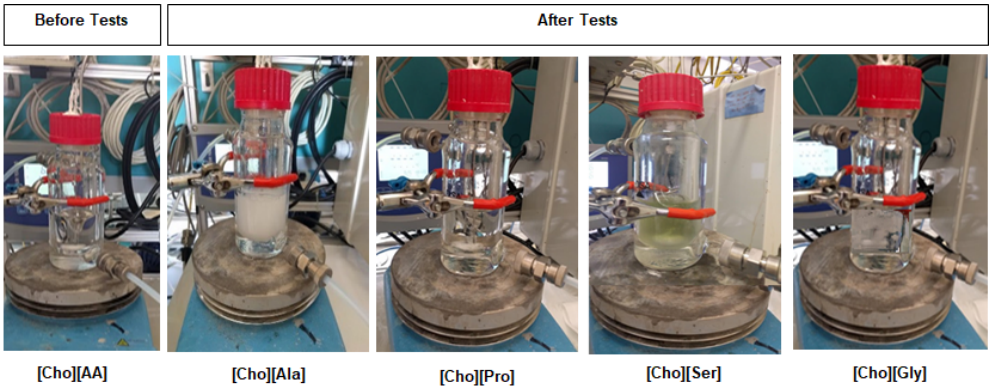

Figure 5-5. The state of [Cho][AA]s after absorption test in the laboratory due to precipitation of the solution.

To investigate the absorption process from a chemical point of view and to elucidate the origin of that precipitate, additional characterizations were performed. The IR spectra of each IL-DMSO solution were acquired before and after the CO_2 absorption experiments and are reported in **Figure 5-6**. The spectra modifications after CO_2 exposition are a clear signal that all four IL-DMSO solutions undergo chemical modifications. In the specific, the peak related to the carboxylate group (~1600 cm^{-1}) slightly shifts to higher wavenumbers (see **Figure 5-6** (a), (c), (d), blue dotted line 1) or modify its shape (see **Figure 5-6** (b), blue dotted lines 1 and 2), which can be attributed to the formation of the carbamate moiety. In addition, a new signal appears at ~1690 cm^{-1} (see line 2 in **Figure 5-6** (a), (c), (d) and line e in part (b)), related to the formation of the carbamic acid species. The spectra evolution is in accordance with our previous study. [156] Thus, the CO2 fixation occurs via the formation of two different species, carbamate, and carbamic acid. Indeed, two different reactions occur, as depicted in **Scheme 5-3** Carbamate moiety form together with ammonium counter-ion, by the reaction of two amines with one CO_2 molecule (see Scheme 5-3. part (a)), whereas carbamic acid forms *via* 1:1 reaction stoichiometry (see **Scheme 5-3.** part (b)).

Concerning the formation of the precipitates, they were analyzed by IR spectroscopy which revealed to be the AA of the [Cho][AA] ILs. During the CO2 absorption, the ILs lose their composition since part of the AA anions precipitate. To explain the reason for the AA precipitation it is worth to focus on the 2:1 stoichiometry absorption (**Scheme 5-3.** part (a)). Upon ammonium formation, the

AA becomes electrically neutral, since it acquires a positive charge, i.e. it is now in a zwitterionic form. On the other side, the carbamate formation produces an AA with a double negative charge. This double negative charge can be counterbalanced either by the ammonium-bearing AA or by an addition choline cation. Because of the scarce solubility of AAs in DMSO, the zwitterionic AAs can precipitate and the whole electroneutrality is still maintained. This AAs precipitates formation can be considered as the reason for the loss of absorption capacity, the effect of which can be removed by prolonging the regeneration step at a higher temperature. For instance, the regeneration of the ILs from these AAs could be possible through several days of heating under vacuum (being the process is thermodynamically favored) but the high energy consumption would make the process uneconomic.

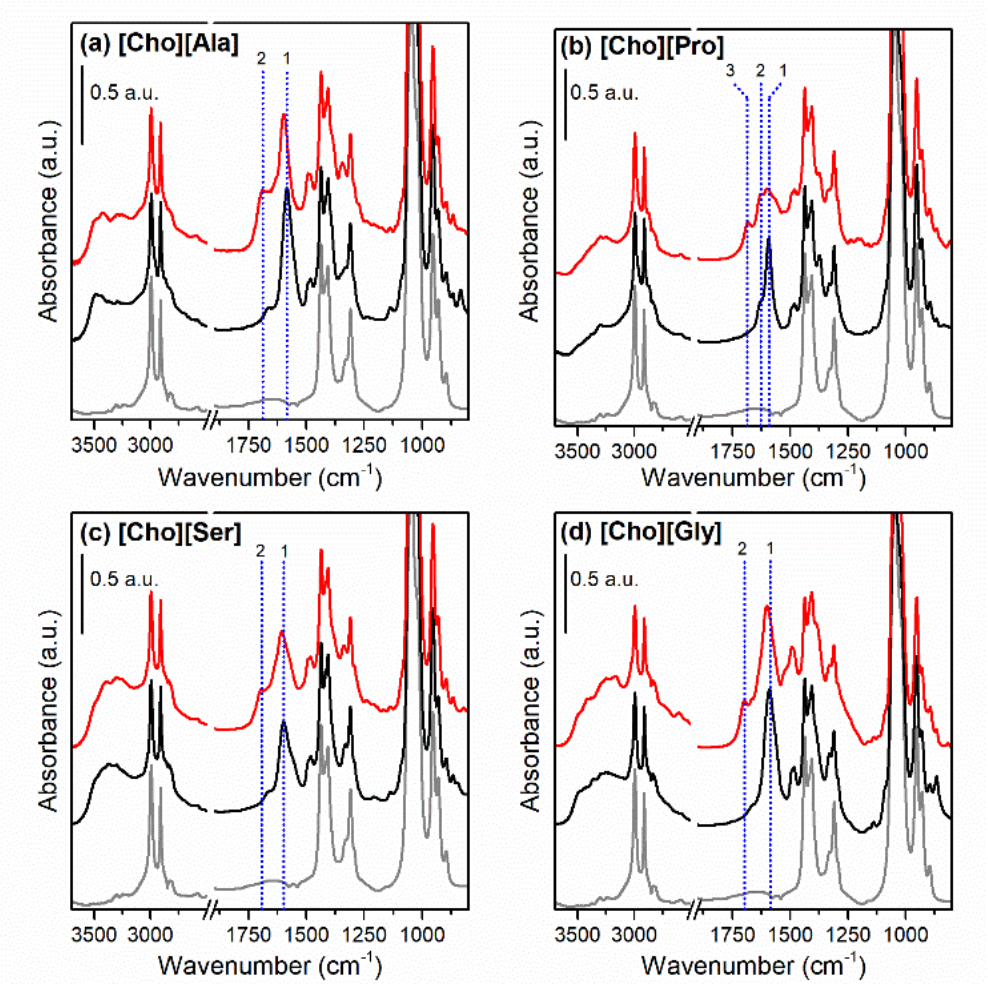

Figure 5-6. ATR-IR spectra of pure DMSO (grey curve) and IL-DMSO solutions before (black curve) and after CO_2 absorption (red curve). Part (a), (b), (c) and (d) report the data related to the DMSO solution with [Cho][Ala], [Cho][Pro], [Cho][Ser] and [Cho][Gly], respectively. The blue dotted lines in each part highlight the relevant modification of the spectra after CO_2 absorption.

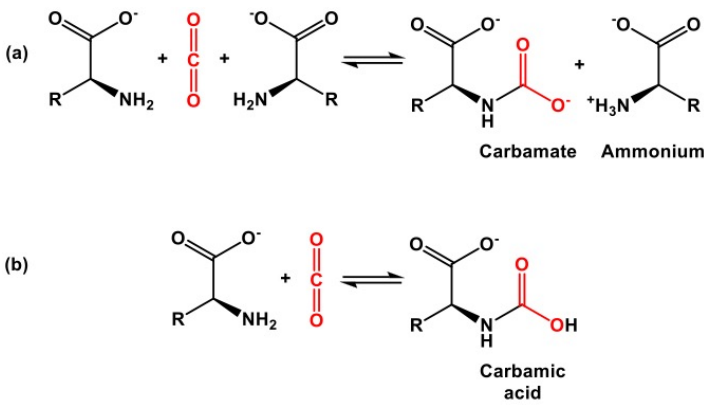

Scheme 5-3. Possible reaction paths of CO_2 and amines. Part (a): formation of ammonium-carbamate species via two amines per one CO_2 (2:1) stoichiometry reaction; part (b): formation of carbamic acid species via one amine per one CO_2 (1:1) stoichiometry reaction.

The desorption process occurred using Ar as an inert gas with a flow rate of 100 mL/min. During the process, the system was heated up to 65 °C with a ramp of 1.3 °C/min. In the 1st cycle, the CO_2 desorption efficiencies were different for all the [Cho][AA] ILs (between 30 and 40%, see **Table 5-5**) but have a relation to their absorption rate. Instead, in the 2nd cycle the [Cho][Pro], [Cho][Ser] and [Cho][Gly] solutions released a higher CO_2 quantity (desorption efficiency ~ 85%) than the [Cho][Ala] (desorption efficiency ~ 42%) at the same operating conditions.

Among all tested solutions, [Cho][Gly] revealed the highest desorption efficiency in the 2nd cycle with the desorption performance equal to 89% which is in agreement with the study by Shengjuan Yuan et al.[157] However, the operating temperature used in their work (110 °C) is much higher than in our study (65 °C).[157]

Table 5-5. Desorption efficiency of the ILs after the different absorption-desorption cycles.

	Desorption Efficiency (%)	
Ionic Liquid	Cycle 1	Cycle 2
[Cho][Ala]	36.3	41.9
[Cho][Pro]	39.9	84.3
[Cho][Ser]	35.4	83.2
[Cho][Gly]	30.4	89.2

The 1st cycle desorption curves of each [Cho][AA] IL are reported in **Figure 5-7**. The shape of the curves are similar and three regimes can be distinguished: (i) in the first minutes, the headspace emptying is responsible for the steep decrease in the CO_2 concentration; (ii) after, the CO_2 is released from the carbamic acid moiety (**Scheme 5-3**. part (a)), which is reversible at room temperature, the CO_2 desorption rates decrease and the CO_2 concentration values reach a plateau at ~25-30 min; (iii) then, the CO_2 desorption speeds again, since the temperature is enough high to

permit CO_2 release from the carbamate species (see **Scheme 5-3.** Part (b), which are more stable than carbamic acid.[156] The temperatures at which the CO_2 release from carbamate become relevant where found to be 38°C, 34°C, 40°C and 43°C for [Cho][Ala], [Cho][Ser], [Cho][Pro], and [Cho][Gly], respectively.

Hence, it is worth to underline that the amounts of captured and released CO_2 are not the same because of the desorption temperature used, which was chosen to preserve the [Cho][AA] IL from progressive aging. The total release can be achieved by increasing the temperature or by extending desorption time. In addition, the observed decrease in the absorption capacity from 1st to 2nd cycle is due to the formation of the precipitate for certain amino acids, which in the absence of CO_2 can be dissolved through the de-saturation of the solution from zwitterionic amino-acid through reversible reaction as shown in **Scheme 5-3**. However, dissolution is slow because of the low total solubility. Thus, this CO_2 can be considered as irreversibly absorbed since the phenomena lead to a decreased amount of available CO_2-reactive amines.

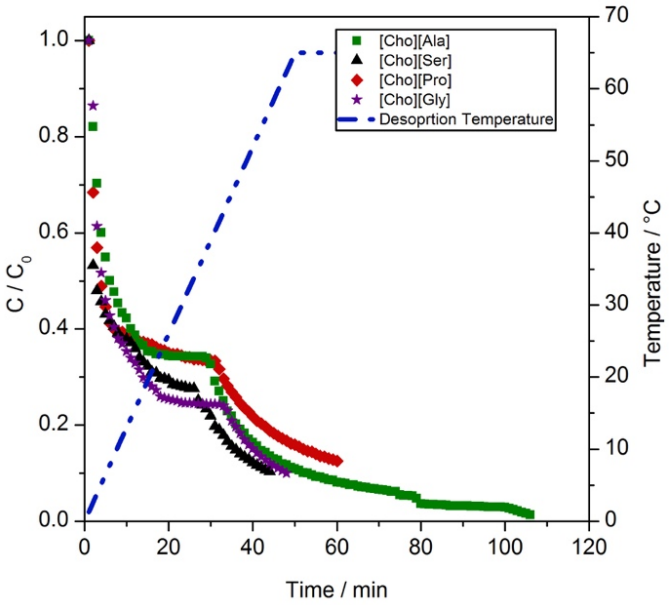

Figure 5-7. Desorption curves after the 1st absorption cycle of the [Cho][AA]-DMSO solution (stripping the gas of Ar with a flow rate of 100 ml/min and a heating rate of 1.3 °C/min up to 65°C).

To the best of our knowledge, the here reported solutions of TSILs in DMSO show better performances than other ILs solutions reported in the literature.[163–166] The CO_2 absorption capacity for [Cho][AA]s reported in **Table5-4** were compared to the results obtained by Biao Li et al. [167] and Shengjuan Yuan. et. al [157] for the same groups of [AA]s in a 5 to 30 wt% solution in water. Such results showed a higher absorption capacity during the 1st cycle for [Cho][AA] in DMSO (~2 times superior) with respect to the same ILs solution in water (~10 wt%) at the temperature of (30 and 35 °C). However, the reversible adsorption/desorption capacities of different solutions reported for the 3rd cycle presented similar CO_2

absorption performances. Indeed, the final absorption capacity in terms of mol CO_2/mol [AA]s for similar concentration is strictly below 0.5 for the 2 to 3 times higher CO_2 partial pressure.

It is necessary to mention that the studies performed previously did not repeat the absorption tests for all of the [Cho][AA]s and reported the results only for the best ILs with the highest CO_2 uptake. For instance, Shengjuan Yuan. et. al [157] investigated the desorption efficiency of only aqueous [Cho][Gly] at a higher temperature (110 °C). For other types of ILs instead, the absorption results were only reported for the 1st cycle, without evaluating the absorption capacity loss after CO_2 desorption. Moreover, a higher CO_2 absorption rate was observed for [Cho][AA]s in the DMSO solution respecting the results of preceding works with the possibility of water present in the CO_2 desorption process. The same amino acids were also tested with Polyethylene glycol with a molecular weight of 200 and the viscosity of about 30 times higher than DMSO.[168] In the same condition as underlined by the kinetic reported for CO_2 absorption where the time for CO_2 capture are 2-3 times higher even considering the higher temperature used (at list 35°C)[149].

5.4 Conclusion

This study introduced the application of choline-based ILs in solution with an organic solvent (DMSO) as a promising approach for CO_2 separation from flue gases. The viscosity of the ILs significantly diminished through their dissolution in DMSO, thus the limits to CO_2 diffusion into the system are decreased. The four [Cho][AA] ILs synthesized in this work: [Cho][Ala], [Cho][Ser], [Cho][Pro], and [Cho][Gly] were tested to measure their CO_2 absorption capacity, from a synthetic flue gas (17 vol% CO_2 in Ar), through different absorption/desorption cycles.

The absorption results indicated a decrease in the CO_2 loading capacity of ILs from the 2nd absorption/desorption cycle. IR spectroscopy analysis showed that such a decrease in the CO_2 absorption performance is due to the formation of carbamic acid species, which appeared in the solution as precipitates. Among the studied ILs, [Cho][Gly], [Cho][Pro] and [Cho][Ser] revealed comparable absorption efficiencies of about 0.3 mol CO_2/mol ILs.

The choline-based amino acids synthesized in this study reported aspiring absorption capacities. Even though their behavior for CO_2 absorption became stable after the secondary runs, on the contrary to what has been reported in previous works were only the first absorption cycle has been studied. The drawbacks related to the high viscosity and high cost of ILs were here limited by applying DMSO as a solvent.

With respect to previous reports, the here reported bio-based TSILs solutions or combine a series of additional advantages: low cost, low environmental impact, easy processability because of their low viscosity, low energy consumption and high regenerability (up to 89% desorption efficiency at steady-state conditions). These characteristics make of these [Cho][AA]-DMSO solutions the most

competitive IL-based absorbents at the state-of-the-art for industrial flue gas treatment, which would allow the CO_2 capture of for its subsequent use as raw material with high purity.

Chapter 6

6 Conclusion

6.1 Conclusion and future works

The research presented in this dissertation focuses on the application of solid and liquid sorbent for post-combustion carbon capture processes. The main materials studied are natural clinoptilolite (a porous zeolite) and bio-based ionic liquids (or amino acid-based ionic liquids). The principal findings of this thesis are divided into two groups as follows, firstly the adsorption behavior of the solid clinoptilolite and its modified forms is described, secondly a mathematical model developed for describing the behavior of adsorption process and finally the CO_2 absorption process with the ionic liquid is reported.

6.1.1 General conclusion on CO_2 adsorption by Clino

The CO_2 adsorption features of Clino were investigated at a range of operational conditions with a mixture of CO_2/N_2 (10:90 v/v). The adsorption capacities of the sorbent were improved through a cation exchange modification with Na^+ and Ca^{2+}. The calculated CO_2 uptake for each sorbent showed an increase in the adsorption loading capacity of Na-Clino, whereas the adsorption capacity of Ca-Clino was not improved. Here, the commercial zeolite of 13X was used as a reference due to its high CO_2 adsorption capturing efficiency. Indeed, the adsorption capacity of Z13X was almost 3 times higher than the untreated Clino at ambient temperature.

By performing experiments at higher temperatures, i.e. up to 65 °C, a highest CO_2 uptake was obtained with Clino, in comparison to Z13X and Na-Clino. To explain such behavior the isosteric heat of adsorption was calculated by performing CO_2 adsorption measurments at two different temperatures. The approximated values of isosteric heat for Z13X, Clino and Na-Clino related to the CO_2 coverage of 1.5 mmol g^{-1} are respectively 50 kJ/mol, 37 kJ/mol and 32 kJ/mol. The obtained q_{iso} values are in agreement with the CO_2 breakthrough curves found at different

temperatures, since the greater the q_{iso}, the less favored is the adsorption at high temperature.

The interaction mechanism between CO_2 and the adsorbents was investigated by means of FTIR spectroscopy. CO_2 upon interaction with Clino, forms linear adducts onto K^+ and (less abundant) Mg^{2+} cations, and carbonate-like species onto basic sites, all the species being only partially reversible at beam temperature. The exchange with Na^+ ions led to a decrease in surface basicity, and to the formation of both single (Na+···O=C=O) and dual (Na+···O=C=O···Na+) cationic sites, available for linear adducts formation.

The research on Clino was continued by modifying the sorbent with other alkaline cations including Na^+, K^+, Cs^+ where the behavior of the system was investigated by using the ZLC column analysis. This method allows measurements of both kinetics and CO_2 uptake. The results obtained indicated that the mechanism of mass transfer on Clino is equilibrium-controlled. The adsorption loading capacities of those materials change in the following order: K-Clino > Na-Clino > Clino > Cs-Clino, providing evidences of higher electrostatics charges for Na^+ and K^+. The largest CO_2 uptake for K-Clino and Na-Clino are respectively 1.3 and 1.2 mol/kg at 20 °C and a partial pressure of 0.1 bar. The adsorption/ desorption tests performed during three consecutive cycles indicate the irreversible adsorption behavior of all samples. Such irreversibility can be described by the formation of strong bonds or carbonate species on the zeolitic framework upon interaction with CO_2. This behavior was later verified by performing TPD analysis at 300ºC.

Overally, from a practical point of view, the improved adsorption capacity of Clino at high temperature (over 55 °C) versus the state-of-the-art zeolite Z13X makes it a potential sorbent for CO_2 removal from flue gases by minimizing the input energy required to the system.

6.1.2 Conclusion points on the adsorption model

In practice, to apply zeolites in industrial applications for carbon capture or biogas upgrading, mathematical models needs to be developed. The model developed in this thesis work can be used for simulating the adsorption behavior of any type of material, once there are enough information on the equilibrium and kinetics behavior of the sorbent. As part of this thesis, the behavior of a fixed-bed reactor packed with Z13X for biogas upgrading was investigated. The mathematical model was constructed based on the material, energy and momentum balances together with the kinetics and equilibrium equations. The parameters of mass and heat transfer including K_{CO2}, K_{CH4} and h_L were estimated using a adsorption test results from a single experiment and by implementing several empirical correlations. The model validation was performed with experimental data at different temperatures, 20 °C, 40 °C and 80 °C, with a CO_2/CH_4 molar fraction of 20 vol% and 40 vol%.

The results from the model showed to be in agreement with the experimental data depending on the operating conditions. However, the simulated breakthrough

curves are consistent with the experimental ones, at all the operating temperatures, indicating a stable pressure gradient inside the column. Instead, the temperature behaviors exhibited discrepancies at different operating temperatures as compared to the validation test condition. This can be attributed to the feed velocity and the assumption of a constant adsorption heat.. This model is used to predict the cyclic behavior of the adsorption process. In perspective, this type of model can be used to simulate the scale-up of new adsorbent materials such as Clino.

6.1.3 Concluding remarks on Amino acid-based Ionic Liquids

This study introduced the application of choline-based ILs in solution with an organic solvent (DMSO) as a promising approach for CO_2 separation from flue gases. The viscosity of the ILs significantly diminished through their dissolution in DMSO, thus the limits to CO_2 diffusion into the system are decreased. The four [Cho][AA] ILs synthesized in this work: [Cho][Ala], [Cho][Ser], [Cho][Pro], and [Cho][Gly] were tested to measure their CO_2 absorption capacity, from a synthetic flue gas (17 vol% CO_2 in Ar), through different absorption/desorption cycles.

The absorption results indicated formation of carbamic acid species, which appeared in the solution as precipitates upon interaction of CO2 with the ILs by means of IR spectroscopy analysis. Among the studied ILs, [Cho][Gly], [Cho][Pro] and [Cho][Ser] revealed comparable absorption efficiencies of about 0.3 mol CO_2/mol ILs. The drawbacks related to the high viscosity and high cost of ILs were here limited by applying DMSO as a solvent.

The advantages of using bio-based TSILs solutions are compromising low cost, low environmental impact, easy processability because of their low viscosity, low energy consumption and high regenerability (up to 89% desorption efficiency at steady-state conditions). These characteristics make of these [Cho][AA]-DMSO solutions the most competitive IL-based absorbents at the state-of-the-art for industrial flue gas treatment, which would allow the CO_2 capture of for its subsequent use as raw material with high purity.

6.1.4 Future work

Future work should focus on broadening the effect of cation exchange in the the adsorption features of Clino to be applicable of clinoptilolite in a large-scale CO_2 separation treatment process. This can be accomplished by finding practical and novel methods to apply Clino and exchanged-Clino as coating materials on porous solid structures, such as monolith. Alternately, a three-dimensional (3D)-printed Clino monolith with desired geometries can be fabricated and put into practice for CO_2 removal from air. Furthermore, the adsorption capacity and selectivity of Clino can be tunned by further synthesis including adaptation of framework composition, increase of pore volume and introduction of cation gataing.

Nonetheless, to make industrially viable the application of Clino in the CO_2 separation processes, several actions need to be undertaken including: the integration of the adsorption model with the experimental data obtained for CO_2 adsorption on Clino, tunning the model and implementation of control strategies.

7 References

[1] D.Y.C. Leung, G. Caramanna, M.M. Maroto-Valer, An overview of current status of carbon dioxide capture and storage technologies, Renew. Sustain. Energy Rev. 39 (2014) 426–443. doi:10.1016/j.rser.2014.07.093.

[2] S.D. Kenarsari, D. Yang, G. Jiang, S. Zhang, J. Wang, A.G. Russell, Q. Wei, M. Fan, Review of recent advances in carbon dioxide separation and capture, RSC Adv. 3 (2013) 22739–22773. doi:10.1039/c3ra43965h.

[3] J. Beck, Efficient Targeted Optimisation for the Design of Pressure Swing Adsorption Systems for CO2 Capture in Power Plants, Biotechnol. Lett. 22 (2000) 777–781. doi:10.1023/A:1005645606616.

[4] I. Hinkov, F.D. Lamari, P. Langlois, M. Dicko, C. Chilev, I. Pentchev, Carbon dioxide capture by adsorption (review), J. Chem. Technol. Metall. 51 (2016) 609–626.

[5] D. Marchon, Research Collection, ETH Zurich Res. Collect. (2016). doi:10.3929/ethz-a-010782581.

[6] R.D. Rogers, K.R. Seddon, S. Volkov, eds., Green Industrial Applications of Ionic Liquids, Springer Netherlands, Dordrecht, 2002. doi:10.1007/978-94-010-0127-4.

[7] A. Rafiee, K. Rajab Khalilpour, D. Milani, M. Panahi, Trends in CO2 conversion and utilization: A review from process systems perspective, J. Environ. Chem. Eng. 6 (2018) 5771–5794. doi:10.1016/j.jece.2018.08.065.

[8] K.A. Mumford, N.R. Mirza, G.W. Stevens, Review: Room Temperature Ionic Liquids and System Designs for CO2 Capture, Energy Procedia. 114 (2017) 2671–2674. doi:10.1016/j.egypro.2017.03.1450.

[9] N. MacDowell, N. Florin, A. Buchard, J. Hallett, A. Galindo, G. Jackson, C.S. Adjiman, C.K. Williams, N. Shah, P. Fennell, An overview of CO2 capture technologies, Energy Environ. Sci. 3 (2010) 1645–1669. doi:10.1039/c004106h.

[10] A. Samanta, A. Zhao, G.K.H. Shimizu, P. Sarkar, R. Gupta, Post-combustion CO 2 capture using solid sorbents: A review, Ind. Eng. Chem. Res. 51 (2012) 1438–1463. doi:10.1021/ie200686q.

[11] A.-H. Lu, G.-P. Hao, Porous materials for carbon dioxide capture, Annu. Reports Prog. Chem. Sect. A. 109 (2013) 484–503. doi:10.1039/c3ic90003g.

[12] D. Bonenfant, M. Kharoune, P. Niquette, M. Mimeault, R. Hausler, Advances in principal factors influencing carbon dioxide adsorption on zeolites, Sci. Technol. Adv. Mater. 9 (2008). doi:10.1088/1468-6996/9/1/013007.

[13] M.M. Lozinska, Investigation of Inorganic Porous Solids as Adsorbents for the Separation of Carbon Dioxide from Flue Gas A thesis presented for the degree of by Magdalena Malgorzata Lozinska , MSc, (2013).

[14] H.-S. Choi, M.P. Suh, Highly Selective CO $_2$ Capture in Flexible 3D Coordination Polymer Networks, Angew. Chemie Int. Ed. 48 (2009) 6865–6869. doi:10.1002/anie.200902836.

[15] M. Younas, M. Sohail, L.L. Kong, M.J.K. Bashir, S. Sethupathi, Feasibility of CO2 adsorption by solid adsorbents: a review on low-temperature systems, Int. J. Environ. Sci. Technol. 13 (2016) 1839–1860.

doi:10.1007/s13762-016-1008-1.
[16] J.C. Poshusta, V.A. Tuan, E.A. Pape, R.D. Noble, J.L. Falconer, Separation of light gas mixtures using SAPO-34 membranes, AIChE J. 46 (2000) 779–789. doi:10.1002/aic.690460412.
[17] J.A.C. Silva, K. Schumann, A.E. Rodrigues, Sorption and kinetics of CO2 and CH4 in binderless beads of 13X zeolite, Microporous Mesoporous Mater. 158 (2012) 219–228. doi:10.1016/j.micromeso.2012.03.042.
[18] Z. Zhang, W. Zhang, X. Chen, Q. Xia, Z. Li, Adsorption of CO2 on zeolite 13X and activated carbon with higher surface area, Sep. Sci. Technol. 45 (2010) 710–719. doi:10.1080/01496390903571192.
[19] Q.H. Dirar, K.F. Loughlin, Intrinsic adsorption properties of CO2on 5A and 13X zeolite, Adsorption. 19 (2013) 1149–1163. doi:10.1007/s10450-013-9543-2.
[20] S.K. Lakhera, S. Suman, Synthesis and Characterization of 13X Zeolite/ Activated Carbon Composite, 2014. http://sphinxsai.com/2015/ch_vol7_no3_ICONN/14/ON40 (1364-1368).pdf (accessed July 8, 2019).
[21] † Jong-Seok Lee, ‡ Jong-Hwa Kim, † Jin-Tae Kim, † Jeong-Kwon Suh, † and Jung-Min Lee, ‡ Chang-Ha Lee*, Adsorption Equilibria of CO2 on Zeolite 13X and Zeolite X/Activated Carbon Composite, (2002). doi:10.1021/JE020050E.
[22] Q.H. Dirar, K.F. Loughlin, Intrinsic adsorption properties of CO2 on 5A and 13X zeolite, Adsorption. 19 (2013) 1149–1163. doi:10.1007/s10450-013-9543-2.
[23] R.W. Stevens, R. V Siriwardane, J. Logan, In Situ Fourier Transform Infrared (FTIR) Investigation of CO 2 Adsorption onto Zeolite Materials, (n.d.). doi:10.1021/ef800209a.
[24] M.M. Lozinska, E. Mangano, J.P.S. Mowat, A.M. Shepherd, R.F. Howe, S.P. Thompson, J.E. Parker, S. Brandani, P.A. Wright, Understanding carbon dioxide adsorption on univalent cation forms of the flexible zeolite Rho at conditions relevant to carbon capture from flue gases, J. Am. Chem. Soc. 134 (2012) 17628–17642. doi:10.1021/ja3070864.
[25] S. Cavenati, C.A. Grande, A.E. Rodrigues, Adsorption Equilibrium of Methane, Carbon Dioxide, and Nitrogen on Zeolite 13X at High Pressures, J. Chem. Eng. Data. 49 (2004) 1095–1101. doi:10.1021/je0498917.
[26] K.T. Chue, J.N. Kim, Y.J. Yoo, S.H. Cho, R.T. Yang, Comparison of Activated Carbon and Zeolite 13X for CO2 Recovery from Flue Gas by Pressure Swing Adsorption, Ind. Eng. Chem. Res. 34 (1995) 591–598. doi:10.1021/ie00041a020.
[27] P.J.E. Harlick, F.H. Tezel, An experimental adsorbent screening study for CO2 removal from N2, Microporous Mesoporous Mater. 76 (2004) 71–79. doi:10.1016/j.micromeso.2004.07.035.
[28] R. V. Siriwardane, M.S. Shen, E.P. Fisher, Adsorption of CO2, N2, and O2on natural zeolites, Energy and Fuels. 17 (2003) 571–576. doi:10.1021/ef020135l.
[29] * Ranjani V. Siriwardane, and Ming-Shing Shen, E.P. Fisher, J. Losch, Adsorption of CO2 on Zeolites at Moderate Temperatures, (2005). doi:10.1021/EF040059H.
[30] C. Falamaki, A. Mohammadi, M. Sohrabi, N2 and O2 adsorption properties of an Iranian clinoptilolite-rich tuff in the original and pre-exchanged forms, Colloids Surfaces A Physicochem. Eng. Asp. 246 (2004) 31–37.

doi:10.1016/J.COLSURFA.2004.07.015.
[31] D.S. Karousos, A.A. Sapalidis, E.P. Kouvelos, G.E. Romanos, N.K. Kanellopoulos, A study on natural clinoptilolite for CO2/N2gas separation, Sep. Sci. Technol. 51 (2016) 83–95. doi:10.1080/01496395.2015.1085880.
[32] D.A. Kennedy, F.H. Tezel, Cation exchange modification of clinoptilolite – Screening analysis for potential equilibrium and kinetic adsorption separations involving methane, nitrogen, and carbon dioxide, Microporous Mesoporous Mater. 262 (2018) 235–250. doi:10.1016/j.micromeso.2017.11.054.
[33] A. Jayaraman, R.T. Yang, D. Chinn, C.L. Munson, Tailored Clinoptilolites for Nitrogen/Methane Separation, (2005). doi:10.1021/ie0492855.
[34] No Title, (n.d.) http://www.iza-online.org/natural/Datasheets/Clino.
[35] K. Hasegawa, A. Matsumoto, Role of cation in target adsorption of carbon dioxide from CO2-CH4 mixture by low silica X zeolites, in: AIP Conf. Proc., AIP Publishing LLC , 2017: p. 020002. doi:10.1063/1.4993321.
[36] S.-T. Yang, J. Kim, W.-S. Ahn, CO2 adsorption over ion-exchanged zeolite beta with alkali and alkaline earth metal ions, Microporous Mesoporous Mater. 135 (2010) 90–94. doi:10.1016/J.MICROMESO.2010.06.015.
[37] E.L. Uzunova, H. Mikosch, Cation site preference in zeolite clinoptilolite: A density functional study, Microporous Mesoporous Mater. 177 (2013) 113–119. doi:10.1016/J.MICROMESO.2013.05.003.
[38] N. V. Plechkova, K.R. Seddon, Applications of ionic liquids in the chemical industry, Chem. Soc. Rev. 37 (2007) 123–150. doi:10.1039/B006677J.
[39] L. A.Blanchard, D. Hancu, E. J.Beckman, J. F.Brennecke, Green processing using ionic liquids and CO2, Nature. 399 (1999) 28–29. https://www.nature.com/articles/19887.pdf (accessed September 17, 2019).
[40] S. Babamohammadi, A. Shamiri, M.K. Aroua, A review of CO<inf>2</inf> capture by absorption in ionic liquid-based solvents, Rev. Chem. Eng. 31 (2015) 383–412. doi:10.1515/revce-2014-0032.
[41] M. Ramdin, T.W. De Loos, T.J.H. Vlugt, State-of-the-art of CO 2 capture with ionic liquids, Ind. Eng. Chem. Res. 51 (2012) 8149–8177. doi:10.1021/ie3003705.
[42] S. Sarmad, J.-P. Mikkola, X. Ji, Carbon Dioxide Capture with Ionic Liquids and Deep Eutectic Solvents: A New Generation of Sorbents, ChemSusChem. 10 (2017) 324–352. doi:10.1002/cssc.201600987.
[43] M.J. Muldoon, S.N.V.K. Aki, J.L. Anderson, J.K. Dixon, J.F. Brennecke, Improving carbon dioxide solubility in ionic liquids, J. Phys. Chem. B. 111 (2007) 9001–9009. doi:10.1021/jp071897q.
[44] Jacob M. Crosthwaite, Sudhir N. V. K. Aki, and Edward J. Maginn, J.F. Brennecke*, Liquid Phase Behavior of Imidazolium-Based Ionic Liquids with Alcohols, (2004). doi:10.1021/JP037774X.
[45] X. Zhang, Z. Liu, W. Wang, Screening of ionic liquids to capture CO 2 by COSMO-RS and experiments, AIChE J. 54 (2008) 2717–2728. doi:10.1002/aic.11573.
[46] M. Ramdin, Experiments and Molecular Simulations Delft University of Technology, (n.d.).
[47] † Jennifer L. Anthony, Jessica L. Anderson, * and Edward J. Maginn, J.F. Brennecke*, Anion Effects on Gas Solubility in Ionic Liquids, (2005). doi:10.1021/JP046404L.
[48] Jennifer L. Anthony, * and Edward J. Maginn, J.F. Brennecke*, Solubilities and Thermodynamic Properties of Gases in the Ionic Liquid 1-n-Butyl-3-

methylimidazolium Hexafluorophosphate, (2002). doi:10.1021/JP020631A.
[49] J.L. Anderson, J.K. Dixon, J.F. Brennecke, Solubility of CO_2, CH_4, C_2H_6, C_2H_4, O_2, and N_2 in 1-Hexyl-3-methylpyridinium Bis(trifluoromethylsulfonyl)imide: Comparison to Other Ionic Liquids, Acc. Chem. Res. 40 (2007) 1208–1216. doi:10.1021/ar7001649.
[50] J. Palomar, M. Gonzalez-Miquel, A. Polo, F. Rodriguez, Understanding the Physical Absorption of CO_2 in Ionic Liquids Using the COSMO-RS Method, Ind. Eng. Chem. Res. 50 (2011) 3452–3463. doi:10.1021/ie101572m.
[51] B.F. Goodrich, J.C. De La Fuente, B.E. Gurkan, D.J. Zadigian, E.A. Price, Y. Huang, J.F. Brennecke, Experimental measurements of amine-functionalized anion-tethered ionic liquids with carbon dioxide, Ind. Eng. Chem. Res. 50 (2011) 111–118. doi:10.1021/ie101688a.
[52] D. Firaha, Molecular Approach toward Gases Absorption by Ionic Liquids, (2016).
[53] X. Wang, N.G. Akhmedov, Y. Duan, D. Luebke, D. Hopkinson, B. Li, Amino acid-functionalized ionic liquid solid sorbents for post-combustion carbon capture, ACS Appl. Mater. Interfaces. 5 (2013) 8670–8677. doi:10.1021/am402306s.
[54] X.Y. Luo, X. Fan, G.L. Shi, H.R. Li, C.M. Wang, Decreasing the Viscosity in CO2 Capture by Amino-Functionalized Ionic Liquids through the Formation of Intramolecular Hydrogen Bond, J. Phys. Chem. B. 120 (2016) 2807–2813. doi:10.1021/acs.jpcb.5b10553.
[55] J.L. McDonald, R.E. Sykora, P. Hixon, A. Mirjafari, J.H. Davis, Impact of water on CO 2 capture by amino acid ionic liquids, Environ. Chem. Lett. 12 (2014) 201–208. doi:10.1007/s10311-013-0435-1.
[56] S. Sjostrom, H. Krutka, Evaluation of solid sorbents as a retrofit technology for CO2capture, Fuel. 89 (2010) 1298–1306. doi:10.1016/j.fuel.2009.11.019.
[57] D. Saha, Z. Bao, Adsorption of CO2, CH4, N2O and N2 on MOF-5 , MOF-177 , and Zeolite 5A, Environ. Sci. Technol. 44 (2010) 1820–1826. doi:10.1021/es9032309.
[58] A.A.Z. Vassilis J. Inglezakis, Handbook of Natural Zeolites, (n.d.). https://www.amazon.it/dp/B00C1DQU76/ref=dp-kindle-redirect?_encoding=UTF8&btkr=1 (accessed November 26, 2019).
[59] Database of Zeolite Structures, (n.d.). http://www.iza-structure.org/databases/ (accessed May 16, 2019).
[60] R.A. Snellings, A.F. Gualtieri, J. Elsen, The Rietveld structure refinement of an exceptionally pure sample of clinoptilolite from Ecuador and its Na-, K-, and Ca-exchanged forms, Zeitschrift Für Krist. Suppl. 2009 (2009) 395–400. doi:10.1524/zksu.2009.0058.
[61] O. Korkuna, R. Leboda, J. Skubiszewska-Zięba, T. Vrublevs'ka, V.M. Gun'ko, J. Ryczkowski, Structural and physicochemical properties of natural zeolites: Clinoptilolite and mordenite, Microporous Mesoporous Mater. 87 (2006) 243–254. doi:10.1016/j.micromeso.2005.08.002.
[62] G. Aguilar-Armenta, G. Hernandez-Ramirez, E. Flores-Loyola, A. Ugarte-Castaneda, R. Silva-Gonzalez, C. Tabares-Munoz, A. Jimenez-Lopez, E. Rodriguez-Castellon, Adsorption kinetics of CO2, O2, N2, and CH4 in cation-exchanged clinoptilolite, J. Phys. Chem. B. 105 (2001) 1313–1319. doi:10.1021/jp9934331.
[63] M.W. Ackley, R.T. Yang, Diffusion in ion-exchanged clinoptilolites, AIChE

J. 37 (1991) 1645–1656. doi:10.1002/aic.690371107.
[64] M.W. Ackley, R.F. Giese, R.T. Yang, Clinoptilolite: Untapped potential for kinetics gas separations, Zeolites. 12 (1992) 780–788. doi:10.1016/0144-2449(92)90050-Y.
[65] R.T. Pabalan, F.P. Bertetti, Cation-Exchange Properties of Natural Zeolites, Rev. Mineral. Geochemistry. 45 (2001) 453–518. doi:10.2138/rmg.2001.45.14.
[66] D.A. Kennedy, M. Mujčin, C. Abou-Zeid, F.H. Tezel, Cation exchange modification of clinoptilolite –thermodynamic effects on adsorption separations of carbon dioxide, methane, and nitrogen, Microporous Mesoporous Mater. 274 (2019) 327–341. doi:10.1016/j.micromeso.2018.08.035.
[67] D.A. Kennedy, F.H. Tezel, Cation exchange modification of clinoptilolite – Screening analysis for potential equilibrium and kinetic adsorption separations involving methane, nitrogen, and carbon dioxide, Microporous Mesoporous Mater. 262 (2018) 235–250. doi:10.1016/j.micromeso.2017.11.054.
[68] A. Jayaraman, A.J. Hernandez-Maldonado, R.T. Yang, D. Chinn, C.L. Munson, D.H. Mohr, Clinoptilolites for nitrogen/methane separation, Chem. Eng. Sci. 59 (2004) 2407–2417. doi:10.1016/j.ces.2003.10.030.
[69] G. Aguilar-Armenta, G. Hernandez-Ramirez, E. Flores-Loyola, A. Ugarte-Castaneda, R. Silva-Gonzalez, C. Tabares-Munoz, A. Jimenez-Lopez, E. Rodriguez-Castellon, Adsorption Kinetics of CO 2 , O 2 , N 2 , and CH 4 in Cation-Exchanged Clinoptilolite, (2001). doi:10.1021/jp9934331.
[70] D. Fragoulis, E. Chaniotakis, M.G. Stamatakis, Zeolitic tuffs of Kimolos Island, Aegean Sea, Greece and their industrial potential, Cem. Concr. Res. 27 (1997) 889–905. doi:10.1016/S0008-8846(97)00072-0.
[71] A.F. Gualtieri, Accuracy of XRPD QPA using the combined Rietveld–RIR method, J. Appl. Crystallogr. 33 (2000) 267–278. doi:10.1107/S002188989901643X.
[72] A.C. Larson, R.B. Von, D. Lansce, GSAS GENERAL STRUCTURE ANALYSIS SYSTEM, n.d. https://permalink.lanl.gov/object/tr?what=info:lanl-repo/lareport/LA-UR-86-0748_REV (accessed August 6, 2019).
[73] B.H. Toby, ¯ Expgui, EXPGUI, a graphical user interface for GSAS Applied Crystallography EXPGUI, a graphical user interface for GSAS, J. Appl. Cryst. 34 (2001) 210–213. https://ncnr.nist.gov/programs/crystallography/software/EXPGUI_reprint.pdf (accessed August 6, 2019).
[74] G. Kahr, F.T. Madsen, Determination of the cation exchange capacity and the surface area of bentonite, illite and kaolinite by methylene blue adsorption, Appl. Clay Sci. 9 (1995) 327–336. doi:10.1016/0169-1317(94)00028-O.
[75] K. Sato, Y. Nishimura, N. Matsubayashi, M. Imamura, H. Shimada, Structural changes of Y zeolites during ion exchange treatment: effects of Si/Al ratio of the starting NaY, Microporous Mesoporous Mater. 59 (2003) 133–146. doi:10.1016/S1387-1811(03)00305-6.
[76] M. Thommes, K. Kaneko, A. V. Neimark, J.P. Olivier, F. Rodriguez-Reinoso, J. Rouquerol, K.S.W. Sing, Physisorption of gases, with special reference to the evaluation of surface area and pore size distribution (IUPAC Technical Report), Pure Appl. Chem. 87 (2015) 1051–1069.

doi:10.1515/pac-2014-1117.
[77] Y. Li, H. Yi, X. Tang, F. Li, Q. Yuan, Adsorption separation of CO2/CH4 gas mixture on the commercial zeolites at atmospheric pressure, Chem. Eng. J. 229 (2013) 50–56. doi:10.1016/j.cej.2013.05.101.
[78] E.P. Favvas, C.G. Tsanaktsidis, A.A. Sapalidis, G.T. Tzilantonis, S.K. Papageorgiou, A.C. Mitropoulos, Clinoptilolite, a natural zeolite material: Structural characterization and performance evaluation on its dehydration properties of hydrocarbon-based fuels, Microporous Mesoporous Mater. 225 (2016) 385–391. doi:10.1016/j.micromeso.2016.01.021.
[79] V.J. Inglezakis, M. Stylianou, M. Loizidou, Ion exchange and adsorption equilibrium studies on clinoptilolite, bentonite and vermiculite, J. Phys. Chem. Solids. 71 (2010) 279–284. doi:10.1016/J.JPCS.2009.12.077.
[80] S. Brandani, E. Mangano, H. Ahn, D. Friedrich, X. Hu, Diffusion mechanism of CO2 in 13X zeolite beads, Adsorption. 20 (2013) 121–135. doi:10.1007/s10450-013-9554-z.
[81] P.A. Jacobs, F.H. van Cauwelaert, E.F. Vansant, J.B. Uytterhoeven, Surface probing of synthetic faujasites by adsorption of carbon dioxide. Part 1.—Infra-red study of carbon dioxide adsorbed on Na-Ca-Y and Na-Mg-Y zeolites, J. Chem. Soc. Faraday Trans. 1 Phys. Chem. Condens. Phases. 69 (1973) 1056. doi:10.1039/f19736901056.
[82] D.S. Karousos, A.A. Sapalidis, E.P. Kouvelos, G.E. Romanos, N.K. Kanellopoulos, Separation Science and Technology A study on natural clinoptilolite for CO 2 /N 2 gas separation A study on natural clinoptilolite for CO 2 /N 2 gas separation, (2016). doi:10.1080/01496395.2015.1085880.
[83] J.A. Dunne, M. Rao, S. Sircar, R.J. Gorte, A.L. Myers, Calorimetric Heats of Adsorption and Adsorption Isotherms. 2. O 2 , N 2 , Ar, CO 2 , CH 4 , C 2 H 6 , and SF 6 on NaX, H-ZSM-5, and Na-ZSM-5 Zeolites, 1996. https://pubs.acs.org/sharingguidelines (accessed August 6, 2019).
[84] D. Shen, M.B.¨ Ulow, F. Siperstein, M.E. And, A.L. Myers, Comparison of Experimental Techniques for Measuring Isosteric Heat of Adsorption, 2000. https://link.springer.com/content/pdf/10.1023%2FA%3A1026551213604.pdf (accessed August 6, 2019).
[85] H. Fang, P. Kamakoti, P.I. Ravikovitch, M. Aronson, C. Paur, D.S. Sholl, First principles derived, transferable force fields for CO2 adsorption in Na-exchanged cationic zeolites, Phys. Chem. Chem. Phys. 15 (2013) 12882. doi:10.1039/c3cp52246f.
[86] L. Grajciar, J. Čejka, A. Zukal, C. Otero Areán, G. Turnes Palomino, P. Nachtigall, Controlling the adsorption enthalpy of CO2 in zeolites by framework topology and composition, ChemSusChem. 5 (2012) 2011–2022. doi:10.1002/cssc.201200270.
[87] D. Nicholson, T. Stubos, Simulation of Adsorption in Micropores, in: 2000: pp. 231–256. doi:10.1016/S0927-5193(00)80011-X.
[88] C. Zanzottera, M. Armandi, S. Esposito, E. Garrone, B. Bonelli, CO <inf>2</inf> adsorption on aluminosilicate single-walled nanotubes of imogolite type, J. Phys. Chem. C. 116 (2012). doi:10.1021/jp3061637.
[89] F.X. Llabrés i Xamena, A. Zecchina, FTIR spectroscopy of carbon dioxide adsorbed on sodium- and magnesium-exchanged ETS-10 molecular sieves, Phys. Chem. Chem. Phys. 4 (2002) 1978–1982. doi:10.1039/b110483g.
[90] B. Bonelli, M. Armandi, E. Garrone, Surface properties of alumino-silicate single-walled nanotubes of the imogolite type, Phys. Chem. Chem. Phys. 15 (2013). doi:10.1039/c3cp51508g.

[91] G. Busca, Acidity and basicity of zeolites: A fundamental approach, Microporous Mesoporous Mater. 254 (2017) 3–16. doi:10.1016/j.micromeso.2017.04.007.
[92] M. Armandi, E. Garrone, C.O. AreÃ¡n, B. Bonelli, Thermodynamics of Carbon Dioxide Adsorption on the Protonic Zeolite H-ZSM-5, ChemPhysChem. 10 (2009) 3316–3319. doi:10.1002/cphc.200900561.
[93] C.L. Angell, Carbon Dioxide Adsorbed on Linde X and Y Zeolites, J. Phys. Chem. 70 (1966) 2420–2420. doi:10.1021/j100879a509.
[94] † B. Bonelli, † B. Civalleri, † B. Fubini, † P. Ugliengo, ‡ and C. Otero Areán, †,§ E. Garrone*, Experimental and Quantum Chemical Studies on the Adsorption of Carbon Dioxide on Alkali-Metal-Exchanged ZSM-5 Zeolites, (2000). doi:10.1021/JP000555G.
[95] L. Bertsch, H.W. Habgood, AN INFRARED SPECTROSCOPIC STUDY OF THE ADSORPTION OF WATER AND CARBON DIOXIDE BY LINDE MOLECULAR SIEVE X [1], J. Phys. Chem. 67 (1963) 1621–1628. doi:10.1021/j100802a013.
[96] P.A. Jacobs, F.H. van Cauwelaert, E.F. Vansant, Surface Probing of Synthetic Faujasites by Adsorption of carbon Dioxide, J. Chem. Soc. Faraday Trans.1. 69 (1973) 2130. doi:10.1039/F19736901056.
[97] J.W. Ward, H.W. Habgood, The Infrared Spectra of Carbon Dioxide Adsorbed on Zeolite X, J. Phys. Chem. 70 (1966) 1178–1182. doi:10.1021/j100876a034.
[98] T. Frising, P. Leflaive, Extraframework cation distributions in X and Y faujasite zeolites: A review, Microporous Mesoporous Mater. 114 (2008) 27–63. doi:10.1016/j.micromeso.2007.12.024.
[99] B. Bonelli, B. Onida, B. Fubini, C. Otero Areá, E. Garrone, Vibrational and Thermodynamic Study of the Adsorption of Carbon Dioxide on the Zeolite Na-ZSM-5, (2000). doi:10.1021/la991363j.
[100] B. Bonelli, B. Civalleri, B. Fubini, P. Ugliengo, C.O. Areán, E. Garrone, Experimental and Quantum Chemical Studies on the Adsorption of Carbon Dioxide on Alkali-Metal-Exchanged ZSM-5 Zeolites, J. Phys. Chem. B. 104 (2002) 10978–10988. doi:10.1021/jp000555g.
[101] H.V. Thang, L. Grajciar, P. Nachtigall, O. Bludský, C.O. Areán, E. Frýdová, R. Bulánek, Adsorption of CO 2 in FAU zeolites: Effect of zeolite composition, Catal. Today. 227 (2014) 50–56. doi:10.1016/j.cattod.2013.10.036.
[102] T. Yamazaki, M. Katoh, S. Ozawa, Y. Ogino, Adsorption of CO2 over univalent cation-exchanged ZSM-5 zeolites, Mol. Phys. 80 (1993) 313–324. doi:10.1080/00268979300102281.
[103] H. Forster, M. Shumann, Infrared Spectroscopic Studies on Carbon Dioxie adsorption in Alkali-metal and Alkaline-earth-metal Ion-eschanged A-type Zeolites, J. Chem. Soc. Faraday Trans. 1. 85 (1989) 1149–1158.
[104] A. Zukal, C.O. Arean, M.R. Delgado, P. Nachtigall, A. Pulido, J. Mayerová, J. Čejka, Combined volumetric, infrared spectroscopic and theoretical investigation of CO2 adsorption on Na-A zeolite, Microporous Mesoporous Mater. 146 (2011) 97–105. doi:10.1016/j.micromeso.2011.03.034.
[105] P.A. Lacobs, F.H. van Cauwelaert, E.F. Vansant, J.. Uytterhoeven, Surface Probing of Synthetic Faujasites by Adsorption of carbon Dioxide, J. Chem. Soc. Faraday Trans.1. 69 (1973) 1056–1068.
[106] J. Zhang, R. Singh, P.A. Webley, Alkali and alkaline-earth cation exchanged chabazite zeolites for adsorption based CO2 capture, Microporous

Mesoporous Mater. 111 (2008) 478–487. doi:10.1016/j.micromeso.2007.08.022.
[107] J. Shang, G. Li, R. Singh, P. Xiao, D. Danaci, J.Z. Liu, P.A. Webley, Adsorption of CO2, N2, and CH4 in Cs-exchanged chabazite: A combination of van der Waals density functional theory calculations and experiment study, J. Chem. Phys. 140 (2014). doi:10.1063/1.4866455.
[108] Y. Garcia-Basabe, A.R. Ruiz-Salvador, G. Maurin, L.C. De Menorval, I. Rodriguez-Iznaga, A. Gomez, Location of extra-framework Co 2+, Ni 2+, Cu 2+ and Zn 2+ cations in natural and dealuminated clinoptilolite, Microporous Mesoporous Mater. 155 (2012) 233–239. doi:10.1016/j.micromeso.2012.01.018.
[109] G. Aguilar-Armenta, G. Hernandez-Ramirez, E. Flores-Loyola, A. Ugarte-Castaneda, R. Silva-Gonzalez, C. Tabares-Munoz, A. Jimenez-Lopez, E. Rodriguez-Castellon, Adsorption kinetics of CO2, O2, N2, and CH4 in cation-exchanged clinoptilolite, J. Phys. Chem. B. 105 (2001) 1313–1319. doi:10.1021/jp9934331.
[110] S. Krishnamurthy, R. Blom, M.C. Ferrari, S. Brandani, Adsorption and diffusion of CO2 in CPO-27–Ni beads, Adsorption. (2019). doi:10.1007/s10450-019-00162-x.
[111] School of Engineering Institute for Materials and Processes The University of Edinburgh, Training Manual for the Zero Length Column System School, 2012.
[112] X. Hu, S. Brandani, A.I. Benin, R.R. Willis, Testing the stability of novel adsorbents for carbon capture applications using the zero length column technique, Chem. Eng. Res. Des. 131 (2018) 406–413. doi:10.1016/j.cherd.2018.01.023.
[113] T. Gelles, Diffusion kinetics in promising adsorbents for gas capture processes, (2019).
[114] E. Mangano, Rapid screening of novel nanoporous materials for carbon capture separations, (2012).
[115] D. Ruthven, F. Brandani, ZLC response for systems with surface resistance control, Adsorption. 11 (2005) 31–34. doi:10.1007/s10450-005-1090-z.
[116] S. Brandani, M.A. Jama, D.M. Ruthven, ZLC measurements under non-linear conditions, Chem. Eng. Sci. 55 (2000) 1205–1212. doi:10.1016/S0009-2509(99)00411-X.
[117] S. Brandani, D.M. Ruthven, Analysis of ZLC desorption curves for liquid systems, Chem. Eng. Sci. 50 (1995) 2055–2059. doi:10.1016/0009-2509(95)00048-A.
[118] F. Brandani, A. Rouse, S. Brandani, D.M. Ruthven, Adsorption Kinetics and Dynamic Behavior of a Carbon Monolith, Adsorption. 10 (2004) 99–109. doi:10.1023/B:ADSO.0000039866.37214.6a.
[119] F. Brandani, D. Ruthven, C.G. Coe, Measurement of adsorption equilibrium by the zero length column (ZLC) technique part 1: Single-component systems, Ind. Eng. Chem. Res. 42 (2003) 1451–1461. doi:10.1021/ie020572n.
[120] S. Brandani, A Simple Graphical Check of Consistency for Zero Length Column Desorption Curves, Chem. Eng. Technol. 39 (2016) 1194–1198. doi:10.1002/ceat.201500634.
[121] S. Brandani, D.M. Ruthven, Analysis of ZLC Desorption Curves for Gaseous Systems, 1996. https://link.springer.com/content/pdf/10.1007%2FBF00127043.pdf

(accessed June 7, 2019).
[122] M. Beil, W. Beyrich, Biogas upgrading to biomethane, in: Biogas Handb., Elsevier, 2013: pp. 342–377. doi:10.1533/9780857097415.3.342.
[123] N. Hedin, L. Andersson, L. Bergström, J. Yan, Adsorbents for the post-combustion capture of CO2 using rapid temperature swing or vacuum swing adsorption, Appl. Energy. 104 (2013) 418–433. doi:10.1016/J.APENERGY.2012.11.034.
[124] L. Riboldi, O. Bolland, Overview on Pressure Swing Adsorption (PSA) as CO2 Capture Technology: State-of-the-Art, Limits and Potentials, Energy Procedia. 114 (2017) 2390–2400. doi:10.1016/j.egypro.2017.03.1385.
[125] S.D. Kenarsari, D. Yang, G. Jiang, S. Zhang, J. Wang, A.G. Russell, Q. Wei, M. Fan, Review of recent advances in carbon dioxide separation and capture, RSC Adv. 3 (2013) 22739. doi:10.1039/c3ra43965h.
[126] A.S. Bhown, B.C. Freeman, Analysis and Status of Post-Combustion Carbon Dioxide Capture Technologies, Environ. Sci. Technol. 45 (2011) 8624–8632. doi:10.1021/es104291d.
[127] J.C. Glier, E.S. Rubin, Energy Procedia 00 (2013) 000-000 Assessment of solid sorbents as a competitive post-combustion CO 2 capture technology Selection and/or peer-review under responsibility of GHGT, 2013. www.sciencedirect.comwww.elsevier.com/locate/procediaGHGT-11 (accessed July 12, 2019).
[128] L. Jiang, A.P. Roskilly, R.Z. Wang, Performance exploration of temperature swing adsorption technology for carbon dioxide capture, Energy Convers. Manag. 165 (2018) 396–404. doi:10.1016/j.enconman.2018.03.077.
[129] J. He, S. Deng, L. Zhao, R. Zhao, S. Li, A numerical analysis on energy-efficiency performance of temperature swing adsorption for CO 2 capture, Energy Procedia. 142 (2017) 3200–3207. doi:10.1016/j.egypro.2017.12.490.
[130] R. Ben-Mansour, M.A. Habib, O.E. Bamidele, M. Basha, N.A.A. Qasem, A. Peedikakkal, T. Laoui, M. Ali, Carbon capture by physical adsorption: Materials, experimental investigations and numerical modeling and simulations – A review, Appl. Energy. 161 (2016) 225–255. doi:10.1016/j.apenergy.2015.10.011.
[131] D. Marx, L. Joss, M. Hefti, M. Gazzani, M. Mazzotti, CO2 Capture from a Binary CO2/N2 and a Ternary CO2/N2/H2 Mixture by PSA: Experiments and Predictions, Ind. Eng. Chem. Res. 54 (2015) 6035–6045. doi:10.1021/acs.iecr.5b00943.
[132] D. Marx, L. Joss, M. Hefti, M. Mazzotti, Temperature Swing Adsorption for Postcombustion CO2 Capture: Single- and Multicolumn Experiments and Simulations, Ind. Eng. Chem. Res. 55 (2016) 1401–1412. doi:10.1021/acs.iecr.5b03727.
[133] M. Heftia, D. Marxa, L. Jossa, M. Mazzottia, Model-based process design of adsorption processes for CO2 capture in the presence of moisture, Energy Procedia. 63 (2014) 2152–2159. doi:10.1016/j.egypro.2014.11.234.
[134] L. Bisone, S. Bittanti, S. Canevese, A. De Marco, V. Prandoni, Cyclic Automation of a Plant for the Removal of CO2 from Biogas, IFAC-PapersOnLine. 50 (2017) 10802–10807. doi:10.1016/J.IFACOL.2017.08.2348.
[135] M. Clausse, J. Merel, F. Meunier, Numerical parametric study on CO2 capture by indirect thermal swing adsorption, Int. J. Greenh. Gas Control. 5 (2011) 1206–1213. doi:10.1016/j.ijggc.2011.05.036.
[136] Edinburgh Research Explorer, (n.d.).

doi:10.1016/j.compchemeng.2016.07.020.
[137] D.M. Ruthven, M.F.M. Post, Chapter 12 Diffusion in zeolite molecular sieves, in: 2001: pp. 525–577. doi:10.1016/S0167-2991(01)80254-8.
[138] N. Casas, J. Schell, R. Pini, M. Mazzotti, Fixed bed adsorption of CO 2/H 2 mixtures on activated carbon: Experiments and modeling, Adsorption. 18 (2012) 143–161. doi:10.1007/s10450-012-9389-z.
[139] S. Topham, A. Bazzanella, S. Schiebahn, S. Luhr, L. Zhao, A. Otto, D. Stolten, Carbon Dioxide, Wiley-VCH Verlag GmbH & Co. KGaA, Weinheim, Germany, 2014. doi:10.1002/14356007.a05_165.pub2.
[140] M.T. M. Fischedick, K. Görner, CO2: Abtrennung, Speicherung, Nutzung, Ganzheitliche Bewertung im Bereich von Energiewirtschaft und Industrie, Berlin, Heidelberg, 2015. doi:10.1007/978-3-642-19528-0.
[141] S. Schiebahn, Effizienzoptimierte CO2 -Abtrennung in IGCC-Kraftwerken mittels Wassergas-Shift-Membranreaktoren, Schriften des Forschungszentrums Jülich Reihe Energie & Umwelt / Energy & Environment, 2015.
[142] I. International Energy Agency, 20 Years of Carbon Capture and Storage - Accelerating Future Deployment, 2016. www.iea.org/t&c/ (accessed March 6, 2019).
[143] M. Bui, C.S. Adjiman, A. Bardow, E.J. Anthony, A. Boston, S. Brown, P.S. Fennell, S. Fuss, A. Galindo, L.A. Hackett, J.P. Hallett, H.J. Herzog, G. Jackson, J. Kemper, S. Krevor, G.C. Maitland, M. Matuszewski, I.S. Metcalfe, C. Petit, G. Puxty, J. Reimer, D.M. Reiner, E.S. Rubin, S.A. Scott, N. Shah, B. Smit, J.P.M. Trusler, P. Webley, J. Wilcox, N. Mac Dowell, Carbon capture and storage (CCS): the way forward, Energy Environ. Sci. 11 (2018) 1062–1176. doi:10.1039/C7EE02342A.
[144] Pathways to a Low-Carbon Economy:Energy System Modelling, 2009. https://www.mckinsey.com/~/media/mckinsey/dotcom/client_service/sustainability/cost curve pdfs/pathways_lowcarbon_economy_version2.ashx (accessed March 6, 2019).
[145] P. Markewitz, W. Kuckshinrichs, W. Leitner, J. Linssen, P. Zapp, R. Bongartz, A. Schreiber, T.E. Müller, Worldwide innovations in the development of carbon capture technologies and the utilization of CO2, Energy Environ. Sci. 5 (2012) 7281. doi:10.1039/c2ee03403d.
[146] A. Goeppert, M. Czaun, G.K. Surya Prakash, G.A. Olah, Air as the renewable carbon source of the future: an overview of CO2 capture from the atmosphere, Energy Environ. Sci. 5 (2012) 7833. doi:10.1039/c2ee21586a.
[147] S. Bocchini, C. Castro, M. Cocuzza, S. Ferrero, G. Latini, A. Martis, F. Pirri, L. Scaltrito, V. Rocca, F. Verga, D. Viberti, Politecnico di Torino Porto Institutional Repository The Virtuous CO 2 Circle or the Three Cs: Capture, Cache, and Convert, J. Nanomater. 2017 (2017) 1–14. doi:10.1155/2017/6594151.
[148] C. De Conno, GPSA Engineering Data Book [Gas Processing], 12th ed., Gas Processors Suppliers Association, Tulsa, Oklahoma, 2004. https://www.academia.edu/11912717/GPSA_Engineering_Data_Book_Gas_Processing_12th_ed_2004 (accessed April 15, 2019).
[149] X. Li, M. Hou, Z. Zhang, B. Han, G. Yang, X. Wang, L. Zou, Absorption of CO2 by ionic liquid/polyethylene glycol mixture and the thermodynamic parameters, Green Chem. 10 (2008) 879. doi:10.1039/b801948g.
[150] W. Gouveia, T.F. Jorge, S. Martins, M. Meireles, M. Carolino, C. Cruz, T.V. Almeida, M.E.M. Araújo, Toxicity of ionic liquids prepared from

biomaterials, Chemosphere. 104 (2014) 51–56. doi:10.1016/j.chemosphere.2013.10.055.
[151] K.D. Weaver, H.J. Kim, J. Sun, D.R. MacFarlane, G.D. Elliott, Cyto-toxicity and biocompatibility of a family of choline phosphate ionic liquids designed for pharmaceutical applications, Green Chem. 12 (2010) 507. doi:10.1039/b918726j.
[152] B.E. Gurkan, J.C. de la Fuente, E.M. Mindrup, L.E. Ficke, B.F. Goodrich, E.A. Price, W.F. Schneider, J.F. Brennecke, Equimolar CO_2 Absorption by Anion-Functionalized Ionic Liquids, J. Am. Chem. Soc. 132 (2010) 2116–2117. doi:10.1021/ja909305t.
[153] Y.S. Sistla, A. Khanna, CO2 absorption studies in amino acid-anion based ionic liquids, Chem. Eng. J. 273 (2015) 268–276. doi:10.1016/j.cej.2014.09.043.
[154] M. Petkovic, J.L. Ferguson, H.Q.N. Gunaratne, R. Ferreira, M.C. Leitão, K.R. Seddon, L.P.N. Rebelo, C.S. Pereira, Novel biocompatible cholinium-based ionic liquids—toxicity and biodegradability, Green Chem. 12 (2010) 643. doi:10.1039/b922247b.
[155] Q.-P. Liu, X.-D. Hou, N. Li, M.-H. Zong, Ionic liquids from renewable biomaterials: synthesis, characterization and application in the pretreatment of biomass, Green Chem. 14 (2012) 304–307. doi:10.1039/C2GC16128A.
[156] G. Latini, M. Signorile, V. Crocellà, S. Bocchini, C.F. Pirri, S. Bordiga, Unraveling the CO2 reaction mechanism in bio-based amino-acid ionic liquids by operando ATR-IR spectroscopy, Catal. Today. (2019). doi:10.1016/j.cattod.2018.12.050.
[157] S. Yuan, Y. Chen, X. Ji, Z. Yang, X. Lu, Experimental study of CO2absorption in aqueous cholinium-based ionic liquids, Fluid Phase Equilib. 445 (2017) 14–24. doi:10.1016/j.fluid.2017.04.001.
[158] S. De Santis, G. Masci, F. Casciotta, R. Caminiti, E. Scarpellini, M. Campetella, L. Gontrani, Cholinium-amino acid based ionic liquids: a new method of synthesis and physico-chemical characterization, Phys. Chem. Chem. Phys. 17 (2015) 20687–20698. doi:10.1039/C5CP01612F.
[159] Q.-P. Liu, X.-D. Hou, N. Li, M.-H. Zong, Ionic liquids from renewable biomaterials: synthesis, characterization and application in the pretreatment of biomass, Green Chem. 14 (2012) 304–307. doi:10.1039/C2GC16128A.
[160] D.-J. Tao, Z. Cheng, F.-F. Chen, Z.-M. Li, N. Hu, X.-S. Chen, Synthesis and Thermophysical Properties of Biocompatible Cholinium-Based Amino Acid Ionic Liquids, (2013). doi:10.1021/je301103d.
[161] S.P. Pinho, E.A. Macedo, Solubility of NaCl, NaBr, and KCl in Water, Methanol, Ethanol, and Their Mixed Solvents, J. Chem. Eng. Data. 50 (2005) 29–32. doi:10.1021/je049922y.
[162] S. De Santis, G. Masci, F. Casciotta, R. Caminiti, E. Scarpellini, M. Campetella, L. Gontrani, Cholinium-amino acid based ionic liquids: A new method of synthesis and physico-chemical characterization, Phys. Chem. Chem. Phys. 17 (2015) 20687–20698. doi:10.1039/c5cp01612f.
[163] B. Gurkan, B.F. Goodrich, E.M. Mindrup, L.E. Ficke, M. Massel, S. Seo, T.P. Senftle, H. Wu, M.F. Glaser, J.K. Shah, E.J. Maginn, J.F. Brennecke, W.F. Schneider, Molecular Design of High Capacity, Low Viscosity, Chemically Tunable Ionic Liquids for CO_2 Capture, J. Phys. Chem. Lett. 1 (2010) 3494–3499. doi:10.1021/jz101533k.
[164] J. Zhang, S. Zhang, K. Dong, Y. Zhang, Y. Shen, X. Lv, Supported Absorption of CO2 by Tetrabutylphosphonium Amino Acid Ionic Liquids,

Chem. - A Eur. J. 12 (2006) 4021–4026. doi:10.1002/chem.200501015.
[165] C. Wang, H. Luo, H. Li, X. Zhu, B. Yu, S. Dai, Tuning the Physicochemical Properties of Diverse Phenolic Ionic Liquids for Equimolar CO2 Capture by the Substituent on the Anion, Chem. - A Eur. J. 18 (2012) 2153–2160. doi:10.1002/chem.201103092.
[166] M. Aghaie, N. Rezaei, S. Zendehboudi, A systematic review on CO2 capture with ionic liquids: Current status and future prospects, Renew. Sustain. Energy Rev. 96 (2018) 502–525. doi:10.1016/j.rser.2018.07.004.
[167] B. Li, Y. Chen, Z. Yang, X. Ji, X. Lu, Thermodynamic study on carbon dioxide absorption in aqueous solutions of choline-based amino acid ionic liquids, Sep. Purif. Technol. (2019) 128–138. doi:10.1016/j.seppur.2018.01.058.
[168] J. Wu, C. Zhao, W. Lin, R. Hu, Q. Wang, H. Chen, L. Li, S. Chen, J. Zheng, Binding characteristics between polyethylene glycol (PEG) and proteins in aqueous solution, J. Mater. Chem. B. 2 (2014) 2983–2992. doi:10.1039/c4tb00253a.